



MARK BRYAN ALIVIO

**EVALUATION OF FLOOD DAMAGE CAUSED BY
RISING SEA LEVELS**

MASTER'S THESIS

MASTER STUDY PROGRAMME FLOOD RISK MANAGEMENT



IHE
DELFt



TECHNISCHE
UNIVERSITÄT
DRESDEN



UNIVERSITAT POLITÈCNICA
DE CATALUNYA
BARCELONATECH

Univerza v Ljubljani



Ljubljana, 2021



Candidate

MARK BRYAN ALIVIO

EVALUATION OF FLOOD DAMAGE CAUSED BY RISING SEA LEVELS

Master's thesis no.:

Mentor:
doc. dr. Simon Rusjan

Chairman of the Commission
prof. dr. Matjaž Četina, Ph.D.

Co-mentor:
izr. prof. dr. Andrej Kryžanowski

Commission member:

Ljubljana, 2021



IHE
DELFIT

TECHNISCHE
UNIVERSITÄT
DRESDEN



UNIVERSITAT POLITÈCNICA
DE CATALUNYA
BARCELONATECH

Univerza v Ljubljani



ERRATA

Error page

Error bar

Instead

Let it be

ACKNOWLEDGEMENTS

"The only impossible journey is the one you never begin." - Anthony Robbins

Every page of this thesis reflects my diligent work and steadfast hope to meet the day when I can finally celebrate its completion and acknowledge the people that made it possible. I have finally made it to this day, thankfully not all by myself. It is a genuine privilege and pleasure to express my deepest sense of thanks, gratitude, and appreciation for the guidance and support of the following individuals who greatly contributed to the success of making this master's thesis.

To my research mentors, Dr. Simon Rusjan and Dr. Andrej Kryžanowski, for their supervision, unwavering support, and dedicated involvement in every step of the process towards the accomplishment of this thesis. My sincerest gratitude to Dr. Simon Rusjan for his great deal of guidance, suggestions, insightful comments, and most especially for sharing his knowledge about the subject of research which I am indeed fortunate to experience. Thus, his continuous supervision and constant response to my queries regarding the limitations of my study have steered me in the right direction of the research which led me to the completion and success of my thesis. I also want to thank Dr. Andrej Kryžanowski, for guiding me to have a better understanding of the present situation of the case study area and for his valuable inputs and comments on a particular aspect of my thesis. In addition, I wish to extend my thanks to Dr. Matjaž Mikoš and Dr. Micha Werner, for their examining inputs and suggestions in improving the quality of my thesis. I am particularly grateful for the assistance of Mr. Andrej Vidmar in carrying out the flood damage estimation using the KRPLAN model and for giving me a brief explanation about the concept and operation of this application.

To the European Commission and selection committee of the Flood Risk Management program, for providing me the opportunity to study this interdisciplinary and international Master of Science degree program thru the Erasmus+ scholarship which allows me to gain an invaluable wealth of knowledge, experiences, and memories in academics and life in general. I consider this Flood Risk Master a turning point in my professional career as a civil engineer because not only it widens my horizons but also it strengthens my decision to pursue a research career that contributes to the sustainable development goals, protection of the environment, and the betterment of the people.

To my Floodies 8 (FRM Batch 8) family, even with our diverse backgrounds, I thank you so much for widening my horizons, travelling Europe with me, and for sharing your life stories, cuisines, and laughter with me which have enriched my life in general. I am truly grateful for our wonderful experiences and memories, both in academics and travelling, which I will treasure forever.

To my friends and cousins back home, for their encouragements, emotional support, and virtual shoulders that I can lean on even through the thousands of kilometers during my discouraging moments.

To my beloved parents, for their unparalleled love, never-ending moral support, and votes of confidence from the start until the last part of my Erasmus journey and making this master thesis;

To finish, I also place on record, my sense of gratitude to one and all, who, directly and indirectly, have lent and extended their helping hands in this venture, Thank you very much and lots of love!

Mark Bryan Alivio
Ljubljana, Slovenia

BIBLIOGRAPHIC-DOCUMENTALISTIC INFORMATION AND ABSTRACT

UDC:	627.33:627.5:556.18(497.4coast)(043.3)
Author:	Mark Bryan Alivio
Supervisor:	Assist. Prof. Simon Rusjan, Ph.D.
Co-supervisor:	Assoc. Prof. Andrej Kryžanowski, Ph.D.
Title:	Evaluation of flood damage caused by rising sea levels
Document type:	Master thesis
Notes:	82 p., 8 tab., 32 fig., 8 eq., 241 ref.
Keywords:	Bathtub inundation model, coastal flooding, damage-probability curves, expected annual damage, KRPAN model, the city of Piran, sea level rise

Abstract

The inexorability of climate change-driven accelerated sea level rise (SLR) poses consequential threats to the majority of the coastal cities around the world through a range of coastal hazards which include more frequent and intense sea flooding. The historic center of the city of Piran in Slovenia is predicted to face a considerable increase in flood risk and consequences of rising sea levels due to its specific topographical coastal relief and high concentration of socio-economic activities and cultural value. However, no existing study explores the impacts of SLR on the recurring coastal flood hazards and extreme sea level events in Piran. This research investigates the return period variation of sea level extremes and evaluates the economic costs of coastal flood damage at the local level according to the varying magnitude of SLR scenarios.

The impact of future SLR on the return period of extreme sea levels was investigated by superposing an array of SLR scenarios onto the Gumbel-fitted current extreme sea levels data. Along with the digital elevation model derived from LiDAR scanning, these scenario-based water levels were translated into a spatial extension of coastal floods using a bathtub inundation model operated in a geographic information system (GIS) raster environment. Exposure assessment of population and sectoral economic elements in Piran was performed by overlaying the hydrologically connected flood surface areas with various geospatial datasets. The extent of inundation and water depth distribution were used as inputs to the KRPAN model (Vidmar et al., 2019) to estimate the economic costs of flood damage for different inundation scenarios. The damage estimates based on six return periods were utilized to construct damage-probability curves and calculate the total expected annual flood damage (EAD) caused by the varying magnitudes of SLR.

The results of the study revealed that the recurrence intervals of the present-day extreme sea level events in the coast of Slovenia have drastically shortened by about a factor of 2 for every 10 cm of SLR. The current low-frequency events with a return period of 100- to 1000-year is projected to be exceeded by almost normal high tide cycle if the increments in sea level follow the two high-end SLR scenarios of 0.84 m and 1.46 m which suggest a higher frequency of extreme sea level in the future. The amplification of the sea level extremes frequency is highly evident, a 30 cm SLR in 2100 will trigger the low probability events to inundate the entire low-lying parts of the city. The inundation will affect 38% of the buildings in the narrow old city center and the majority of cultural heritage sites while causing displacement of 47% of the total inhabitants in the area which further escalates tremendously with higher increments of SLR. Consequently, the EAD associated with this level of SLR is about 2.4 million euros per year and 65% of this damage is borne from residential buildings and household contents. The EAD dramatically escalates to 10.2 million euros per year under a high-impact SLR scenario from a baseline cost of 0.68 million euros per year. The study clearly shows that the economic impact of SLR in the old town of Piran is expected to become costly and in view of its local character, the residential properties and cultural heritage were demonstrated to face the greatest consequences of rising sea levels in the future. This degree of damages is very unlikely to be tolerated and will cause many additional concerns to the state ministries, municipality, and society in the near future which emphasizes the crucial role of long-term coastal adaptation measures implementation.

BIBLIOGRAFSKO – DOKUMENTACIJSKA STRAN IN IZVLEČEK

UDK:	627.33:627.5:556.18(497.4Obala)(043.3)
Avtor:	Mark Bryan Alivio
Mentor:	doc. dr. Simon Rusjan
Somentor:	izr. prof. dr. Andrej Kryžanowski
Naslov:	Ocena poplavne škode zaradi naraščanja gladine morja
Tip dokumenta:	magistrsko delo
Obseg in oprema:	82 str., 8 pregl., 32 sl., 8 en., 241 ref.
Ključne besede:	model poplavljanja morja, obalne poplave, verjetnostne škodne krivulje, pričakovana letna škoda, model KRPAN, mesto Piran, dvig morske gladine

Izvleček:

Neizogibno in pospešeno dviganje morske gladine zaradi podnebnih sprememb ogroža številna obalna mesta po svetu z različnimi obalnimi nevarnostmi, ki vključujejo vse pogostejše in intenzivnejše poplavljajanje morja. Zgodovinsko središče mesta Piran v Sloveniji se bo zaradi specifične topografije obale in visoke koncentracije družbeno-ekonomskega dejavnosti in kulturnih vrednot soočalo s precejšnjim povečanjem poplavnega tveganja zaradi dviga morske gladine. Doslej še ni bila izvedena raziskava, ki bi preučila vpliv povečane pogostosti obalnih poplav in ekstremnih poplavnih dogodkov v mestu Piran. V naši raziskavi je bil preučen vpliv spremenjene pojavnosti poplav morja kot posledice dviga morske gladine ter ocenjena ekonomska škoda obalnih poplav na lokalni ravni glede na različno obseg scenarijev dviga gladine morja.

Vpliv prihodnjega pričakovanega dviga morske gladine na pojavnost ekstremnih nivojev gladine morja je bil raziskan tako, da smo izvedli statistično analizo pojavnosti nivojev morske gladine z uporabo Gumblove porazdelitve. Ob tako statistično izvrednotenih gladinah smo upoštevali še dodatne dvige morske gladine z upoštevanjem različnih podnebnih scenarijev. Z uporabo digitalnega modela višin, pridobljenega na osnovi LiDAR snemanja obalnega območja, so bili izvrednoteni nivoji gladin morja nadalje upoštevani pri določitvi poplavnih območij z uporabo modela poplavljanja morja, ki deluje v rastrskem okolju geografskega informacijskega sistema (GIS). Ocena izpostavljenosti prebivalstva in sektorskih gospodarskih elementov znotraj mesta Piran je bila izvedena s prekrivanjem hidrološko povezanih poplavnih površin z različnimi nabori prostorskih podatkov. Obsegi poplavljanja in porazdelitev globine vode na poplavnih območjih so bili uporabljeni kot vhodni podatki v model KRPAN (Vidmar et al., 2019) za oceno poplavne škode za različne scenarije dviga morske gladine. Ocene škode izvrednotene z upoštevanjem 6 različnih povratnih dob poplav morja, so bile uporabljene za izdelavo verjetnostnih škodnih krivulj, na osnovi le-teh pa smo nadalje preračunali skupno pričakovano letno škodo zaradi poplav ob upoštevanju različnih scenarijev dviga morske gladine.

Rezultati študije so pokazali, da so se intervali pojavljanja sedanjih ekstremnih visokovodnih dogodkov na slovenski obali drastično skrajšali in sicer za približno faktor 2 na vsakih 10 cm dviga morske gladine. Na osnovi izračunov lahko predvidevamo, da bodo trenutni nizkofrekvenčni dogodki s povratnimi dobbami od 100 do 1000 let doseženi s skoraj normalnim ciklom plime v primeru, da bo dvig morske gladine sledil dvema kritičnima scenarijema dviga gladine za 0,84 m oz. 1,46 m. Povečanje pogostosti nastopa ekstremnih poplavnih dogodkov bo zelo očitno, 30 cm dvig morske gladine do leta 2100 bo povzročil, da bodo že pri pogostih poplavnih dogodkih poplavljeni celotni nižje ležeče predeli mesta Piran. Poplave morja bodo po naših ocenah prizadela 38% stavb v ožjem starem mestnem jedru in večino lokacij kulturne dediščine, hkrati pa bo v najverjetnejšo izselitev prisiljen 47% delež celotnega prebivalstva na območju, v primeru upoštevanja najbolj kritičnih scenarijev dviga gladine se posledice še dodatno stopnjujejo. Pričakovana letna škoda povezana s to stopnjo dviga morske gladine je približno 2,4 milijona evrov na leto, 65% te škode pa je vezano na stanovanjske zgradbe in gospodarske dejavnosti. Pričakovana letna škoda dramatično naraste na 10,2 milijona evrov na leto v primeru upoštevanja najbolj kritičnih scenarijev dviga morske gladine, kar predstavlja izjemno veliko povečanje izhodiščnih stroškov s sedanje ocene 0,68 milijona evrov na leto. Rezultati jasno kažejo, da bo

gospodarski učinek dviga morske gladine na območju starega mestnega jedra Pirana izjemno velik in da se bo glede na lastnosti stanovanjskih nepremičnin in kulturne dediščine lokalna skupnost morala soočiti z velikimi posledicami naraščajoče gladine morja v prihodnosti. Poplavne škode v takšnem obsegu bodo v prihodnosti prav gotovo postale nesprejemljive ter bodo povzročile številne dodatne skrbi ministrstvom, lokalni skupnosti ter družbi v najširšem pomenu, kar jasno kaže na bistveno vlogo in pomen načrtovanja ter izvajanja dolgoročnih protipoplavnih ukrepov.

TABLE OF CONTENTS

ERRATA	I
ACKNOWLEDGEMENTS	II
BIBLIOGRAPHIC-DOCUMENTALISTIC INFORMATION AND ABSTRACT	III
TABLE OF CONTENTS	VI
LIST OF FIGURES.....	VIII
LIST OF TABLES.....	X
ABBREVIATIONS AND SYMBOLS	XI
1 INTRODUCTION	1
1.1 Motivation	1
1.2 Objectives of the study	3
1.3 Research questions	4
1.4 Scientific innovation and practical value	4
2 LITERATURE REVIEW	6
2.1 Climate change – driven sea level rise	6
2.2 Characteristics of coastal flooding	8
2.3 Coastal inundation mapping imposed with SLR using GIS tools and LiDAR-DEM data	10
2.3.1 Bathhtub inundation model	11
2.3.2 Role of LiDAR-DEM in sea-level rise inundation mapping.....	13
2.4 Flood damage estimation	15
3 CASE STUDY AREA.....	19
3.1 Past flood events	20
3.2 Sea level rise in Slovenian coast	22
4 RESEARCH METHODOLOGY	24
4.1 Methodological framework	24
4.2 Data acquisition	25
4.2.1 Elevation Data - LiDAR DEM.....	25
4.2.2 Land use data	26
4.2.3 Other geospatial datasets.....	27
4.2.4 Annual maximum sea level.....	29
4.2.5 Sea level rise projections.....	30
4.3 Development of sea level rise scenarios	31
4.4 Extreme value analysis.....	32
4.5 Inundation scenarios	34
4.6 Delineation of potential inundated areas (PIAs).....	35
4.7 Exposure analysis	36
4.8 Flood damage estimation	37
4.8.1 KRPAN model	38
4.8.2 Damage-probability Curve.....	40
5 RESULTS AND DISCUSSION	42

5.1	Estimates of current and scenario-based extreme sea levels	42
5.1.1	Return period variation of extreme sea levels.....	44
5.2	Elevation-based inundation maps (PIAs).....	46
5.3	Exposure analysis.....	48
5.3.1	Population	50
5.3.2	Built-up structures.....	51
5.3.3	Public infrastructures	52
5.3.4	Cultural heritage	55
5.4	Estimated costs of coastal flood damages.....	57
5.5	Response strategies and adaptation measures to reduce the impacts of SLR	64
6	CONCLUSIONS AND RECOMMENDATIONS	65
6.1	Summary.....	65
6.2	Conclusions	66
6.3	Recommendations	68
7	REFERENCES	69

LIST OF FIGURES

Figure 1: Global mean sea-level rise projections over the 21 st century relative to 1986 – 2005 for the four RCP scenarios (Source: IPCC, 2013)	8
Figure 2: Classification of flood damages adapted from Penning-Rowsell et al. 2003; Smith and Ward 1998 as cited in Messer et al. (2007).....	15
Figure 3: Location of the study area.....	21
Figure 4: Annual mean sea level trend (10-year moving average) at Koper tide gauge station over the period of 1960 to 2020 (Source: Ličer et al., 2021)	23
Figure 5: Methodological flowchart.....	24
Figure 6: Elevation Map of Piran	27
Figure 7: Land use map of Piran	28
Figure 8: Land use classification of the study area	28
Figure 9: Spatial distribution of population (left) and cultural heritage sites (right) in Piran	29
Figure 10: Annual maximum sea level and the number of days it exceeded the flood level of 300 cm at the tide gauge station Koper (Source: ARSO)	30
Figure 11: Hydrologic Connectivity using 4-side and 8-side rule (Poulter and Halpin, 2008).....	36
Figure 12: KRPAN model application	39
Figure 13: Diagnostic plots from fitting a GEV (left) and Gumbel (right) distribution to the annual maximum sea level dataset.....	44
Figure 14: Changes in the return period of extreme sea levels in Piran under different sea level rise scenarios.....	46
Figure 15: Inundation maps of Piran for 2-year (left) and 5-year (right) return period imposed with varying SLR values	48
Figure 16: Inundation maps of Piran for 10-year (left) and 100-year (right) return period imposed with varying SLR values	48
Figure 17: Inundation maps of Piran for 500-year (left) and 1000-year (right) return period imposed with varying SLR values	49
Figure 18: Inundated land area in Piran for a series of SLR scenarios.....	49
Figure 19: Number of endangered population in Piran for a series of SLR scenarios	50
Figure 20: Number of exposed residential buildings in Piran for a series of SLR scenarios	52
Figure 21: Number of exposed non-residential buildings in Piran for a series of SLR scenarios.....	52
Figure 22: Estimated length of local roads exposed to a series of SLR scenarios	53
Figure 23: Estimated length of underground electric cables exposed to a series of SLR scenarios.....	54
Figure 24: Estimated length of water supply networks exposed to a series of SLR scenarios.....	54
Figure 25: Estimated length of sewer systems exposed to a series of SLR scenarios	55

Figure 26: Endangered cultural heritage sites in Piran for 2-year return periods at different SLR scenarios.....	56
Figure 27: Endangered cultural heritage sites in Piran for 1000-year return periods at different SLR scenarios.....	56
Figure 28: Some of the most notable cultural heritage properties located in the low-lying center of Piran	57
Figure 29: Shares of flood damages by sectors for (a) 2-year; (b) 5-year; (c) 10-year; (d) 100-year; (e) 500-year; and (f) 1000-year recurrence intervals at varying SLR scenarios.....	59
Figure 30: Damage-probability curves for Piran according to different SLR scenarios	60
Figure 31: Total Expected Annual Flood Damage in Piran for different SLR scenarios.....	61
Figure 32: Shares of EAD in Piran by categories for different SLR scenarios	63

LIST OF TABLES

Table 1: Projected global mean sea level rise (m) by 2100 from different authors.....	7
Table 2: Datasets used in the study	25
Table 3: Sea level rise scenarios.....	32
Table 4: Identified elements at risk in Piran.....	37
Table 5: Extreme sea level for various return periods using GEV and Gumbel distribution models (with 95% confidence interval inside the brackets).....	43
Table 6: Distribution parameters of the GEV and Gumbel ($\xi = 0$) model (with standard error estimates inside the brackets) using MLE technique.....	43
Table 7: Model performance of GEV and Gumbel distribution using criterion-based goodness-of-fit test.....	43
Table 8: Average recurrence intervals of scenario extreme sea levels for different SLR projections...	45

ABBREVIATIONS AND SYMBOLS

μ	Location parameter
σ	Scale Parameter
ξ	Shape Parameter
AIC	Akaike Information Criterion
ARSO	Agencija Republike Slovenije za Okolje
BIC	Bayesian Information Criterion
CEWL	Current Extreme Water Level
DEM	Digital Elevation Model
EAD	Expected Annual Damage
ESL	Extreme Sea Level
EVA	Extreme Value Analysis
GIS	Geographic Information System
GDP	Gross Domestic Product
GMSL	Global Mean Sea Level
IPCC	Intergovernmental Panel on Climate Change
KRPAN	Kumulativni Računi Poplavnih škod in ANalize
LiDAR	Light Detection and Ranging
RCP	Representative Concentration Pathway
SEWL	Scenario Extreme Water Level
SLR	Sea Level Rise

"This page is intentionally blank"

1 INTRODUCTION

This chapter briefly explains the general background of the problem to be addressed, the motivation of the study, and the rationale behind the project. A short introduction of the case study is also provided, followed by the identification of the objectives to be achieved, research questions to be answered, and the significance of the study.

1.1 Motivation

In recent years, the global mean sea level (GMSL) is persistently rising at an accelerating rate of $5 \text{ mm} \cdot \text{year}^{-1}$ over the five-year period of 2014 to 2019 (WMO, 2019) which is substantially faster than the average rate of $3.2 \text{ mm} \cdot \text{year}^{-1}$ recorded between 1993 and 2010. This can further increase up to an overwhelming rate of 4 to $9 \text{ mm} \cdot \text{year}^{-1}$ under the Representative Concentration Pathway (RCP) 2.6 scenario and 10 to $20 \text{ mm} \cdot \text{year}^{-1}$ by 2100 for RCP8.5 (Oppenheimer et al., 2019). Thus, a 2°C increase in global temperature will additionally cause sea levels to rise between 0.3 m and 0.93 m at the end of the 21st century (IPCC, 2013) while other researchers have stressed out that it could eventually reach 2 m or even more in the following period (Horton et al., 2018; Kopp et al., 2014; Le Bars et al., 2017). The inevitability of sea-level rise (SLR) caused by climate change will double the frequency and intensity of severe coastal flooding in the next few decades with dire consequences and impacts to the social, ecological, and economic conditions of the country. It is widely recognized that coastal zones are the “frontline” of climate change due to their geographical setting and topography while the increased frequency and severity of storm surges and SLR pose direct threats to people, property, infrastructure, and economic activities of the region (Nicholls et al., 2008; Nicholls and Cazenave 2010). Oppenheimer et al. (2019) clearly stated the exponential relationship of SLR and flood frequency which shows that rising sea levels will consequentially trigger historically rare events with a return period of 100 years or larger to occur annually or even more frequently by the end of 2100 under the RCP 8.5 scenario at a high confidence level. However, for most vulnerable coastal areas in the lower altitudes, the amplification of the average occurrence frequency of extreme sea levels is particularly high which implies that even the RCP 2.6 scenario will lead to the annual occurrence of such rare events as early as mid-century. This shortening of recurrence interval of extreme water levels under future SLR was explored by Wu et al. (2016) and found out that under the RCP8.5 scenario, the 50-year return period event will occur once in 3–11 years by 2050 and in 1–3 years by 2100; and the 100-year period will shift to a 1-in-5–19-year event in 2050 and 1-in-1–5-year event in 2100; while, the 1000-year recurrence event will occur every 34–172 years by 2050 and every 2–30 years by 2100. Furthermore, the result of the study by Haigh and Pattiarchi (2010) also revealed that the projected rise in sea level by 2100 will potentially decrease the current average recurrence intervals in Southwest Australian coast such as a 100-year event in 1900 will become today’s 1-in-10 to 20-year event which is about 50 times increase in exceedance frequency. Despite this, coastal areas have experienced tremendous growth and are interestingly becoming the center of important economic and commercial activities in many countries and regions which provide critical inputs for industry and transport; opportunities for tourism and recreation; and home to the growing world’s population and wildlife habitat. This paradoxical situation could be exacerbated by the aforementioned human-induced changes on ocean and land which played an important role in escalating the exposure and vulnerability of coastal zones to future SLR and extreme sea level events (IPCC, 2013; OECD, 2019). The effects are manifested in the episodic event of coastal inundation that can last from hours to days of which the increasing frequency of high water under extreme conditions is expected to grow by a factor of 100 in most coastal cities around the globe in the following century (IPCC, 2019) with accompanying socio-economic costs and cascading impacts on coastal landscapes, their ecosystem services, and coastal inhabitants. The intensification of coastal

flood risk in the future could result in unprecedented coastal flood losses where the corresponding economic cost of damage and affected population are projected to increase during the 21st century.

A study of Jevrejeva et al. (2016) estimates that 90% of the coastal areas will experience an above-average rise in sea level by 2040 in case the temperature reaches 2°C under the RCP8.5 scenario. This is an alarming phenomenon that significantly proliferates coastal flood damages during the 21st century and gains widespread attention among researchers, scientists, and policymakers due to the ecological importance of coastal zones and their high concentration in socio-economic values. It is therefore essential from economic, social, and ecological points of view to obtain the most accurate insights of the extent of SLR-driven hazards for planning of future development, management, and protection of the coastal environment. In response to rising sea levels, there is a growing necessity of efforts and investments on coastal adaptation measures, impact assessment, risk management, and long-term decision plans to better prepare the ensuing consequences of SLR and reduce the associated cost of the phenomenon. Pursuant to the findings of the study conducted by Vousdoukas et al. (2020), around 95% of the projected economic losses due to coastal flooding could be avoided when coastal adaptation measures are implemented in European coastlines. Whilst, the consequences of doing nothing are expected to cause an annual flood damage of €209.8 billion and €1268.4 billion for RCP 4.5 and 8.5 scenarios, respectively at the end of 2100 from a baseline of €1.4 billion per year. Similarly, the additional coastal flood protection will reduce the number of affected people along the entire coastlines in Europe by 59% for RCP 4.5 and 66% for RCP 8.5 compared to a “do nothing” scenario. On a global scale, Kirezci et al. (2020) found out that in the absence of coastal protection measures, 0.5–0.7% of the world’s land area will be at risk of periodic sea flooding by 2100 which will expose 2.5–4.1% of the world’s population and imperil valuable assets with a worth of 12–20% of the current global economy. These key numbers show that implementing measures to adapt to rising sea levels makes economic sense in reducing some of the coastal impacts by several orders of magnitude.

Numerous studies have explored and developed different techniques and methods to assess the impacts of sea level rise on coastal areas at global, regional and local scales. The use of Geographic Information System (GIS) and digital elevation models (DEMs) in simulating and mapping the potential inundation and vulnerability scenarios of the coasts related to sea level rise throughout the years has grown and progressed as a global endeavor (Breili, et al., 2020; Cooper, et al., 2013; Gesch, 2009; Gracia, et al., 2019; Lichter and Felsenstein, 2012; Poulter and Halpin, 2008; Rowley et al., 2007; Stanchev, et al., 2009). Hence, GIS paved the way for establishing a method to evaluate the risk of coastal flooding due to sea level rise where the availability of high-resolution DEM as the foundation of the analysis plays an indispensable role in the operational workflow. The most commonly used method to evaluate the impact of SLR-induced inundation in coastal areas is the “bathtub” fill technique which solely takes into consideration the ascending of water level rather than the changes in ocean dynamics. As an elevation-based approach, the process is carried out in a GIS raster environment, with any cells in the DEM having an elevation value lower than the specified water level (e.g. projected sea level rise) are delineated as vulnerable to inundation (Elkabbany, 2019; Gallien et al., 2011; Gesch, 2009; Murdukhayeva, 2013; NOAA, 2012; Poulter and Halpin, 2008). Furthermore, these previous studies seek to communicate the risk to coastal communities via interactive maps which is a great utility for intelligent land-use planning, cost-benefit analysis of adaptation measures (Kulp and Strauss, 2019), and informed policymaking related to climate change, particularly sea level rise (Malik and Abdalla, 2016; Kuleli et al., 2009). In light of this, though scientific records have shown the successful application of readily available data, tools, and platforms (GIS, DEMs, etc.) in identifying, delineating, and mapping lands vulnerable to rising sea levels at a more localized scale, the attention given to utilize these by-products in estimating the associated cost of socio-economic damages is often limited.

With a coastline length of 46.6 km on the Adriatic Sea, the Slovenian coast is of extreme importance to the state because of its well-developed touristic infrastructure, cultural heritage, and

nature protected areas and also, it serves the country's only international cargo port, the Port of Koper which connects the Central and Eastern Europe and the Mediterranean. Furthermore, tourism as the most important activity in the coastal municipalities, especially in the city of Piran, contributes 12.3% to the total gross domestic product (GDP) of Slovenia and generates 110,700 jobs in 2018. Sitting snugly at the tip of its narrow peninsula, the old port town of Piran is best known as the "Slovenia's Seaside Paradise" (Burton, 2016) that is protected as a cultural and historical monument (Benčič, 2018). The authentic image of this well-preserved medieval town reflects the extremely diverse and rich architectural history of the Slovenian coast (Ložar, 2019) complemented by the Mediterranean ambience and various cultural attractions which give the town its heart and soul. The labyrinth of cobbled streets with closely constructed buildings (Deu, 2016) is characterized by lively market squares, ornamented fountains, monuments, museums, galleries and coastal cafes and restaurants. However, these Slovenian coastal regions are facing the ominous threats of repeated coastal flooding which is primarily governed by the tides and sea level changes. The flooded area is most extensive in the historic center of Piran due to its location in sensitive coastal landscapes (Vahter, 2006) and exposure to both high tides and strong southerly wind. It experiences an increase of high tide events with consequent flooding several times in a year, frequently during autumn and winter, and occasionally in spring, with large part of the old city center is under water. Given a 0.5 m rise in sea level, it has been roughly estimated that a normal high tide flooding will inundate 14 km² of the coastal municipalities which are 3% of the combined land surface areas of Koper, Izola and Piran (Kolega, 2006). Hence, these hazards and losses could be prevented or at least controlled by making out detailed mid- and long-term plans on coastal protection measures. Despite being regularly flooded during high tide events which inflicted damages to infrastructure and disrupted the economic activities and social system in the area, no studies considering the sea flooding problems in a holistic way are found concerning the exposure and vulnerability of Piran and its neighboring coastal municipalities to coastal flooding while the potential consequences of sea level rise on the location in terms of damage are not yet explored and elucidated.

Coupled with the interest of reducing the catastrophic impacts of rising sea levels and coastal flooding, a study on the estimation of flood damage according to the different sea level rise scenarios has become the subject of this research. Correspondingly, in response to the burgeoning necessity of better disaster preparedness and flood protection plans in the historic town of Piran, this study utilized the capabilities of GIS tools and LiDAR-derived DEM which are technologically available to users and managers to define the areas exposed to inundation and potentially endangered by sea level rise. This is particularly imperative as the existing studies and past flood events clearly show the critical vulnerability of Piran to coastal flooding and the adverse consequences of sea level rise to its population and economy in the next few decades. The assessed flood damage and generated inundation-related information along the coastal areas will assist actors at various levels of government (from municipal to state level) and stakeholders in robust decision-making processes and in developing the most appropriate site-specific flood protection measures as the baseline information. Furthermore, the results of this study could be used for cost-benefit analysis of the flood protection measures.

1.2 Objectives of the study

The primary objective of this research is to evaluate the impact of coastal flooding and the associated flood damage caused by rising sea levels in Piran, Slovenia. Moreover, the study was carried out with the intention to meet the following specific objectives:

- a. Determine the impact of sea level rise on the return period of extreme water levels;
- b. Generate detailed inundation maps for different sea level rise scenarios;

- c. Determine the extent of coastal floods in the location according to the different sea level rise scenarios;
- d. Assessment of the exposure of built-up structures and other socio-economic factors endangered by sea floods according to the different sea level rise scenarios;
- e. Estimate the flood damage cost inflicted to each sector present in the study area for different return period events;
- f. Generate damage – probability curves for different sea level rise scenarios based on the damage estimates of every return period events; and
- g. Calculate the expected annual flood damage of different sea level rise scenarios.

1.3 Research questions

In relation to the problem definition, this research shall address the following research questions:

- a. How will the future sea level rise change the recurrence interval of extreme water levels?
- b. How will the future sea level rise affect the extent and depth of coastal floods and its associated cost of damage in the city of Piran under present situation and the case of different assumed emission scenarios, namely RCP 2.6, 4.5 and 8.5?
- c. What part of the city is heavily flooded in case of extreme sea level rise scenarios?
- d. What land-use types and economic sectors are severely affected by coastal flooding due to sea level rise?
- e. What percentage of the current population would be directly affected by potential inundation?
- f. How will the future sea level rise affect the expected annual damage of coastal floods in Piran?

1.4 Scientific innovation and practical value

As the coastal flood risks are set to intensify in the future along with the socio-economic development in the coastal floodplain, a tremendous increase in flood damage is expected due to rising sea levels induced by climate change. Even though these challenges are basically relatively well known, studies concerning sea-level rise vulnerability assessment and flood risk mitigation in the peninsula of Piran are still minimal and require a deeper understanding. There is an urgency to expand sea level rise impact assessments as this coastal location becomes increasingly vulnerable to the effects of SLR-induced flooding. As an initial step in developing adaptation plans, this study defines the areas that are most likely inundated from sea level rise and the exposure of population, infrastructures, and assets to coastal floods which are the key components in flood risk assessment, spatial planning, and emergency services operation. Thus, the novelty of the present research lies in illuminating the impact of SLR on the occurrence probability of extreme sea level events on the Slovenian coast. The study also lays a contribution to scientific records on the successful application of GIS and LiDAR DEM in simulating and mapping the spatial distribution of coastal flooding with the potential effects of future sea-level rise and the associated cost of damage in the wider Gulf of Trieste area. It will also serve as a springboard for future researchers with underpinning information to incorporate more detailed information on the influence of storm surges, winds, and wave actions on sea-level rise scenarios as well as its extent and application to the neighboring coastal municipalities especially in the potential changes of the operability of port of Koper due to sea-level rise. Additionally, this study will present an important step towards practical methodology to estimate location-specific damage and derive the corresponding damage-probability curves for different sea level rise scenarios.

Estimates of future damages due to sea level rise and the adaptation costs are essential in supporting the efforts to reduce the consequences of climate change-driven sea level rise as well as in

designing strategies to adapt to increasing coastal flood risk. Considering the local nature of damages and adaptation, the generated flood damage-probability curves from this study play a pivotal role in the workflow of estimating the economic loss due to sea level rise and damage assessments of coastal impacts and adaptations. Integrating the use of damage-probability curves and expected annual damage of coastal floods provides valuable information on the risk profile of Piran that can be used to prioritize flood mitigation measures that can effectively cope with the potential impacts of sea level rise. Furthermore, as a decision-support tool aiding local governments, stakeholders, and other actors, this research provides a simplified means of predicting the extent of inundation during sea flood events for emergency action, planning site-specific flood protection measures, and identifying this hazard zone with special attention and utmost importance.

2 LITERATURE REVIEW

This chapter presents the overview of existing literature and studies on sea flood characteristics and the associated impacts of sea level rise as well as the methods developed for GIS-based assessments of sea level rise and coastal flooding exposure that have relevance to the present research study. The information provided from previous research shall serve as background and guide in the development of appropriate methodology to satisfy the research objectives of the study.

2.1 Climate change – driven sea level rise

The Intergovernmental Panel on Climate Change (IPCC) is the leading scientific and intergovernmental body under the umbrella of the United Nations that provides policymakers and the world with scientific information on human-induced climate change, its implications and potential impacts, as well as options for adaptation strategies. IPCC (2013) Fifth Assessment Report (AR5) gives a comprehensive assessment of sea level rise over the past few decades. As one of the major consequences of climate change, sea level rise has raised a widespread concern globally over the centuries and is therefore, attracted the attention of many climate scientists, researchers, and various actors in the policymaking body to study its projections, causes, impacts and the ways to adapt to this pressing phenomenon. The changes in sea level are strongly studied in the scientific arena as they play a crucial value for the development, management, and protection of coastal areas from environmental, social, and economic points of view (Marcos et al., 2012). They can be measured using tide gauges with more than 100 years of measurements which are recently supported by better spatial coverage of data from satellite laser altimetry. Increasing sea levels are generally driven by the warming of global mean temperature which in turn depends on the atmospheric greenhouse gas concentrations. Future sea-level rise scenarios should be projected based on different Representative Concentration Pathways (RCP) which encompasses a varied range of potential future greenhouse gas concentration trajectories (OECD, 2019).

The two dominant physical processes responsible for global mean sea level (GMSL) rise are ocean thermal expansion and glacier mass loss (without considering Antarctica and Greenland ice sheets) which accounts for about 30 to 55% and 15 to 35% of the projections, respectively. More than 90% of the heat trapped by greenhouse gas emissions between 1971 and 2010 are being absorbed by the ocean while the continuous shrinking and mass loss of glaciers could increase the sea level by as much as 16 cm by the end of the 21st century (Church et al., 2013). Table 1 presents the estimated increase in GMSL for different climate scenarios according to various authors. According to the IPCC Fifth Assessment Report (2013), GMSL has risen 19 cm over the period of 1901 to 2010. Whereas, a projected rise of between 26 and 82 cm in sea level is the range the IPCC considers likely (66% confidence) for 2081–2100 (relative to 1986–2005) from 18 to 59 cm in the 2007 IPCC report which is strongly dependent on the RCP emission scenarios. As stipulated in the report, process-based projections on GMSL rise in 2100 will likely be in the range of 0.44 m [0.28–0.61 m] if there is a drastic decline of greenhouse emissions from 2020 onward (RCP2.6), 0.53 m [0.36–0.71 m] when emissions stabilize by 2050 (RCP4.5), 0.55 m [0.38–0.73 m] for a scenario where emission starts declining after 2080 (RCP6.0), and 0.74 m [0.52–0.98 m] (RCP8.5) if the emissions continue to rise rapidly until 2100. However, the latest report of Oppenheimer et al. (2019) on ocean and cryosphere in a changing climate eloquently stated that GMSL is predicted to increase between 0.43 m (0.29–0.59 m) under RCP 2.6 and 0.84 m (0.61–1.10 m) under RCP 8.5 by 2100 which includes the contribution of Antarctic ice-sheet melting. Several researchers have fuelled discussions on the growing possibility of considerably higher future GMSL rise than suggested by IPCC AR5. They have explored the future contribution of Greenland and Antarctic ice sheets to sea level rise and figured out that GMSL is estimated to increase

up to 2 meters or even more by 2100 under high emission scenarios (Bamber et al., 2019; Jevrejeva et al., 2014; Kopp et al., 2014; Le Bars et al., 2017; Oppenheimer et al., 2019). According to the study of Kopp et al. (2014) on the sea-level projections for the 21st and 22nd century using probabilistic model, the mean global sea-level will rise within the very likely range (90% confidence) of 0.5–1.2 m by 2100 and 1.0–3.7 m by 2200 under RCP8.5 while with the effort to curb the emissions, for RCP2.6 it is lowered to 0.3–0.8 m by 2100 and 0.3–2.4 m by 2200. In addition, there is high confidence that GMSL is soaring at an accelerating rate of 3.2 mm·year⁻¹ over the period 1993–2015 to 3.6 mm·year⁻¹ over the period 2005–2015 as shown in Figure 1. On the other hand, the World Meteorological Office (2019) has recently published an article indicating that between 2014 and 2019, the rate of GMSL rise has amounted to 5 mm·year⁻¹ which is considerably faster than the average rate of 3.2 mm·year⁻¹ since 1993. Despite the large uncertainty of sea level rise projections beyond 2100, Horton et al. (2018) stressed out that the median estimates of GMSL rise by 2300 range from 1.0–2.0 m, 1.7–4.2 m, and 3.2–11.7 m under RCP2.6, 4.5 and 8.5 scenarios.

The probabilistic projections made by Jevrejeva et al. (2016) on global sea level rise disclosed that with a warming of 2°C, more than 90% of coastal areas will experience a sea level rise higher than the global estimate of 0.2 m by 2040 under RCP8.5 scenarios. If the global temperature continues to rise above 2°C after 2040, the rate of GMSL rise will surpass 10 mm·year⁻¹ by 2083. As a result, more than 80% of the coastlines in the world will surpass the median GMSL rise of 0.6 m. Further, a 5°C warming by 2100 will result in a rapid rise in sea level at a rate of 14 mm·year⁻¹ reaching 0.9 m and 80% of the coastline will exceed the 95th percentile upper limit of 1.8 m of the global sea level rise.

Table 1: Projected global mean sea level rise (m) by 2100 from different authors

Scenarios	AR5 (IPCC, 2013)	SROCC (IPCC, 2019)	Kopp et al. (2017)*
RCP2.6	0.44 (0.28–0.61)	0.43 (0.29–0.59)	0.56 (0.37–0.78)
RCP4.5	0.53 (0.36–0.71)	0.55 (0.39–0.72)	0.91 (0.66–1.25)
RCP6.0	0.55 (0.38–0.73)	-	-
RCP8.5	0.74 (0.52–0.98)	0.84 (0.61–1.10)	1.46 (1.09–2.09)

*2000 is the baseline year up to 2100

Sea level changes and variability in regional (~100 km) and local (~10 km) scales will significantly deviate from global mean values because of geological, oceanographic and meteorological influences. Local mean sea level trends at any coastal areas of interest are affected by global sea level fluctuations, regional and local factors (Mimura, 2013; Nicholls, 2002; Williams and Lück-Vogel, 2020) which is termed as the relative sea level (RSL) change (Aucan, 2018). Also, local responses to SLR are based on the RSL changes of a particular location which may be higher or lower than the global average due to several local changes in land subsidence, ocean currents, land height variations and other non-climatic drivers (Oppenheimer et al., 2019). From the perspective of a location-specific frame of reference relative to the land, RSL from tidal stations is considered to be more relevant for coastal protection along with the superimposed influences of tides, wave actions, and surges (Arns et al., 2017) as the risk is geographically variable. The ascent in RSL poses a risk to coastal communities, economy, and ecosystems by influencing the magnitude and frequency of coastal flooding.

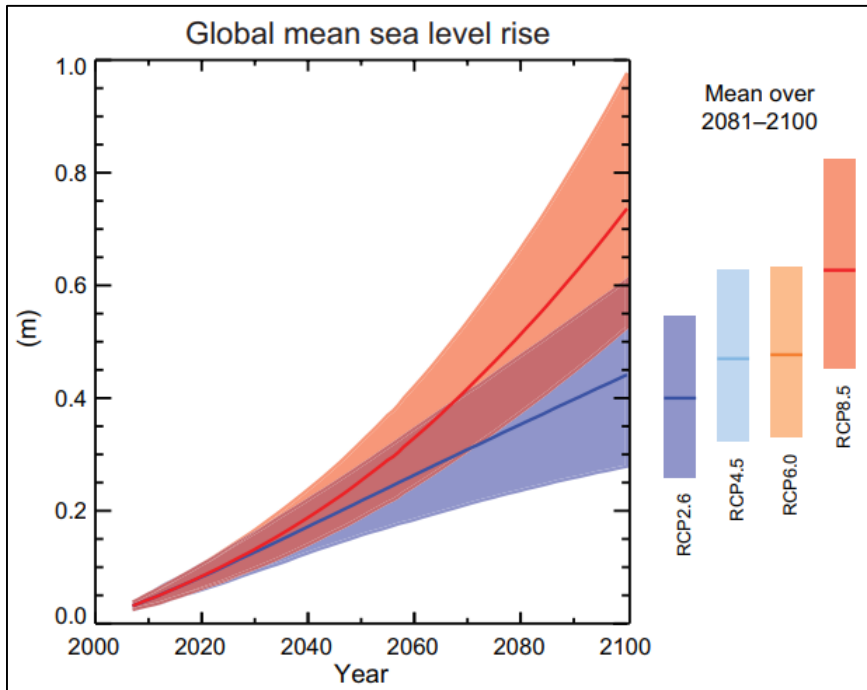


Figure 1: Global mean sea-level rise projections over the 21st century relative to 1986 – 2005 for the four RCP scenarios (Source: IPCC, 2013)

2.2 Characteristics of coastal flooding

Located at the interface between land and sea, coastal zones consist of natural and built environments which undergo dynamic changes due to anthropogenic-driven interactions of land and sea. Its attractive environment, favorable climatic conditions and economic opportunities are strong drivers fuelling urban development, population growth and socio-economic income from tourism, navigation (ports), trade centers and resource-based activities such as fisheries, aquaculture and agriculture (Scialabba, 1998). As reported by Griggs (2017), human history undoubtedly established a longstanding relationship with the coastal environments as it offers flat and fertile land with easy access to water which is ideal for agricultural production, settlements and other amenities. However, coasts are exposed to extreme weather events which are also exacerbated by climate change-driven sea level rise. The future impacts of accelerating sea level rise due to climate change have emerged as a defining societal concern that is seen to be widespread in coastal areas. Rising sea level inundates and threatens low-lying coastal zones through an array of coastal hazards including more severe and frequent coastal flooding, erosion, wetland or coastal ecosystem loss (change), saltwater intrusion, impeded drainage, and permanent submergence of land by higher mean sea level or high tides (OECD, 2019; Oppenheimer et al., 2019). Thus, in most coastal areas, sea level is rising faster relative to land because of the effects of winds, waves, ocean currents and non-climatic anthropogenic drivers which magnifies the exposure and vulnerability of the area to the upward trend of sea level. Additionally, the crucial factor that is often overlooked is the impact of local geological stresses, particularly for coastal areas located in the subduction zones, which can cause either an upward or downward movement of the land affecting the variability of relative sea level for decades (Kominz, 2013). The combined effects of earthquake-related land subsidence and absolute regional sea level rise have resulted to increased coastal flooding and sea incursions in the inhabited low-lying areas of Torres Islands in Australia. (Ballu et al., 2011). Thus, a minor shift in relative sea level can significantly impact the frequency of sea floods at any location along the coasts disrupting its physical processes, economic operations and social fabric. As studied by Oppenheimer et al. (2019), human-induced subsidence and change in wave height and period strongly

contribute to the future changes of RSL at the coast which implies the critical role of these local processes in projecting the impacts of sea level rise at local scales. They added that in the absence of adaptation efforts, the aforementioned risk related to increasing sea levels is expected to proliferate by the end of the century along with all the low-lying coastal settings.

Furthermore, scientific evidence indicates that sea level rise will also intensify storm surges (Dasgupta, 2009) as it extends the pathway of the storms upland (Tahvildari and Castrucci, 2021) by providing a higher “launch point” for the surge that can result in an abnormally greater inland extent of seawater intrusion (Neumann et al., 2015). As a result, it exacerbates the severity of coastal and inland flooding by magnifying the extent and depth of inundation in areas already vulnerable to coastal storms and consequently, the accompanying flood damage. Nevertheless, recent studies have recognized that as sea level increases, it no longer takes a hurricane or strong storm to cause flooding in most coastal cities around the globe (Jacobs et al., 2018; Moftakhar et al., 2017; NOAA National Centers for Environmental Information, 2018; Sweet et al., 2014). Nowadays, flooding occurs more often at fairly normal high tides in many seaside locations without the interference of low atmospheric pressures and rains. The National Oceanic and Atmospheric Administration (NOAA) officially termed this phenomenon as ‘nuisance flooding’ or high tide flooding (NOAA National Centers for Environmental Information, 2018; Sweet et al., 2014) which is primarily governed by the RSL change. The visible manifestation of local mean sea level rise can be understood in the reduction of the gap between the mean sea level (MSL) and flood threshold point (Sweet et al., 2013) which amplifies the frequency of tidal-induced nuisance flooding. The latest report from NOAA (2018) revealed that nuisance flooding nowadays is growing more common along the U.S. coastlines which are 60% higher compared to the typical flooding about 20 years ago and 100% higher than 30 years ago, particularly in the city of Boston with 19 days of flooding, a more than 200% growth from 2000. Although this phenomenon is categorized as not catastrophic in nature (Ray and Foster, 2016), it is indeed capable of causing significant socio-economic damages to the affected area (Moftakhar et al., 2015) and thus, provides an early localized indication of community-specific impacts and areas that will eventually be affected by a more severe major flooding. This perennial sea flooding disrupts routine activities and economic operations in the location leading to loss of income; decreases the service and real-estate values of various infrastructures; interrupts the flow of daily traffic by making the roads inaccessible; discourages tourism; overwhelms the capacity of the sewer system causing it to become ineffective; and causes property damage including the contents, facilities and structures. Aside from those tangible impacts, the recurrent high-tide flooding also poses risk to public health (including psychological stress) and safety because flood water could sweep cars and people that may increase human injuries and fatalities; it threatens water quality due to contamination from drainage problems whereas ponded water serves as the breeding ground of disease-carrying mosquitoes and bacteria (Moftakhar et al., 2018; NOAA National Centers for Environmental Information, 2018). A study by Moftakhar et al. (2017) revealed that even though it is not catastrophic at the time, this type of flooding happens multiple times in a month or year leaving the hotspot areas to experience greater cumulative exposure of assets compared to infrequent extreme flooding events and thus, presented it as a cumulative hazard. They articulately added that over time, in places where such floods occur more frequently, the accumulated costs of impacts are comparable to devastating events. It represents a considerable economic burden for communities and local governments as they will be forced to expend resources for maintenance cost of infrastructures, for necessitating occasional clean-up (pumping water out of the streets) and for financial assistance to the affected inhabitants. This highlights the fact that due to the ongoing sea level rise, the substantive impacts from coastal flooding of higher frequency and duration will regularly occur and when concurrent with localized rainfall or storm surge, the effects could become disastrous leading to extremely high-cost economic consequences.

The global assessment conducted by Hinkel et al. (2014) on the costs of flood damage and the associated adaptation measures under 21st century sea level rise revealed that with constant protection (without adaptation) of the coasts, 0.2 to 2.9% of the global population will experience an annual flooding in 2100 for RCP2.6 and 0.5 to 4.6% for RCP8.5 under a GMSL rise ranging from 25 to 123 cm. For the same scenario, flood damage costs grow significantly equal to the magnitude of the flooded population throughout the century with an estimated annual loss of 0.3 to 5.0% of the global GDP under RCP2.6 and 1.2 to 9.3% under RCP8.5. This degree of impact caused by rising sea levels is very unlikely to be accepted by society. Hence, the continuous development of the socio-economic conditions in the coastal areas will attract more people and value of assets towards the zone which consequently pushed every country to plan and implement adaptation strategies. Considering the common approach of protection, the cost of constructing and maintaining a dike in 2100 requires a yearly investment of US\$ 12 to 71 billion which is much smaller compared to the cost of avoided direct damages. It was shown in this study that protection measures reduce the affected population by about 2 orders of magnitude while the annual GDP losses are lowered by approximately 2 to 3 orders of magnitude. Moreover, the study of Jevrejeva et al. (2018) estimated an economic loss of US\$ 10.2 trillion per year accounting for 1.8% of the global GDP by 2100 due to a sea level rise of 0.52 m under a 1.5°C of warming and US\$ 11.7 trillion per year (2.0% of global GDP) for a rise of 0.63 m from a 2°C of warming, if no additional adaptation is undertaken. In case that the target temperature of 2°C is missed and the warming continues to follow the RCP8.5 scenario, the global annual flood costs without further adaptation will escalate rapidly to US\$ 14.3 trillion (2.5% of global GDP) for 0.86 m of sea level and US\$ 27.0 trillion (4.7% of global GDP) under the 95th percentile sea level rise of 1.8 m. Furthermore, the recent study of Kirezci et al. (2020) confirmed that in 2100, the increase in the inundated area, affected population and threatened assets is projected to be 48%, 52% and 46%, respectively under the RCP8.5 scenario. The results indicate that a flooding extent of 661,000–1,009,000 km² due to sea level rise will endanger 176–287 million people worldwide in 2100 from 128–171 million people affected by the current 100-year return period extreme sea level. Meanwhile, the cost of damage to valuable assets escalates from US\$ 6.5–9.1 trillion to US\$ 8.8–14.2 trillion. These key figures underline the unprecedented growth in damages caused by rising sea levels and the importance of adaptation measures in reducing flood losses and increasing the resilience of coastal societies. In response to the urgency of the need to adapt to the amplifying coastal flood risk, mapping the areas exposed to potential inundation amalgamated with long-term sea level rise plays a pivotal role in developing and implementing an adaptation framework.

2.3 Coastal inundation mapping imposed with SLR using GIS tools and LiDAR-DEM data

In an era of rising sea levels, the number and frequency of flooding events occurring in the coastal communities provide the latest scientific consensus of mapping the specific areas at risk of flooding from sea level rise and assessing its potential impacts on the socio-economic condition of the area and the coastal ecosystem. As a vital component of responding to the rising seas, the generated maps offer valuable information to local authorities in increasing public awareness about the hazard, improving emergency response, and planning for coastal adaptation strategies (Mullin and French, 2016; Webster et al., 2006). The concept of mapping sea level rise based on emission scenarios predicated from IPCC is drawing much attention in the scientific arena. Hence, the application of GIS in integrating coastal hazards and sea level rise has been extensively used as a tool for understanding, modelling, visualizing and predicting their accompanying inundation impacts (Chang et al., 2013; Gallien et al., 2011; Li et al., 2009; Lichter and Felsenstein, 2012; Malik and Abdalla, 2016; Marcy et al., 2011; Williams and Lück-Vogel, 2020).

2.3.1 Bathtub inundation model

One of the most widely used GIS-based techniques to simulate sea level rise inundation is the single-value water surface model, popularly known as Bathtub (NOAA, 2012), equilibrium (Gallien et al., 2011), or static inundation (Breilh et al., 2013) model which only requires high-resolution and accurate topographic data in the form of DEM as the primary input. A bathtub modelling approach considers any area below the user-specified water level (e.g. projected SLR) as being flooded (Elkabbany, 2019; Gallien et al., 2011; Gesch, 2009; Murdukhayeva, 2013; NOAA, 2012; Poulter and Halpin, 2008). Moreover, as it is integrated with elevation data, the quality and resolution of DEM have a significant effect on the accuracy of the inundation model and assessment results (Gallien et al., 2011; Gesch, 2018; Paprotny and Terefenko, 2017; Prahl et al., 2018; Schmid et al., 2014) where in this context, several researchers have proven the use of Light Detection and Ranging (LiDAR) DEM because of its high vertical accuracy and better spatial resolution (Gesch, 2009; Webster et al., 2006). The advantage of using this GIS-based sea level rise mapping tool is its simple, inexpensive and straightforward model construction which attracts many organizations, researchers and individuals to produce an interactive graphical display of the inundated areas and provide analysis of vulnerability at local, regional and global scales. On one hand, the drawbacks of this method limit its functionality because it does not consider the dynamic processes of coastal inundation, hydrological connectivity of adjacent flooded cells to the ocean, existing built protection structures, land movement, storm surges and other local factors that may have an influence on the model (Doyle et al., 2015; Siebentritt, 2016; Williams and Lück-Vogel, 2020). An improvement to this method necessitates spatial continuity between the ocean and flooded areas for them to be defined. Consequently, several attempts have been made to improve and modify the simple bathtub model that accounts for more than just static elevation and integrate the additional information such as drainage infrastructures, dikes, groundwater levels, wave height, storm surge and among others to enhance the accuracy of model predictions (NOAA, 2012; Poulter and Halpin, 2008). Nonetheless, there are still many GIS-based studies involving the use of various sources of DEMs that have been successfully applied the simple bathtub inundation model in sea level rise mapping methodology.

The Government of Australia is actively involved in providing sea level rise mapping information to their coastal urban areas using the RCP scenarios from IPCC Fifth Assessment Report. The two main sources of these products can be accessed online for free, namely; OzCoasts (<https://coastadapt.com.au/sea-level-rise-information-all-australian-coastal-councils>) which uses a simple bathtub fill technique to map the sea level rises of 0.5 m, 0.8 m, and 1.1 m combined with tidal data; and Coastal Risk Australia (<https://www.coastalrisk.com.au/home>) which was developed using a high-resolution LiDAR DEM and bathtub inundation model to investigate the extent of coastal flooding as a result from sea level rise, tidal heights and seasonal storm surge (Siebentritt, 2016). While, the Sea Level Rise viewer (<https://coast.noaa.gov/sl/>) established by NOAA Office for Coastal Management employs a modified bathtub approach that incorporates hydrologic connectivity and regional and local tidal variability to map the future inundation along the U.S. coasts from a plausible projection of sea level rise. This digital map viewer provides the following information: the extent of inundation for a sea level rise of 0.3 to 1.8 m at 0.3 m intervals; frequency of and depiction of areas exposed to high tide flooding; simulation and impacts of sea level rise at local or community level; marsh migration due to the different upward trend of relative sea level; spatial uncertainty of mapped sea levels; and social vulnerability index. The underlying digital elevation model used to generate the inundation maps in this tool was sourced out from LiDAR which does not incorporate a comprehensive analysis of pipe network or engineering grade hydrologic analysis and also, future changes in geomorphology and coastline, erosion and land subsidence were not taken into account yet during the development of the maps (NOAA Office for Coastal Management, 2017).

Gallien, Schubert and Sanders (2011) critically examined the performance of equilibrium and hydraulic flood mapping methods in predicting the tidal flooding in an urban embayment using a LiDAR digital terrain model. A total of ten scenarios were considered in their study to investigate the predictive skill of the models and their uncertainties accounting for the effects of ocean heights, floodwall heights, modelling approach and topography. They found out that scenarios using the bathtub approach (scenarios 1 and 2) show an overestimation of flooded areas with an overprediction fit measure value of 0.91 (value of 0 means no overprediction). Whereas, all scenarios that use the hydraulic modelling method (scenarios 3 to 10) yields a more accurate flood prediction performance compared to the first two scenarios but interestingly, scenarios 5 and 6 which incorporate the influence of tidal level and narrow flood wall height from RTK survey data have the highest accuracy performance among all scenarios. This highlights the importance of integrating protective barriers in the inundation model. Henceforth, the sensitivity of flood extent to barrier heights and bay water level implies that the equilibrium flood mapping tool is suitable for undefended terrain because it neither accounts for hydraulic connectivity or flow barriers.

The inundation impact assessment conducted by Chang, Guan and Aral (2013) with the manifestation of space-varying future sea level change in Florida (USA), projected by a dynamic system model (DSM) uses a bathtub modelling approach to determine the severity and extent of inundation in the study area. Based on model predictions, an augment of 1.94°C and 0.55°C in mean sea surface temperature in the Gulf of Mexico and the Atlantic Ocean will trigger a sea level rise of 51 cm and 48 cm, respectively. Under these SLR projections, 5.2% (approximately 7770 square kilometers) of Florida will be inundated by 2100 of which the inundation rate starts accelerating from 2040 and will be decelerating after 2060. Additionally, they also figured out that the lower accuracy of elevation data underestimated the magnitude of inundation and recommended the use of LiDAR. On the contrary, the investigation of Breilh et al. (2013) revealed that the bathtub model can predict well the flooding in small marshes and large marshes drained by an estuary located no more than 3 km from the coastline and landward boundary of the marsh. In the case of large marshes without estuaries or with an estuary that is characterized by a long distance between the coastline and landward boundary of the marsh, the model is found to overpredict the extent of flooding significantly. From this study, it appears that the bathtub model can perform nearly the same as complex models under certain site-specific conditions, e.g., a morphological parameter of marshes.

Williams and Lück-Vogel (2020) modified the simple GIS-based bathtub model by taking into consideration the hydrological connectivity, surface roughness and beach slope using LiDAR digital surface model (DSM) to determine the storm-related coastal inundation imposed with sea level rise. In order to evaluate the model results, the output from the enhanced model was compared to the traditional bathtub model and historical flood data. Accordingly, imposing a sea level rise of 0.38 m and 0.82 m based on the projections made by IPPC (2013) to the baseline scenario amplifies the extent of inundation for both models. The conventional bathtub model exceeds the inundated areas of the improved model by 12% for the baseline scenario and increases to 25% and 30% when the sea level swells to 0.38 m and 0.82 m, respectively. This overestimation in flooded areas could be attributed to the inclusion of low-lying parts of the coasts that are not hydrologically connected to the sea and thus, dependent on the local condition of the coasts. Meanwhile, model validation revealed that the simulated flood lines of the modified method coincide closely with the 2008 storm-induced flood event while the simple bathtub fill technique consistently overestimated the flood extent. The authors concluded that even though the enhanced bathtub model produced more reliable results than the classical bathtub model, the latter still has qualities for application on low-energy coasts.

Li et al. (2009) developed a comprehensive GIS-based model to analyze and visualize the global extent of future inundation due to sea level rise and its impact on land-cover and population by addressing two shortcomings of a simple bathtub inundation model: (1) the water connectivity of

delineated potentially inundated areas (PIAs) to the ocean (2) the exclusion of existing inland water bodies as part of PIAs. Hydrological connectivity is defined based on the eight-side rule of connectivity while the incorporation of inland water bodies in the delineation process uses an iterative, custom algorithm. On one hand, this study did not account for the effect of sea level rise on high water levels and the influence of existing flood protection structures. Similar to other studies, Li et al. (2009) also found out that the classic bathtub modelling approach that does not consider the hydrological connectivity and existing inland water bodies overestimates the extent of PIAs by 86.4% and 50.6% for a sea level rise of 1 m and 6 m, respectively compared to their methods. The results of their analysis showed that 1.055 million km² of land will be under water for a 1-m rise in sea level which escalates to 2.193 million km² when the water level reaches up to 6 m. Respectively, the submersion of land exposes 107.9 (2% of the world's population) to 431.4 (7% of the world's population) million people to the risk of potential inundation of which most of them comes from less developed countries, suggesting a growing demand for humanitarian needs in the future. More than 60% of the land-cover types in the PIAs are forest and grassland for all sea level rise increments. However, there is a steady increase in the percentage of cropland that will be lost due to the swelling of sea level which is alarming as most of the developing countries are dependent on this respect. Whereas, the decreasing trend of percentage lost for forest may imply the existence of natural vegetation in the buffer zone of few meters above the coastline and cropland is inundated once this zone is exceeded. Although, economic impacts were not part of their analysis, Li et al. (2009) included additional features that are intended to promote educational awareness of the future impact of rising sea levels on the natural and built-up environments among the non-specialist community by making it more informative and understandable to K-12 students, teachers, the general public, and policymakers.

2.3.2 Role of LiDAR-DEM in sea-level rise inundation mapping

The prevalent effect of rising sea levels along the world's coastline is manifested in the underlying dynamics of coastal landscapes over time of which due to its low-lying nature, the topography is the principal driver that determines their exposure to the adverse consequences of increased water levels (Gesch, 2018). Therefore, a detailed, accurate and up-to-date representation of coastal topography, most often in the form of a digital elevation model, is necessary to model the inundation in coastal environments and the potential effects of future sea-level rise (Gesch, 2009). The application of DEM in SLR-induced inundation mapping and vulnerability assessment has become a standard practice in the global arena (Cooper et al., 2013). As the primary variable for sea-level rise inundation mapping, it is important that the quality of DEM must be optimized to the greatest resolution as possible (Casas et al., 2006) because its accuracy and resolution greatly influence the reliability and accuracy of results and model outputs (Cooper et al., 2013; Gesch, 2009). Elevation-based mapping of sea-level rise remains a challenge because the augment in sea level every year is about an order of magnitude smaller than the vertical error of most DEMs available nowadays (Gesch, 2009; Poulter and Halpin, 2008; Rowley et al., 2007). The studies of Gesch et al. (2007) and Hinkel et al. (2014) have concluded that DEM with higher resolution and vertical accuracy significantly improve the results of sea-level rise impact assessment. In response to the increasing demand for high-resolution DEM for SLR-related assessments, the use of state-of-the-art LiDAR technology in producing a highly detailed and more accurate representation of coastal topography has received considerable attention from scientific communities and government agencies. LiDAR-derived DEM is well suited for identifying the potential inundation of coastal lands from rising seas and for detailed assessments of its associated social, economic and ecological impacts (Gesch, 2009; Zhang, 2011). The DEMs built from LiDAR have a higher horizontal resolution (e.g. 1 m) and lower vertical error (RMSE at the scale of centimeters) with elevation values quantized in centimeters (Gesch, 2009; 2018). These improvements in data quality

offer a strong advantage for LiDAR DEM in SLR-induced inundation modelling to generate more accurate maps and detailed evaluation of its impacts that will aid adaptation decisions (Cooper et al., 2012; Zhang, 2011).

Gesch (2009) analyzed the role of LiDAR elevation data in the improvements of delineating and mapping the coastal lands vulnerable to sea-level rise by comparing it to the available nationwide contour-based National Elevation Dataset (NED) DEM with approximately 30 m of horizontal resolution and also to the most widely used global DEMs in SLR studies such as GTOPO30 from the U.S. Geological Survey (USGS) with about 1 km of horizontal resolution and a 90-m resolution Shuttle Radar Topographic Mission (SRTM). Gesch (2009) employed a bathtub modelling approach to map the potential inundation zones which are hydrologically connected to the source of flooding. Coarser global elevation datasets from GTOPO30 and SRTM produce very large and uncertain inundation areas due to their high vertical error defined with the RSME values of 3.83 m and 3.13 m, respectively. Even the use of NED 30-m DEM becomes a challenge if the goal is to generate inundation zones from a 1 m sea level rise or lower increment because it has a vertical accuracy of 1.27 m. In this way, Gesch (2009) concluded that the performance of coarser DEM in generating detailed inundation maps is severely constrained by their low vertical accuracy and integer meter quantization of elevation values. Favorably, the 3 m - LiDAR DEM with an RMSE value of 0.14 m delivers a substantial improvement in delineating vulnerable lands compared to the former elevation datasets used in global and regional sea-level rise analysis. LiDAR-derived maps provide more detailed information of inundated areas where the end-user can be certain of the accurate delineation of sea flooding from a 1 m rise in water level.

The investigation of Zhang (2011) on the effect of vertical resolution of DEMs on the extent of inundation revealed that the vertical accuracy of a DEM has more influence on defining the inundated areas than its horizontal resolution which was executed by comparing a LiDAR DEM with USGS DEM of the same 30-m horizontal resolution. The presence of low and high topographic features in the 30-m LIDAR DEM has resulted in a dramatic difference of 9.90% to 29.45% in the area of inundation of the two DEMs for a 1 m increase in sea level. Correspondingly, the over-prediction of inundated areas is in favor of the 30-m USGS DEM implying its inherent lower elevation accuracy. Zhang (2011) has extended its comparison between a 5-m and 30-m LiDAR DEMs to examine the effect of horizontal resolution on the delineation of inundated areas and found out that the latter is only appropriate for estimating the accumulated numbers for inundation areas at the county level and a finer horizontal resolution (5 m) is required in determining the individual properties vulnerable to rising sea levels.

Poulter and Halpin (2008) developed three approaches to simulate coastal flooding from sea level rise which ranges from a simple bathtub fill technique to enforcing the hydrological connectivity of inundating lands using a four- and eight-side connectivity rule. They used 6-m and 15-m resolution LiDAR DEMs to examine the effects of horizontal resolution and hydrological connectivity modelling approach on the extent and timing of potential inundation due to a rising sea level of 0.3 m to 1.1 m. Regardless of the connectivity rule, the extent of possible inundation modelled with a 15-m DEM is larger than the predictions of a 6-m DEM for all scenarios, of which the difference between their areas of inundation is greatest at low increments of sea-level rise (<0.3 m) and decreases at higher values (>0.8 m). Whereas, specifying the hydrological connectivity to the model reduces the inundation estimates for both DEMs relative to the simple bathtub method. As expected, the inundated area using an 8-side rule is greater than the 4-side rule which could be attributed to the increased number of connections between adjacent cells. For a 0.3 m increase in sea level, the inundated areas of 1,112 km² and 1,178 km² generated from a 6-m DEM is much lower than 1,578 km² and 1,868 km² for a 15-m DEM when 4-side and 8-side connectivity was defined, respectively. This large difference in the area of inundation indicates a strong interaction between the rules for hydrological connectivity and DEM horizontal resolution most critically at lower projections of sea level rise.

2.4 Flood damage estimation

Generally, floods of any type bring a wide array of negative consequences and harmful effects to the economy, environment, ecological systems, human health and social fabric as well as damages to various infrastructures, cultural heritage, agriculture, and industrial production. Damages due to floods are usually categorized into direct and indirect damages and further classified into tangible and intangible losses depending on whether these losses can be assessed in monetary terms. Direct flood damages include all varieties of losses that are in direct physical contact with flood water while indirect damages occur primarily because of the disruption of physical and economic linkages induced by the direct impact of flood exposure (Messner et al., 2007). Figure 2 presents the typology of flood damages with examples.

Flood damage estimation is an indispensable task in flood risk assessments (Win et al., 2017) and water resources planning, particularly in evaluating the flood mitigation benefits. The probable damage information will support funding agencies to decide the prioritization of projects by comparing the reductions of flood damage and estimated costs of the project in cost-benefit analysis (USACE, 2013). Moreover, in consonance with the report of the Bureau of Transport and Regional Economics (2002) in Australia, the estimates of flood damages have influenced the decisions of the government regarding the emergency relief aid, land-use planning and research priorities while Middelmann-Fernandes (2010) articulately mentioned that obtaining flood loss data is a challenge shared globally. Similarly, the two basic approaches used to conduct a flood damage estimation are (1) property-by-property assessment of potential damage; and (2) the use of depth-damage functions (Karamouz et al., 2016; Win et al., 2017). As discussed by Dutta et al. (2003), establishing a suitable flood loss estimation model is linked with many issues due to the characteristics of flood damages such as obtaining detailed flood parameters at any specific location, appropriate classification of damage categories and the relationship between the flood parameters and associated damages.

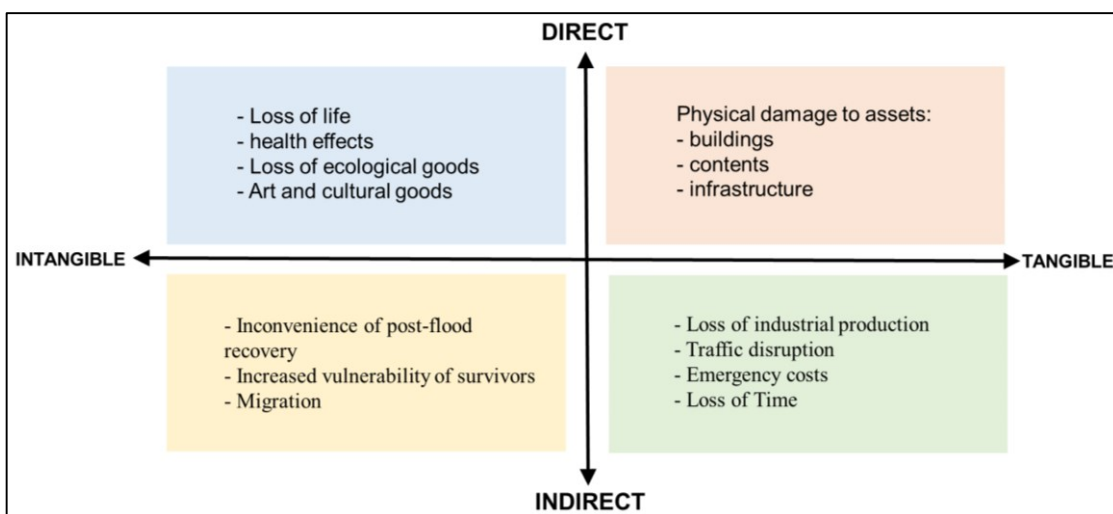


Figure 2: Classification of flood damages adapted from Penning-Rowsell et al. 2003; Smith and Ward 1998 as cited in Messer et al. (2007)

An internationally accepted standard method of damage estimation is the use of depth-damage curves, also known as, stage-damage curves which describe the mathematical relationship between flood depth and the degree of possible economic damage attributed to that water level. Depth-damage functions can be developed in two ways depending on the kind and source of information used: (1) empirical approach which uses damage data from historical flood events in a given location and

therefore represents actual losses from that event (Dutta et al., 2003; Merz et al., 2010; Pistrika et al., 2014); and (2) synthetic approach which collects theoretical data on damages via expert knowledge through “what-if-analysis” (Gerl et al., 2016) and hypothetical estimation based on land use/land cover patterns and object types related to a specific building component (Dutta et al., 2003; Merz et al., 2010; Pistrika et al., 2014). A solid argument is in favor of empirical models because real flood damage information is more accurate than the subjective “what-if” analysis employed in synthetic models (Pistrika et al., 2014). However, Smith, 1994 stressed out that conducting comprehensive damage surveys in the aftermath of any flood events requires much time and effort per unit area while Messner et al. (2007) found biases in the results of using this method in the UK by overestimating the damage to building contents because of trying to incorporate as much actual flood damage data as possible into a database which leads to the underestimation of long term effects on the building fabrics. Moreover, another weakness of empirically-based damage models is the low transferability of functions to other study areas because of the significant errors in temporal and spatial translation due to differences in several flood characteristics, building types, contents and warning time (Merz et al., 2004; Smith, 1994). In contrast, synthetic models have a higher level of standardization of damage functions which are highly suitable for both temporal and spatial transferability that can be applied to any area under investigation (Merz et al., 2010; Smith, 1994). Also, due to the relative scarcity of actual flood damage data, synthetic depth-damage curves are most commonly used. Messner et al. (2007) eloquently stated that the term “synthetic” doesn’t mean arbitrary or artificial but rather it refers to the approach of synthesizing existing data from various secondary sources and actual experience of floods. Referring to the study of McBean et al. (1986 as cited in Middelmann-Fernandes, 2010), the combination of empirical and synthetic depth-damage curves could produce more accurate results of damage assessment by calibrating the latter with the observed flood damage information. Aside from distinguishing the depth-damage functions into empirical and synthetic, they can further be defined either as absolute or relative damage functions. Absolute flood damage estimation is also called the unit area approach which looks at individual properties (Messner et al., 2007) and estimates the damage in monetary amounts per unit area of the element at risk which necessitate regular re-calibration of the damage functions (Gerl et al., 2016; Messner et al., 2007; Olesen et al., 2017; Pistrika et al., 2014). In the UK, this technique is found appropriate for commercial, retail and industrial properties where size is a critical determinant of potential flood damage (Messner et al., 2007). Whilst, relative damage functions express the estimated flood losses as a percentage of the total asset value of a flood-affected property (Gerl et al., 2016; Messner et al., 2007; Pistrika et al., 2014). One of the strengths of this approach is its simplicity because of the multitude of available data sources on the value of properties in flood risk zones which is the most commonly used approach across the European countries (Messner et al., 2007). Several flood damage models have already existed to estimate the losses incurred by floods in different countries. A typical examples of an empirically derived flood damage model are the German HOWAS-database and Flood Loss Estimation MOdel (FLEMO) while sets of synthetically generated damage functions are published in the Multi-Coloured Manual (MCM) in the UK (Messner et al., 2007) and Damage Scanner in the Netherlands while USACE combines both approaches to derive a depth-damage function (Merz et al., 2010). Relative damage functions are widely used in the HAZUS-MH model of USA, Rhine Atlas, Hydrotec and FLEMO of Germany and the Standard Method and Damage Scanner of the Netherlands whereas absolute damage functions are applied in the UK and Australia (Merz et al., 2010). The European Joint Research Centre (JRC) developed a comprehensive global database of depth-damage functions for 214 countries based on historical flood data and an extensive literature survey that converts depth of floods into direct economic damage for different categories, namely residential buildings, commercial, industry, transport, infrastructure and agriculture (Huizinga et al., 2017). Although, other existing parameters such as flood velocity, duration, sediment loads and others have an influence on the occurrence of damage, water depth is still widely used as the main determinant and decisive parameter

to quantify losses due to floods (Büchele et al., 2006; Pistrika et al., 2014) of which various depth-damage curves showing this relationship have been developed. Depth-damage relationships assume that a certain height of water level and its relation to a structure height determines the expected value of damage to buildings such that when similar structures or buildings are exposed to the same flood depths, it can be assumed that they experience damages of similar magnitude or proportion as the actual values (Davis and Skaggs, 1992). The following paragraphs briefly discussed some of the flood loss models that have existed and successfully applied in different countries.

The Multi-Coloured Manual of the UK was developed mainly to estimate the flood damage in economic sectors at micro- and meso-scale levels (Penning-Rowse et al., 2005) for water management policy and quantitative evaluation of investment decisions (Penning-Rowse et al., 2010). It evaluates the damages using absolute depth-damage curves which are derived mostly based on synthetic analysis and expert judgment. It uses water depth as the main parameter to define the potential damage in British Pounds for residential, commercial and industrial buildings. Since it is an object-based model, the estimated maximum damage per square meter describes the expected cost of repair to a specific building and not the damage of the surrounding land (Jongman et al., 2012). On one hand, it describes the indirect damage calculation as a difficult task and does not provide a general approach for such assessment (Penning-Rowse et al., 2010).

The family of FLEMO models has been used in Germany for scientific flood risk analyses ranging from local to national levels. It comprises of two individual models: (a) FLEMO for the private (FLEMOps) which is primarily developed to estimate the direct tangible damage in residential buildings and household contents (Thieken et al., 2008); (b) FLEMO for the commercial sector (FLEMocs) which estimates direct monetary losses of buildings, equipment, goods, and products of companies (Kreibich et al., 2010). These models are derived empirically using historical flood damage data from 2002, 2005 and 2006 in the Elbe and Danube catchments which were validated at micro- and meso-scale levels (Jongman et al., 2012). FLEMOps uses water level, building type, building quality, contamination, and precaution as the determining factors of flood damage (Thieken et al., 2008). On the other hand, FLEMocs adapts the model structure of FLEMOps but considers water depth, contamination, precaution, size of the company (number of employees) and different economic sectors as the influencing factors in estimating the losses (Kreibich et al., 2010).

The Damage Scanner model (DSM) is the simplification of HIS-SSM model, the most comprehensive flood damage model in the Netherlands. The latter is widely used by the Dutch government agencies in estimating the potential direct and indirect flood damage on a regional and national scale but due to the unavailability of highly detailed data on individual buildings, industries and infrastructures, the DSM was developed (Kok et al., 2005). The direct physical damages in DSM are calculated based on a series of stage-damage curves for 13 different types of aggregated land use instead of individual units (Jongman et al., 2012; Messner et al., 2007). The curves employed in this model were primarily obtained using synthetic data with inundation depth as the decisive parameter of flood loss where the estimated maximum damage reflects the reconstruction values of buildings, replacement values of contents and market values of agricultural products (Jongman et al., 2012).

HAZUS Multi-Hazard (HAZUS-MH) software and HEC Flood Damage Reduction Analysis (HEC-FDA) program are developed by FEMA (FEMA, 2020) and USACE Hydrologic Engineering Center, respectively for damage assessments in the United States. HAZUS-MH estimates the potential damages of floods, earthquakes, and hurricane winds on buildings, facilities, infrastructures, utilities, vehicles and agriculture to be used by federal, state, regional and local governments and private sectors for planning risk management and emergency operation. The model combines empirical and synthetic approaches by testing it against experts' judgment and historical records of the mentioned natural hazards. HAZUS-MH has a distinct feature of accommodating additional data and methods which allows localities to refine the loss estimates for localized emergency planning and evaluate the effects

of hazard mitigation measures. The HAZUS Flood model uses a comprehensive inventory of general building blocks, essential facilities, transportations and lifeline systems, population data, vehicles and agriculture. It comes with a suite of damage curves from the Federal Insurance Administration on the basis of 20 years of empirical damage data, and USACE for specific regions in the US using flooding depth as the governing parameter but also takes into account velocity, lead time, timing and water quality (FEMA, 2020). On the other side, HEC-FDA offers the capability to implement integrated hydrologic engineering and economic analysis to assist USACE members in evaluating any flood damage reduction strategies (CEIWR-HEC, 2016). Based on the hydrologic and hydraulic information of the study area, the model can calculate the expected annual damage by considering depth as the assessment index (Mohammadi et al., 2014).

The ANUFLOOD suite of depth-damage curves in Australia is the most prevalently used absolute model in flood damage assessment which uses an empirical approach (Merz et al., 2010; Nafari, 2018; Olesen et al., 2017) based on the damage data from the 1986 flood event in Sydney. It calculates the accumulated value of damage including structural and content losses from stage-damage functions which are classified according to the size of the property and vulnerability of business contents (Nafari, 2018). However, the use of the depth-damage curves is only appropriate when the velocity of water is less than 1 meter per second (Middelmann-Fernandes, 2010) which is supported by the New Zealand Institute of Economic Research (2004) because with faster flowing water, the building is likely to suffer structural failures. Hence, this model also employs a synthetic approach for residential and commercial properties and estimated the indirect damage as 15% and 55% of the direct residential commercial damage, respectively (Gissing and Blong, 2004). Furthermore, the wide array of flood damage estimation models from country to country underline the importance of damage assessment in the context of decision-making for holistic flood risk management.

Although considerable studies have been devoted to the investigation of the impact of future sea level rise on the world's coastal and deltaic cities using both static and hydrodynamic inundation models, their application is confined to hazard zone delineation, exposure and vulnerability assessment while only limited research has focused on the estimation of its associated economic damages at more localized scale. Furthermore, despite the flooding situation in the city of Piran as discussed in Section 3.1, the attention given to study its exposure and vulnerability is often limited and the potential consequences of sea level rise at the local scale in terms of damage are not yet explored and elucidated. In light of the scientific evidence presented above concerning the accelerating pace of sea level rise and the increasing frequency of high tide and coastal flooding, it is therefore advantageous to utilize the capabilities of the GIS-based approach and the high-resolution LiDAR-DEM in generating SLR-induced inundation and estimating the exposure of land, population, assets, and the concomitant annual flood damage caused by a range of sea level rise in the city of Piran.

3 CASE STUDY AREA

Slovenia has an entire coastline length of 46.6 km spanning along the Gulf of Trieste, the northernmost part of the Adriatic Sea which is bordered by four major coastal municipalities, namely Ankaran, Koper, Izola and Piran (Mezek and Bricelj, 2002; UNEP/MAP, 2018). The interface of land and sea is highly varied, consisting of steep cliffs and gentle slopes of land towards the coast (Kolega, 2015), shingle beaches and the coastal plains which are heavily modified by human activities. Despite its short length, the Slovenian coast is of enormous value to the country because of its great strategic importance to the economy, cultural heritage, nature conservation, and marine and coastal ecosystems (Vahter, 2006). Similarly, these Mediterranean coastal areas of Slovenia is tagged as the “window into the world” (UNEP/MAP, 2018) due to their best-preserved touristic medieval town centers, nautical tourism, rich cultural heritage, a wide array of activities ranging from a network of trails to water sports, attractive location relatively close to larger cities of Northern Italy and Croatia and the country’s only international cargo port, the Port of Koper which connects the Central and Eastern Europe and the Mediterranean (Golob, 2020). Tourism is the most important activity in the coastal zone, particularly in the municipality of Piran, aside from maritime transport, industry, commerce and fishery. Tourist activities which are highly concentrated on the coastal strip contribute 12.3% to the total GDP of Slovenia which generates 110,700 jobs in 2018 (Prijatelj, 2019) and hosts 23 - 27% of the total tourists in the country. These coastal municipalities are home to nearly one-third of the accommodation facilities of Slovenian tourists offer with 22,289 beds (UNEP/MAP, 2018; Prijatelj, 2019).

Geographically, the city of Piran (hereinafter: Piran) is the administrative seat of the Municipality of Piran lying between $13^{\circ}34'$ east longitudes and $45^{\circ}31'$ north latitudes with an approximate land area of 0.7 km^2 and a total population of 3,730 based on the 2020 census (SURS, 2020). It is the most densely populated urban settlement in Slovenia with almost 5,355 residents for every square kilometer of its surface area (Razpotnik, 2020). On the other hand, the ancient city center of Piran, which had already been settled during the pre-Roman era, has been given a full monumental protection (Benčič, 2018) as an urban heritage site with several individual monuments and buildings that belongs to the highest category of historical and cultural heritage protection. Besides, the city, which is surrounded by a well-preserved medieval wall (Benčič, 2012), is considered as one of the most important historic urban areas in Slovenia with imprints of diverse architecture and rich history over the past centuries (Deu, 2016). It certainly features an urban structure as the oldest remnant of the city which is characterized by a dense clustering of buildings that reflects the image of most perfectly preserved medieval, gothic and renaissance houses, ornamented façades, magnificent squares and networks of narrow-winding streets intertwined with the millennial flow of constant change, expansion and improvements (Deu, 2016). The town underwent major building changes in the 19th century which began with the filling of the mandrač (an inner harbour for smaller vessels like fishing boats and sailboats), popularly known today as the Tartini Square, the construction of a municipality, a large mill on Punta, hotel facilities on the coast and the removal of parts of the walls (Deu, 2016; Ložar, 2019). This worldly coastal town is home to numerous cultural treasures that are of significant value such as the Tartini monument, Venetian house, the town hall, baroque house, Tartini central square, Tartini’s birth house and among others which are all located in the low-lying parts of the city. In addition to this, some of the finest museums and galleries of the country like the Piran coastal galleries, maritime museum, magical world of shells, museum of underwater activities, etc. are also seated within the vicinity of the old port town (Benčič, 2012). Endowed with its medieval character and the plethora of historic-cultural attractions, it is one of the major tourist icons on the Slovenian coast with the highest number of accommodated tourists and overnight stays in 2018 ranking 2nd next to the country’s capital city of Ljubljana (Prijatelj, 2019). Piran municipality alone has 13,000 tourist beds which are more than 50% of the total number of beds from the four municipalities (UNEP/MAP, 2018). The medieval

harbour town of Piran sitting on a narrow peninsula as shown in Figure 3 is popularly known as “Slovenia’s Seaside Paradise” (Burton, 2016) and has always been included in every tourist promotion of the state due to its picturesque beauty (Weber, 2007).

However, due to its peninsular shape and location, the old city center of Piran, which was expanded by artificially elevating some parts of the coastline, is facing the ominous threats of recurrent coastal flooding because of its exposure to both high tides and southerly winds. It experiences recurrent high tide flooding several times in a year during autumn and winter, and occasionally in spring, with large part of the town center is under water (Kolega, 2006; Vahter, 2006). Furthermore, sea floods in Slovenia are mainly governed by a complex interacting influence of astronomical high tides with a marked influence of low air pressure and a relatively strong south wind (Kolega, 2006) which causes high waves and additional rises in water levels. The sea level measurement on the Slovenian coast is configured relative to the mareographic zero at the tide gauge station in Koper (Kolega, 2006) with a mean sea level value of 218 cm (Strojan and Robič, 2016). Even before the tide gauge station in Koper became operational, records of small-scale and large-scale events of sea flooding have reported that the low-lying parts of Sečovlje, Piran, and Strunjan are the most affected parts in the Slovenian coast. The Adriatic Sea begins to flood the most exposed parts of the coast when it exceeded the flood stage of 300 cm (or 0.91 m based on the national altitude coordinate system) above the mareographic zero (Robič and Vrhovec, 2002) which corresponds to the level of yellow warning issued by the Slovenian Environment Agency (Agencija Republike Slovenije za Okolje, ARSO). In case the water level reaches 330 cm (1.21 m), an orange warning is issued as it starts to inundate the Tartini Square and the Punta (the oldest town quarter at the very end of the peninsula) while the Piran mandrač is already filled with sea water. Subsequently, ARSO raises the warning level to code red when the height of the water level at the coast rises above or equal to 350 cm (1.41 m) causing complete inundation of Tartini Square and submersion of the Piran Punta and Mandrač (Ličer, 2019). Over the period of 1960 to 2015, the sea level has exceeded the flooding threshold of 300 cm for 471 times with an average number of exceedances of more than 8 times per year which causes severe coastal inundation and economic damage (Strojan and Robič, 2016). Unfortunately, these can occur up to 16 (Robič and Vrhovec, 2002) to 31 (Strojan and Robič, 2016) times a year like in 2000 and 2010, respectively, most commonly from October to December. The following records of flood events on the Slovenian coast, particularly in the study area are taken from a published study by Kolega (2006) and Ujma journal of the Administration for Civil Protection and Disaster Relief of Slovenia.

3.1 Past flood events

A simultaneous occurrence of high tide and storm on the night of November 3, 1966 flooded the Tartini Square and all the coastal streets in Piran while huge waves had shaken and undermined the coastal wall causing heavy damage to the nearby establishments. The event continued until the maximum value of the water level was reached on the 4th of November at 8 pm measuring 352 cm (1.43 m in the national altitude coordinate system) which submerges the Tartini Square in approximately half a meter of flood water. The concurrence of storm events and high sea levels inflicted a severe economic damage to Piran as most of its facilities and assets are directly exposed to the sea. Likewise, it also affected the neighboring parts of the Slovenian coast causing a whole-day road closure between Lucija and Piran and destruction of wooden piers, cabin doors and small boats in Portorož. Subsequently, the flood, which occurred on the 25th and 26th of November 1969, recorded the highest measured sea level to date in the Slovenian coast at a value of 394 cm (1.85 m in the national altitude coordinate system). This two-day flood incident inundated the entire coastal area of Slovenia which is considered an extreme flood event because of the unusually high water level. It caused a great deal of damage to private properties, houses and businesses in the city center as well as to the cars parked in Tartini Square as the

sea water flooded them to a height of nearly 1 m. Also, all road sections towards Izola, Portorož and Piran have closed all day and the traffic connectivity between Koper and Piran was disrupted.



Figure 3: Location of the study area

Another flood was reported on December 22, 1979 when the strong south wind raised the waves crashing against the rocks and drove the water level to swell at a height of 356 cm (1.47 m) penetrating the squares and streets of the old town. In the following year, the sea level reached an overwhelming elevation of 361 cm (1.52 m) on October 25, 1980 which was only caused by an astronomical high tide while the same height of sea level was recorded in December 1982 with the influence of both southerly wind and drop of air pressure. These have caused inconveniences to the inhabitants and paralysis of social and economic activities of the area (Kolega, 2006). The floods in the old city of Piran became more frequent during the 21st century as the number of exceedances of the specified flooding threshold increases (i.e. 2002, 2004, 2005, and 2007) which leads to higher economic losses due to the continuous socio-economic development in Piran. During the astronomical high tide in December 2008, which coincided with a strong southerly wind, the sea level surged to its second highest measured level of 372 cm (1.63 m) in the monitored period for the last fifty years pushing the water masses from the open sea towards the coast. As a result, the duration of flooding was prolonged because the sea water from the lowest parts of the coast only receded after seven hours which incurred an estimated damage of 1 million euro (Ličer et al., 2009). It entirely flooded the lower ends of the coast and parts of the coastal towns, salt pans and roads in areas where floods are usually not frequent. In Koper, it inundated the city promenade, the interior of Bonifika stadium, parking lot of the market, Ukmajev Square which caused road closure and damage to about a hundred of cars while the Great Square, customs pier and some residential and commercial buildings in Izola were flooded as well as the premises of the Manzioli Palace and Marina Hotel. Similarly, the Tartini Square in Piran was under a half meter deep water impacting the nearby buildings of Tartini Hotel, the Tartini Theater, the municipal building, the library and many residential buildings while disrupting the access road to the city, destroying about 50 vehicles and distressing its economic activities. On one hand, the Sečovlje salt pans suffered the most damage where the flood water breached through the dilapidated embankments in several places (Robič and Strojan, 2009). The most

recent coastal flooding in Piran on the night of November 13, 2019 was synchronized with intense precipitation from the cyclone over the Mediterranean, southerly wind and full moon. It recorded a sea level height of 373 cm (1.64 m) which continued to flood the core of the city until morning and the worst hit was Izola (STA, 2019). According to Blatnik (2019) of the Radio-Television Slovenia Broadcasting, the mayor of Izola reported that their municipality suffered a damage of approximately 1.8 million euros while in Piran, about 2 million euros of damage was appraised. Whereas, the concurrence of high tides and persistent heavy rains in December 2020 have inundated parts of the coast causing electrical power outages and traffic delays. According to the report of the local government officials, the sea flooding has not caused substantial damage to Piran because it was prevented by a precautionary measure protecting the most exposed parts of the town from the intrusion of water with a barrage (STA, 2020). This event underscores the importance and necessity of appropriate flood protection measures and comprehensive implementation plans to ensure the protection and preservation of the city.

The records of past flood events reflect the increasing vulnerability and risk of Slovenian coastal towns to sea flooding predominantly due to astronomical high tides and winds where the old city of Piran is one of the main weak points in this regard. The apparent upward trend of global sea level, especially in recent decades and projections, could exacerbate this ongoing problem as it amplifies the magnitude, frequency and duration of sea flooding in the study area by amplifying the number of cases in which the sea level exceeds the flood threshold. The resonant effect of simultaneous occurrence of high tides, strong wind and high-intensity rainfall will drastically intensify the extent and magnitude of coastal flooding with fatal consequences to the affected area.

3.2 Sea level rise in Slovenian coast

Sea level changes along the Slovenian coast have been measured since 1960 at the mareographic station in Koper which is primarily used for monitoring and forecasting the water level of the sea during coastal flooding. Whereas, the archived data from long-term tidal gauge observations provide information on the variability and trend of local sea level and the impact of climate change. Figure 3.2 depicts the increasing trend of annual mean sea levels in Koper over the last six decades of observation. This data from the long-term set of measured values shows that within the period of 1960 to 2015, the local mean sea level in the coast has risen by 10 cm at a rate of $1.7 \text{ mm} \cdot \text{year}^{-1}$ (Strojan and Robič, 2016). However, Ličer (2019) claimed that the recorded sea level between 1961 and 1995 does not have a statistically significant trend, but during the 1990s, it gradually increased until a more realistic trend of sea level rise was observed. Specifically, over the observation period of 1995 to 2015, a statistically significant growth in the rate of mean sea level is about $5 \text{ mm} \cdot \text{year}^{-1}$ which is faster than the European and global average. These data are in accordance with the sea level information of the Italian part of the Adriatic coast where the measurements from the Punta Della Salute station in the Venetian Lagoon and Trieste station show similar variability in water level as in Figure 4 (Ličer, 2019). Likewise, due to the interconnectedness of the world's seas, a similar rise in sea levels is expected around the world but its magnitude and rate will depend on various climate change scenarios and differences in specific regional and local conditions. The higher share of sea level rise is attributed to the thermal expansion of the sea due to ocean warming of which the seawater temperature in the North Adriatic Sea rose by 1.8°C over the last 60 years (Orovic, 2018) and also, the melting of glaciers and ice sheets in Greenland and Antarctica.

For most of the European coastline, the mean sea level change is predicted to be reasonably comparable to the global average except for the northern part of the Baltic Sea and Atlantic coast (EEA, 2020). More specifically, the Mediterranean basin will experience a 40 to 50 cm of SLR while the Adriatic Sea will rise in the range of 30 to 40 cm under the RCP4.5 scenario. As a result, the frequency of sea flooding on the Adriatic coasts is estimated to increase by a factor of 26 to 50 at the end of the

21st century while the estimated 10 cm rise in sea level will proliferate the recurrence of coastal flooding by a factor of 10 (Strojan and Robič, 2016). The most visible effect in this respect is the growing number of cases in which the sea level exceeded the designated flood point of 300 cm implying a periodic sea flooding on the Slovenian coast. Ličer (2019) has demonstrated this aspect of sea level rise along the Slovenian coast with an extremely straightforward approach which is simply raising the measured sea level values of the entire time series from 1961 to 2017 by 30 cm. As a result, the number of incidents in which the sea level was above 330 cm (the orange warning) and 350 cm (red warning) has climbed to 1,153 from 55 and 149 from 8, respectively. This is about a 20-fold increase in the cumulative flood time above the orange and red warning levels which indicate a more often and longer sea flooding in Piran. Moreover, along with other coastal municipalities, Kolega (2006) found out that a 0.5 m rise in sea level will trigger the onset of annual floods to exceed the scale of today's extreme floods inundating 14 km² of the coastal municipalities which are 3% of the combined land surface areas of Ankaran, Koper, Izola and Piran. Relative to the current situation, this would imply more extreme floods every year and in case the exceptional flood occurs, a rise of 0.5 m would submerge the low-lying parts of the coast by 1.44 m. As reported by the Ministry of the Environment, Spatial Planning and Energy (2002), the cultural and historical center of Piran is the most at risk Slovenian coastal town from the consequences of rising sea levels and the city's well-developed touristic infrastructures demand urgency to map and understand this phenomenon while estimating the flood damage caused by rising sea level.

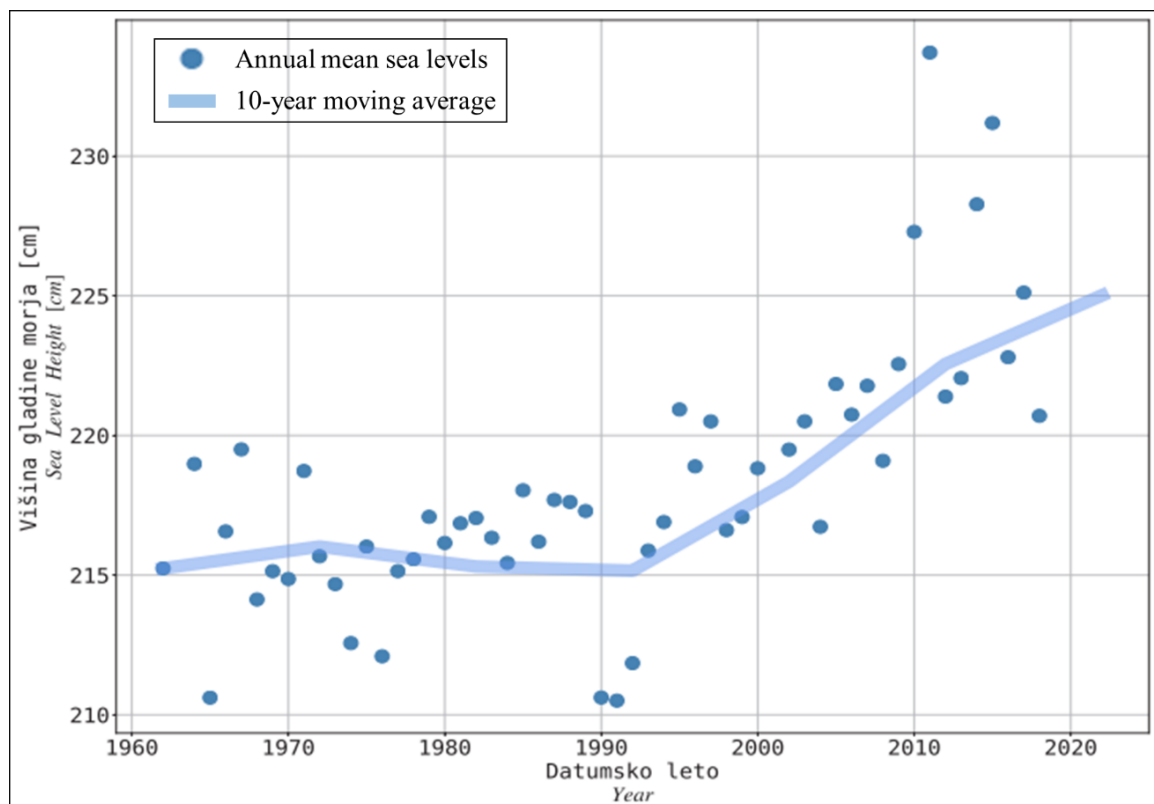


Figure 4: Annual mean sea level trend (10-year moving average) at Koper tide gauge station over the period of 1960 to 2020 (Source: Ličer et al., 2021)

4 RESEARCH METHODOLOGY

This chapter details the methodology implemented in this research to meet the underlying objectives. The approach employed in this study concerns with the quantitative assessment of flood damage caused by rising sea levels. The following sections disclosed the steps involved and introduced the relevant datasets in detail according to the approved framework.

4.1 Methodological framework

The methodological framework in Figure 5 provides a clear overview of the procedures implemented in this study. The research started with a detailed review of scientific literature to maximize the understanding of sea level rise mechanisms (Chapter 2), how it affects the characteristics of coastal floods, the associated impacts and the underlying methods of coastal inundation modelling. Thus, the framework is structured into three major processes: the first part deals with extreme value analysis of annual maximum sea levels and the second stage delineates the potentially inundated areas (PIAs) using a GIS-based bathtub modelling approach, while the third phase estimates the associated flood damage for different sea level rise scenarios to derive a depth-damage curve.

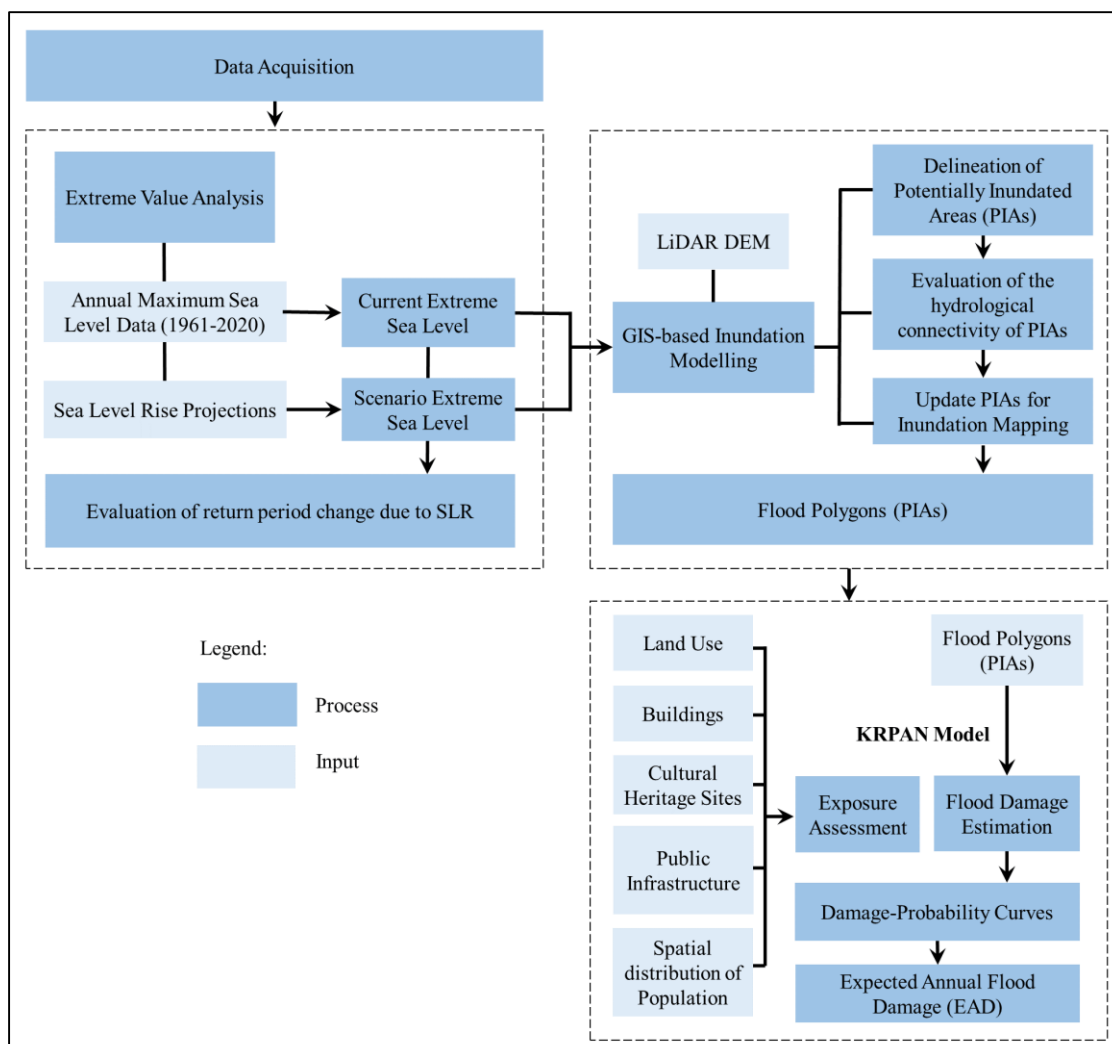


Figure 5: Methodological flowchart

4.2 Data acquisition

Data used in this study were collected from different governmental entities of the Republic of Slovenia which are all freely accessible on their respective websites. Table 2 presents the relevant datasets required to carry out the objectives of the study along with their spatial domain and sources. High-resolution 1m-LiDAR Digital Elevation Model (DEM) as the primary source of elevation measurements was used to generate the PIAs of Piran city along with extreme coastal water level and forecasted sea level rise values. Other geospatial data was also collected for impact assessment such as land use map, population features, cultural heritage sites, public infrastructure, and registry of buildings which are mostly available for free. Furthermore, data on the historical annual maximum sea level of the Slovenian coast was made available upon request, while sea level rise projections were mainly based on a literature review. Thus, the following subheadings briefly discussed the sources, nature and analysis of the datasets used in the study.

Table 2: Datasets used in the study

Dataset	Data Type	Resolution / Scale	Source
LiDAR DEM	Raster	1m	Agencija Republike Slovenije za Okolje (ARSO, Slovenian Environment Agency) of the Ministry of the Environment and Spatial Planning
Orthophoto	Raster	0.25 m	Surveying and Mapping Authority of the Republic of Slovenia of the Ministry of the Environment and Spatial Planning
Land Use Registry of Buildings	Vector	1: 5,000	Ministry of Agriculture, Forestry and Food
Population	Vector	1: 1,000	Surveying and Mapping Authority of the Republic of Slovenia
Cultural Heritage Annual maximum sea level	Vector	100 m by 100 m grid	Slovenian Statistical Office (SURS)
Projected Sea level rise	Hydrological	Yearly	Ministry of Culture
	Hydrological	Global / Regional	ARSO
			Scientific literature

4.2.1 Elevation Data - LiDAR DEM

The quality and reliability of flood hazard analyses greatly depend on the availability of detailed and accurate topographic data. The primary input variable for an accurate SLR-induced inundation modelling is a high-resolution topographic information (Gesch, 2009). DEMs as the predominant source of ground topography have long been an integral part of flood modelling and it is therefore essential that its resolution be improved to the highest possible extent (Casas et al., 2006). In this study, a high-resolution digital elevation model generated through an airborne laser scanning technology was used which is commonly used in assessing the hazard of coastal flooding because of its accuracy (Webster 2010). Light Detection and Ranging (LiDAR) is a remote sensing technique that uses laser light in pulses to measure variable distances of the Earth and these light pulses generate actual, three-dimensional information of Earth's surface characteristics and shape (NOAA Coastal Services Center,

2012). LiDAR data, in particular, has been extensively used for detailed flood modelling, risk assessment and hazard mapping studies due to its highly accurate depiction of features within the landscape which makes it very appropriate to be used as input data in 1D-2D numerical flood simulations and enables the accurate prediction of flooding (Ernst 2010; Erpicum et al. 2010). LiDAR-derived terrain data for the whole of Slovenia were provided by the Ministry of Environment and Spatial Planning through their National Aerial Laser Scanning Project from 2014 to 2015. Most parts of the country were scanned with a density of 5 points per square meter for high mountain range areas and 2 points per square meter for forest areas while areas that are at high risk of flooding and landslide were scanned with a precision of 10 points per square meter (Triglav-Čekada et al., 2015). Free access to a nationwide LiDAR data (http://gis.arso.gov.si/evode/profile.aspx?id=atlas_voda_Lidar@Arso) opens up a wide array of opportunities for applications: from hydraulic evaluation of water conditions, spatial planning, flood simulation and hazard mapping, designing flood control structures to studies on environmental protection, archaeology, agriculture, cultural heritage, geomorphological changes, and many others (Slovenia in the laser scanning data, 2015).

LiDAR datasets are stored in two national coordinate reference datum: D96/TM (geodetic datum 1996) which is based on the European Coordinate System and the old grid coordinate system D48/GK (geodetic datum 1948, Gauss-Krüger projection). LiDAR-derived digital terrain model has a grid size of 1 m by 1m, a horizontal resolution of 30 cm (Triglav-Čekada et al., 2015) and a vertical accuracy of 8 cm as indicated in the technical report of the geodetic consulting agency (Mlasko, 2011).

Figure 6 clearly shows that a large part of the land area in Piran is located in the low-elevation coastal zone (LECZ) which is only 10 m or less in elevation above sea level. According to on-site inspection, the area is protected by submerged rip-rap breakwaters to reduce erosion and dissipate the energy of the waves approaching the promenade. With sea levels predicted to rise and a shift in the frequency of extreme sea level events, this area on the Slovenian coast is inarguably prone to a high risk of sea flooding and its related consequences.

4.2.2 Land use data

Land use is an indicator that describes the condition of the landscape and the management of land which reflects the socio-economic development and spatial management of the area (Vrščaj, 2011) as a result of natural, historical, demographic, and economic influences (Gabrovec and Kladnik, 1997). Land use information plays a requisite role in exposure assessment and damage calculation. Thus, the actual land use map of the study area was acquired from the Land Use Database of the Ministry of Agriculture, Forestry and Food (MAFF), the national record of land use/land cover data of the Republic of Slovenia, which is publicly available at <https://rkg.gov.si/vstop/> in vector shape format (polygon). Accordingly, it is the most detailed study of land use available for the entire country at the micro-level with the primary purpose of determining the actual condition of agricultural land use for the implementation of measures of the common agricultural policy of the European Union (Petek, 2004) but integrating the analysis of urbanization on land and other categories have also been conducted (Vrščaj, 2011). The database is updated annually for about one-third of the territory of Slovenia and the latest data available for the study location is from the year 2017 which was generated using a computer-assisted interpretation of digital orthophoto maps taken from 2004 to 2016 with an image resolution of 25 cm (MAFF, 2019). The ministry categorized the actual land use into 25 different classes, but for this study, it was reclassified into 4 major land use classes as shown in Figure 7.

Built-up areas take up the dominant portion of 73.7% of the total area of interest comprising primarily of residential areas and accommodation facilities which are all situated in the LECZ (Figure 8). It was followed by agriculture constituting 24.2% of the land area but these are located in higher elevations. It clearly indicates that the coastal plains are heavily modified by human activities and are

densely populated despite their size and location in sensitive coastal landscapes as shown in Figure 9. As mentioned previously, Piran has a developed tourist infrastructure and tourism is the major economic driver in the area. This concentration of urban settlements and economic activities in the artificially elevated coastal plain of Piran represents a national and mayoral concern especially in the preservation of its cultural heritage (Figure 9).

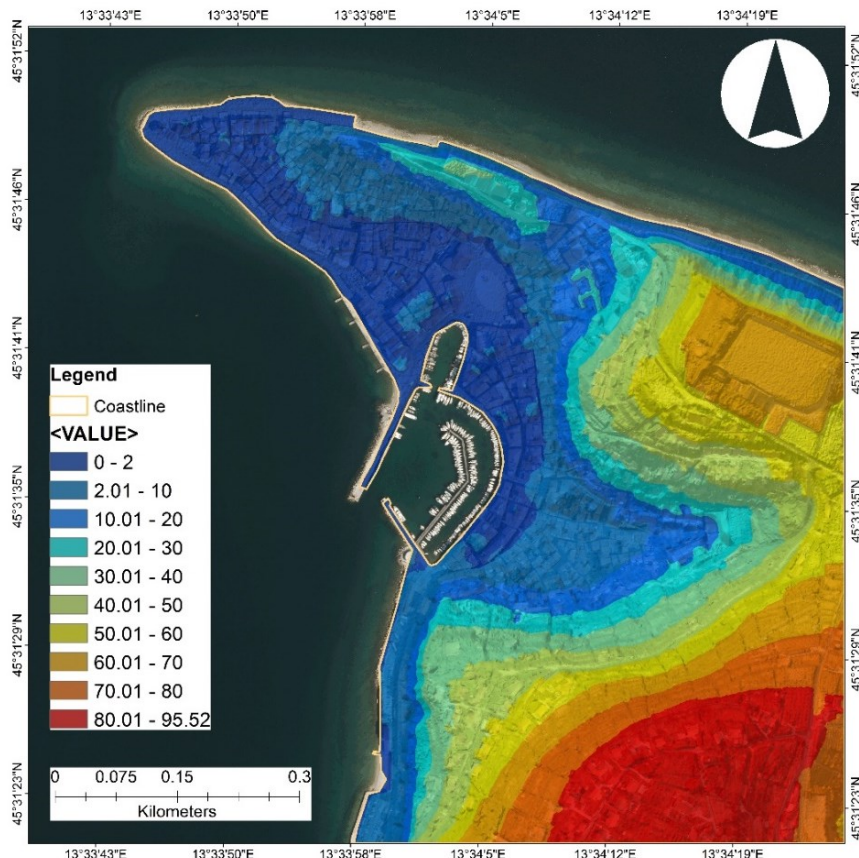


Figure 6: Elevation Map of Piran

4.2.3 Other geospatial datasets

The population distribution in the study area with a spatial level of 100 m by 100 m was obtained from STAGE (<https://gis.stat.si/#lang=en>), a web service application of the Slovenian Statistical Office which offers a freely accessible interactive cartographic tool for presenting and disseminating national statistical data in a different time and spatial units (Kuzma and Merc, 2015). According to this data, 3,568 inhabitants are residing in the investigated area and most of them are highly concentrated in the low-lying town center of Piran as depicted in Figure 8. Whilst, building statistics in the location were accessed from Surveying and Mapping Authority of the Republic of Slovenia (GURS, <https://www.e-prostor.gov.si/access-to-geodetic-data/free-geodetic-data/>) which is an independent body under the Ministry of the Environment and Spatial Planning responsible for the management and maintenance of geodetic databases of the country. The registry of buildings contains information on the real-estate function of the building into residential and non-residential use (industrial, commercial, etc.), construction year and the number of floors (GURS, 2017). In addition to this, a geo-database of the protected cultural heritage sites in Piran (Figure 9) was downloaded for free from an open data website of the Ministry of Culture (<https://data-mk-indok.opendata.arcgis.com/>) which can also be viewed online through their GIS portal. The data comes in a shapefile format containing a registry of immovable cultural heritage and its legal protection regimes (Ministry of Culture, 2018).

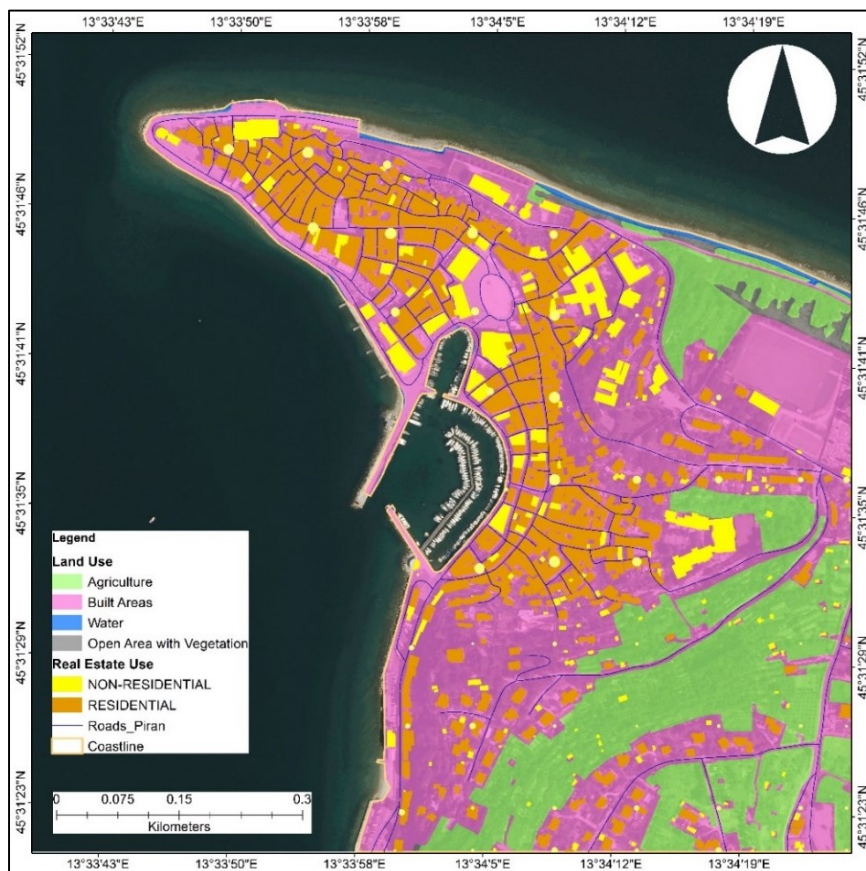


Figure 7: Land use map of Piran

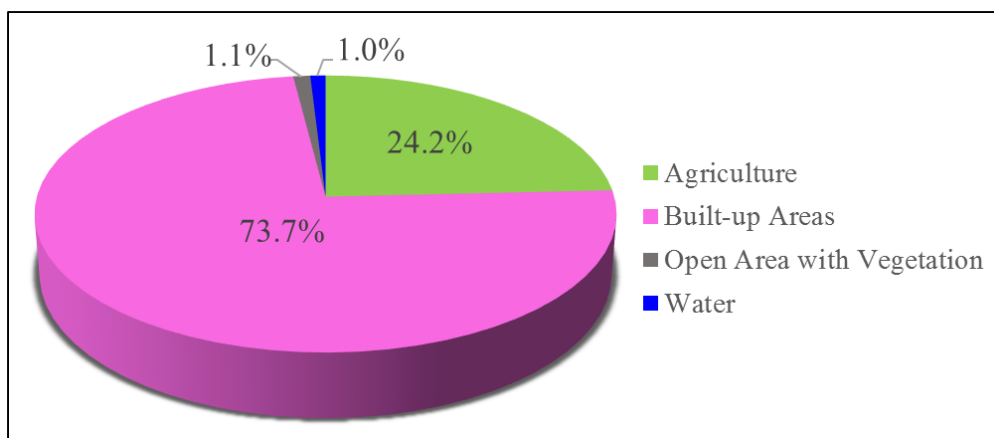


Figure 8: Land use classification of the study area

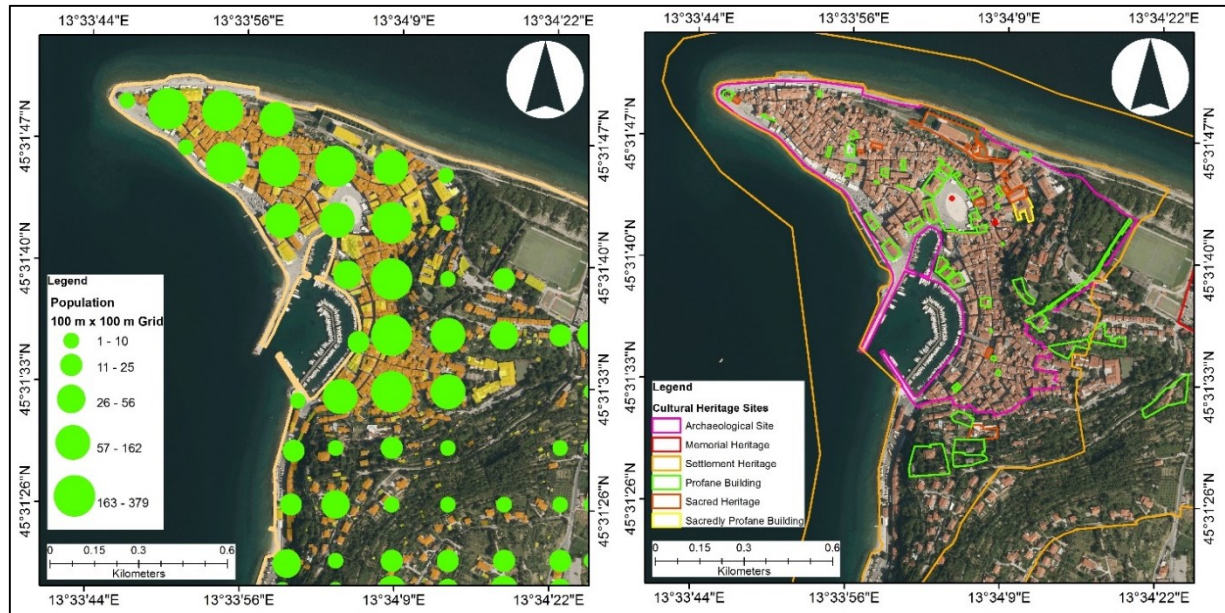


Figure 9: Spatial distribution of population (left) and cultural heritage sites (right) in Piran

4.2.4 Annual maximum sea level

The historical time series of annual maximum sea water level observed at the Koper tide gauge station from 1961 to 2020 as plotted in Figure 10 was extracted from quality monthly extreme values provided by the Slovenian Environment Agency. As mentioned above, the occurrence of flood events begins when the sea level is above 300 cm in relation to the starting point of the water meter bar in Koper. It shows that the frequency and severity of coastal flooding in Piran has increased over the last decades (Figure 4.6). The number of days in which the sea level surpassed the flood point as displayed below shows an increasing trend over the years. These 60 years of data were prepared to estimate the return periods of extreme sea level events in Slovenia using an extreme value technique. On the other hand, the following sea level elevations are measured relative to the zero gauge level located 2.09 m below mean sea level and 4.012 m below the R5486 benchmark in Koper. Thus, the sea level data used in the inundation analysis was converted to the national altitude coordinate system of Slovenia by subtracting 2.09 m to the recorded height of sea level to coincide with the vertical datum of LiDAR DEM used in this study.

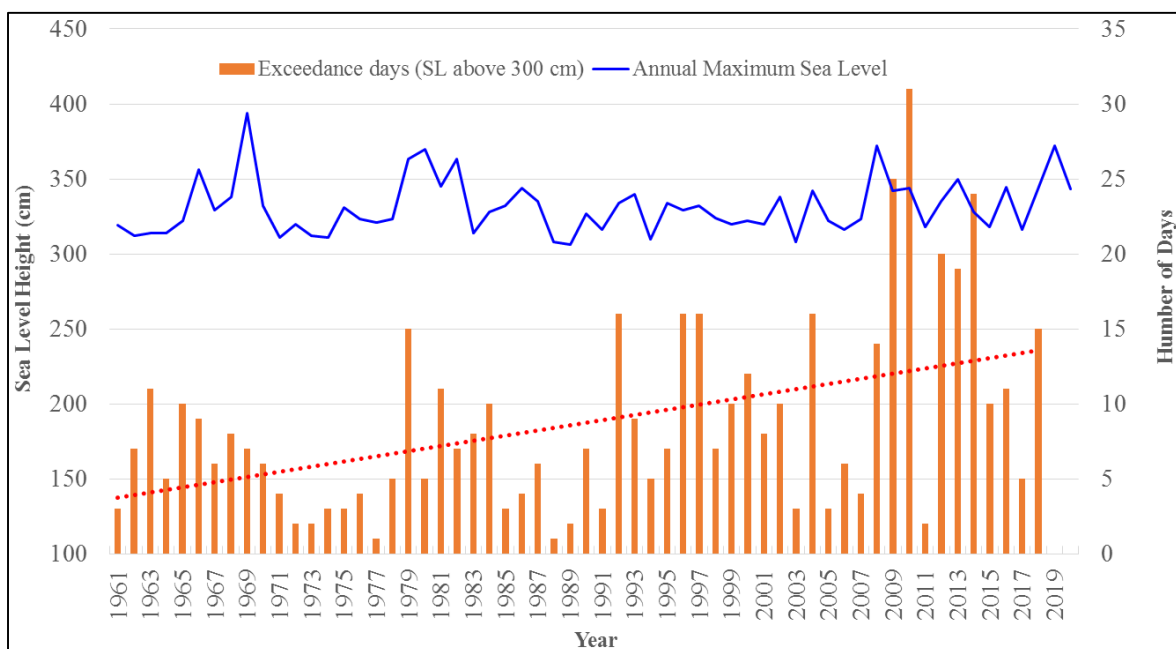


Figure 10: Annual maximum sea level and the number of days it exceeded the flood level of 300 cm at the tide gauge station Koper (Source: ARSO)

4.2.5 Sea level rise projections

The global estimates of mean sea level rise by 2100 show a large spread value, ranging from 0.28 - 0.61 m for RCP2.6 scenario to 0.52 - 0.98 m in the case of RCP8.5 (IPCC, 2013). However, observation data from satellite altimetry and tide gauge stations congruently reveal that sea level is not rising uniformly around the globe and is spatially variable due to various contributing factors such as temperature difference, wind and pressure changes, salinity, ocean currents, vertical land motion and among others (IPCC, 2013). In the Mediterranean context, Tsimplis et al. (2008) predicted a maximum steric sea level rise of 25 cm with a mean value of 13 cm for the 21st century using an atmosphere–ocean regional climate model under the A2 emission scenario, while the work of Galassi and Strada (2014), which combines the terrestrial ice melt, ice-age glaciers and steric sea level components, estimated a 9.8 – 25.6 cm rise across the entire Mediterranean Sea by 2040 to 2050. According to the analysis of sea level trends from satellite altimetry and tide gauge data, the Mediterranean Sea is rising at a rate of $2.44 \pm 0.5 \text{ mm} \cdot \text{year}^{-1}$ between 1993 and 2012 (Bonaduce et al., 2016) which is higher than $1.1 – 1.3 \text{ mm} \cdot \text{year}^{-1}$ of the last century (Tsimplis and Spencer, 1997). More specifically, the positive trend of sea level rise observed across the North Adriatic Sea is among the highest in the Mediterranean basin (Bonaduce et al., 2016; Rocco, 2015) and the low-lying coastal areas of this region, which possess an immense socio-economic, environmental and cultural value, are particularly vulnerable to sea level rise and coastal inundation (Ramieri, 2000; Tsimplis et al., 2012; Torresan et al., 2019). As reported by Rocco (2015), the tide gauge station in Trieste, Italy, which has the longest records of tidal data, indicated a higher sea level trend of $5.05 \pm 1.20 \text{ mm} \cdot \text{year}^{-1}$ throughout 1993 to 2014 compared with the average rate of $1.25 \pm 0.04 \text{ mm} \cdot \text{year}^{-1}$ for the entire Adriatic Sea as per Galassi and Spada (2015). Furthermore, Scarascia and Lionello (2013) predicted a mean sea level rise of 8.9 cm in the North Adriatic region by the end of the 21st century with an uncertainty range between 10th and 90th percentile, from 2.3 to 14.1 cm but considering the contribution of ice melt, the study suggests a rise of 14 to 49 cm. Whereas, according to the findings of Galassi and Spada (2014), the sea level in Trieste and Bakar, Croatia is estimated to escalate by 11.3 to 22.7 cm by 2040–2050 at a rate of 2.2 to 4.5 $\text{mm} \cdot \text{year}^{-1}$ which is generally in line with the projections in the Adriatic basin, ranging from 11.5 to 23.8 cm. On the other side, the application

of a multi-model chain approach to the North Adriatic Sea revealed that most of the area in this region (from Po River Delta to the border of Italy and Slovenia) will experience a sea level rise of 17 cm for a low scenario and 42 cm for the high scenario by 2070 – 2100 (Torresan et al., 2019).

Although, the estimates mentioned above suggest a broad range of values, they unanimously indicate an increase and the available data from RCP scenarios could be used to analyze the impact of sea-level rise induced by climate change.

4.3 Development of sea level rise scenarios

The latest scientific understanding of sea level rise projections from IPCC AR5 (IPCC, 2013) and SROCC (IPCC, 2019) with the contributions of committed experts through scientific journals (Bamber et al., 2019; Horton et al., 2018; Jevrejeva et al., 2014; Jevrejeva et al., 2016; Kopp et al., 2014; Kopp et al., 2017; Le Bars et al., 2017; Mengel et al., 2016; WMO, 2019; Wong et al., 2017) confirms the accelerating pace of global sea level increase as the most plausible effect of climate change. Although, the magnitude and timing of future sea level rise remain uncertain, decision-makers are already now facing urgent need of a reasonably well-justified estimate or range of values to adequately develop policy and adaptation plans (Cooper et al., 2013).

Detailed projections of future sea level rise along the Slovenian coast as a consequence of climate change are not available as well as its impact is not widely studied. However, some authors support a relatively uniform sea-level trend over the North Adriatic Sea (Bonaduce et al., 2016; Ličer, 2019; Zanchettin et al., 2020) and the rise is likely to be at least 30 cm by 2100 (Ličer, 2019). Also, Nicholls et al. (2014) articulately mentioned that performing an impact analysis is still doable even though there is no data available to generate a sea level rise scenario. This is accomplished “by using a nominal value for the change in sea level or a range of values to develop an appreciation of the potential impacts or determine thresholds in the magnitude of impacts” (p. 137). Likewise, due to the large uncertainties in the projection of future sea level rise, it is prudent to consider a range of scenarios to avoid invalidity of the rendered impact analysis every time new estimates of sea level rise become available and to allow the inclusion of uncertainty, sensitivity and risk in the analysis (Nicholls et al., 2014). Seconded by Zhang (2011), it is recommended to estimate the area of inundation and the associated statistics of affected properties, infrastructures and population based on a sequence of sea level rise scenarios determined by the range of uncertainty. On that account, this study considers a total of seven sea level rise scenarios based on the projections in the North Adriatic Sea. The future sea level rise envelope from the scientific literature was discretized in 10 cm increments producing a series of scenarios from 10 to 50 cm to provide a comprehensive overview of the probable effects of sea level rise over the next few decades. This parameter was chosen by taking into account the vertical accuracy of the LiDAR DEM with an RMSE of 8 cm (Mlasko, 2011) and the 10 cm rise being experienced in the Slovenian coast for the past few decades (Strojan and Robič, 2016). In addition to this, the study also includes two additional extreme scenarios that account for the influence of the Antarctic ice-sheet on GMSL rise which is predicted to become the largest contributor in the future (Church et al., 2013; DeConto and Pollard, 2016). Despite their low probability, the inclusion of such high-impact scenarios is essential for long-term coastal risk management (EEA, 2020; Griggs et al., 2017; Hinkel et al., 2015) because “it frames the greatest risk, the largest damages, and highest prospective costs in planning adaptation” (Stammer et al., 2019, p. 924). Besides, it allows long-term projects with high-risk aversion to be included in the analysis, particularly in the coastal areas where high economic, social, environmental and cultural values are of the greatest concern. Thus, the two worst-case scenarios of this study were defined according to the RCP8.5 emission scenario of IPCC (2019) Special Report on the Ocean and Cryosphere in a Changing Climate and Kopp et al. (2017) with a sea level rise value of 0.84

m and 1.46 m, respectively which allows decision-makers to think across the full range of possibility. Table 3 gives the summary of the sea level rise scenarios used in the present study.

Table 3: Sea level rise scenarios

Scenario	Sea level rise (m)
S1	0.1
S2	0.2
S3	0.3
S4	0.4
S5	0.5
S6	0.84
S7	1.46

4.4 Extreme value analysis

Extreme value theory is a widely used statistical discipline to analyze hydrologic phenomena, particularly in predicting the occurrence of extreme events with low probability and its application in coastal protection and management has long been acknowledged by the scientific community (Coles, 2001; Charras-Garrido and Lezaud, 2013; Karz et al., 2002; Fredriksson et al., 2016). The theorem provides a framework for modelling of data maxima (or minima) which allows extrapolation of more extreme and rare events that are outside the range of the available data (Coles, 2001; Fredriksson et al., 2016). Extreme sea levels (ESLs) are commonly assessed by the concept of return levels and return periods which are often required for designing coastal flood defense structures. Return levels represent the water level expected to be exceeded annually while the return period (or recurrence interval) is defined as the inverse of the exceedance probability of a certain event (Ribeiro et al., 2014). ESLs are typically calculated based on parametric extreme value analysis (EVA) of historical sea level data (Mudersbach and Jensen, 2010). EVA can be performed either by using a block maxima approach (e.g. annual maxima) or peaks over threshold method which follows a Generalized Extreme Value (GEV) distribution and Generalized Pareto Distribution (GPD), respectively (Coles, 2001; Fredriksson et al., 2016). The annual maximum series model has been extensively used in analyzing the extreme values, especially in flood frequency analysis (Bezak et al., 2014; Sindhu, and Unnikrishnan, 2011) because it is more robust to temporal and spatial variations (Muis et al., 2016). This method defines the samples by taking the highest value in a year (Bezak et al., 2014; Sindhu, and Unnikrishnan, 2011) with an assumption that these data are independent and identically distributed random variables (Coles, 2001). Thus, it requires at least 25 years of data for a satisfactory analysis (Pugh, 1987) while Stephens (2009) preferred requiring 50 years of sea level records to partially compensate for the loss of data during sampling. On the other hand, the peaks over threshold sample consist of all well-defined peak values that exceed a certain threshold level but choosing an appropriate threshold is a challenge to this method (Bezak et al., 2014). Data on the return periods of extreme sea levels in the Slovenian coast is available through the ARSO report (Centa et al., 2014) however, they were calculated from a series of sea level measurements from 1960 to 2013 and the lowest return period available in the report is only 10-year. Since the research objectives require quantification of extreme sea level events with higher annual exceedance probability than 10-year and evaluation of the future changes in extreme sea levels under the influence of sea level rise, it is prudent to carry out a separate extreme value analysis based on the recent available sea level data. In this study, the extreme coastal water levels in Slovenia for six different return periods were estimated by fitting a GEV and Gumbel distribution to the annual maximum series of sea level using the maximum-likelihood method.

A GEV distribution model is a family of continuous probability distributions that was developed within the extreme value theory as a result of combining the families of Gumbel (type I), Frechet (type II) and Weibull (type III) functions into a single family of models (Eq. 1). It is a three-parameter distribution characterized by a location (μ), scale (σ) and shape (ξ) parameter which describes the behavior of the maxima and the distribution type (Bali, 2003; Huang et al., 2008; Millington et al., 2011). Hence, this parametric statistical model allows a continuous range of possible shapes and has the following probability (Eq. 1) and cumulative (Eq. 2) distribution functions denoted as $f(x)$ and $F(x)$ respectively, for a variable x .

$$f(x) = \frac{1}{\sigma} \left\{ 1 + \xi \left(\frac{x-\mu}{\sigma} \right) \right\}^{-1-\frac{1}{\xi}} \exp \left\{ - \left[1 + \xi \left(\frac{x-\mu}{\sigma} \right) \right]^{-\frac{1}{\xi}} \right\} \quad (1)$$

$$F(x) = \exp \left\{ - \left[1 + \xi \left(\frac{x-\mu}{\sigma} \right) \right]^{-\frac{1}{\xi}} \right\} \quad (2)$$

where in this application x denotes a value of the annual maximum sea level, μ is the location parameter, σ is the scale parameter and ξ is the shape parameter. Thus, the expression $\left[1 + \xi \left(\frac{x-\mu}{\sigma} \right) \right]$ and σ must be greater than 0 while μ and ξ can take any real numbers. The location parameter, μ defines the shift of a distribution in a horizontal direction while the scale parameter describes the variation of the distribution around its center (Millington et al., 2011). The shape parameter, ξ is critically significant in this respect as it governs the tail behavior of each distribution and determines which type of the distribution best fits the data (Tyralis et al., 2019). The GEV model follows a Gumbel or Type I extreme value distribution (EV) when $\xi = 0$; Frechet or Type II EV when $\xi > 0$; and Weibull or Type III EV when $\xi < 0$. In practical applications, GEV distribution is used as an approximation to model the distribution of maximum annual water levels (Hawkes et al., 2008), which is generally unknown.

The two-parameter Gumbel distribution (EV1), also known as the double exponential distribution is a particular case of GEV distribution which only uses location (μ) and scale (σ) parameters as shown in Eq. 3 (Bezak et al., 2014; Fredriksson et al., 2016; Gorgoso-Varela and Rojo-Alboreca, 2014). This allows for Gumbel to have an infinite range of interests while Frechet and Weibull have finite left and right boundaries, respectively (Fredriksson et al., 2016). In addition, the prevalence of Gumbel distribution in any hydrological application can be traced with its simplicity and generality where its mathematical handling can estimate the two parameters more accurately than three (Koutsoyiannis, 2004). However, the main drawback of this approach is that it produces the smallest possible estimates of extremes for longer return periods with low exceedance probabilities but greater hazard intensity which could possibly put design-limited engineering structures at high risk of failure (Jonsson and Ryden, 2017; Koutsoyiannis, 2004). Furthermore, the cumulative distribution function of the Gumbel method can be expressed as:

$$F(x) = \exp \left\{ - \exp \left[- \left(\frac{x-\mu}{\sigma} \right) \right] \right\} \quad (3)$$

Although, several techniques can be used for the estimation of distribution parameters, here the Maximum Likelihood Estimation (MLE) was employed for both GEV and Gumbel distributions because of its ability to provide a more consistent, flexible and efficient approach to parameter estimation problems which in general, shows less biased results than any other methods (e.g. L-moments, method of moments). This technique defines the distribution parameters in such a way that their values maximize the probability of the given observed data. Also, following the guidelines of the

Federal Emergency Management Agency (FEMA), MLE is recommended as the method to estimate the model parameters of the GEV distribution (Huang et al., 2008).

The results obtained from two distribution models were then compared to the official values stipulated in the ARSO report (Centa et al., 2014) and the most appropriate distribution was selected based on Akaike Information Criterion (AIC) and Bayesian information criterion (BIC) goodness-of-fit tests along with a visual inspection of various diagnostic plots. These statistical metrics have been successfully used by several authors as a model selection criteria for finding the best fit distribution model in hydrological extreme analysis (Alahmadi et al., 2014; Bella, et al., 2020; Golian et al., 2020; Méndez et al., 2007; Wong et al., 2020). They are penalized-likelihood information criteria for selecting models estimated by maximum likelihood which consists of a goodness-of-fit term and a penalty to control over-fitting. Their approach of comparing models is more intuitive by finding the right balance between goodness-of-fit and model parsimony, hence lower values of AIC and BIC indicate a better fit of the model to the actual data (Dziak et al., 2012). Each statistical measure was calculated under the maximum likelihood estimation framework in R along with the estimated return periods of extreme sea levels. The model with the smallest AIC and BIC values was preferred and was used in the succeeding analysis.

Moreover, the future variation in the recurrence interval of the current extreme water levels (CEWLs) was evaluated by imposing the defined sea level rise scenarios above the CEWLs as estimated from observed sea level measurements. For this study, the superposition of CEWLs and sea level rise as shown in Eq. 4 is referred to as the scenario EWLs (SEWLs) which is widely applied in coastal risk assessment under sea level rise (i.e. Feng et al., 2018; Haigh and Pattiaratchi, 2010; Haigh et al., 2011; Licher and Felsenstein, 2012; Paprotny and Terefenko, 2017; Wu et al., 2016). The return period of SEWLs was then calculated by fitting a logarithmic curve to the data using trendline analysis in Excel.

$$SEWL = CEWL + SLR \quad (4)$$

where SEWL denotes scenario extreme water level with the influence of future sea level rise (SLR).

In general, the extreme value analysis method in this study was carried out in ‘RStudio’ version 3.6.1 using its Extremes Toolkit (extRemes) (Gilleland and Katz, 2011; 2016) which is an open-source programming language and software environment for statistical computing and graphics (R Core Team, 2020).

4.5 Inundation scenarios

For coastal flood analysis, the inundation scenarios were defined based on the recurrence interval of 2-, 5-, 10-, 100-, 500- and 1000-year return periods, estimated from the extreme value analysis. Hence, the final water level for sea level rise inundation modelling was determined as the combination of the hypothetical water level based on different return periods and 7 projected sea level rise as presented in Table 3. A total of 42 scenarios were developed to examine the changes in land exposure and its associated economic losses as a function of sea level rise.

In the present study, the dynamic coastal processes such as erosion or wave run-up nor the influence of land subsidence, winds and drainage on coastal flooding were not considered. Currently, it is difficult to incorporate these factors in inundation scenarios due to the unavailability of reliable data to estimate site-specific erosion, complexity of specific hydrometeorological conditions and possible impact of land subsidence. This assumption is reasonable for Piran as the sea along the Slovenian coast in periods when the tide is the dominant cause of coastal flooding, in no case exceeds any of the above warning levels and extreme sea level events are nonetheless becoming more often and chronic due to decadal rise in sea level (Ličer, 2019). Thus, it is assumed that there are no changes in the topography

of the study area when inundation modelling was carried out. Needless to say, the effect of storm surges and the associated drop in air pressure, southeasterly winds and wave actions in the Adriatic basin would exacerbate the present condition of sea flooding on the Slovenian coast. Further, these factors are well-acknowledged as part of the limitations of the study and an impulse for future research directions.

4.6 Delineation of potential inundated areas (PIAs)

The extent and probable impacts of sea flooding under the different sea level rise scenarios were delineated using a bathtub inundation modelling approach. The main idea behind this approach is any areas with an elevation of less than the defined water level are flooded like a “bathtub”. For this study, the extent of coastal flooding is determined by two main factors, namely topography and hydrological connectivity. Therefore, the use of existing and publicly available high-resolution LiDAR DEM is an advantage in carrying out this method as it is a key input parameter that determines the inundation domain of the bathtub model. Although, several studies around the globe have shown the successful application of the bathtub model in coastal inundation mapping using both non-connected and hydrologically-connected approaches, they unanimously agreed that the latter option is more appropriate and leads to a more representative model of surface flooding (Habel et al., 2020; Li et al., 2009; Licher and Felsenstein, 2012; Malik and Abdalla, 2016; Poulter and Halpin, 2008; Sahin and Mohamed, 2014; Vaan de Sante et al., 2012; Yunus et al., 2015). Additionally, as Gesch (2018) recommended, imposing hydrologic connectivity ensures that inundated areas are directly connected to the source of flooding which is also regarded as a best practice for coastal impact assessments. According to Poulter and Halpin (2008), hydrologic connectivity can be modelled using either a four-side or eight-side connectivity rule as presented in Figure 11. Under the four-side connectivity rule, the cell is only inundated if at least one of its cardinal directions is adjacent to the flooded cells and directly connected to the sea which can potentially underestimate the surface flow connections and their impacts. On the other hand, an eight-neighbor connectivity rule considers a cell to be inundated if any of its cardinal and diagonal neighborhoods are flooded and directly connected to the source of flooding (Poulter and Halpin, 2008). Though, the eight-side rule may likely overestimate the impacts, it offers a more conservative approach for planning purposes (Cooper et al., 2015; Fu and Song, 2017) which is commonly used in elevation-based SLR impact assessments (Breilh et al., 2013; Fereshtehpour and Karamouz, 2018; Li et al., 2009; Poulter and Halpin, 2008; Yunus et al., 2015).

The potential zones of inundation were generated using a raster calculator in a GIS environment by comparing the elevation in each cell of LiDAR DEM with the user-defined water level (i.e., the SLR scenarios of interest) and all cells with values below that of the chosen threshold are considered flooded. Eq. 5 describes how the task of deriving the flood polygons was executed in ArcGIS version 10.8.1. The output was a two-colored raster map displaying the land and inundation defined with a value of 0 and 1, respectively. All areas from the output raster with an assigned value of 1 represent those cells that are inundated by a rising sea while areas with an assigned value of 0 contain cells that are unlikely to be inundated. For this purpose, raster cells with a value of 0 were reclassified to NoData using a Reclassify tool to better represent the inundation area which satisfies the condition $d \leq h$. However, the hydrological connectivity of these initial delineated inundated surfaces was evaluated and determined based on an eight-neighbor rule. A region group algorithm in ArcGIS Spatial Analyst Tool (ESRI, 2020) was used to filter out the hydrologically connected areas from the binary raster map using an eight-side rule. Hence, this method ensures that each region composed of inundated pixels are hydrologically connected with each other and to the source of flooding (i.e. sea) which was then referred to as the potentially inundated areas (PIAs).

$$S_{x,y} = \begin{cases} d_{x,y} \leq h, 1 \\ d_{x,y} > h, 0 \end{cases} \quad (5)$$

where S represents the cell values after processing, either flooded (1) or not flooded (0), d is the elevation of a given cell stored in LiDAR DEM at location x,y and h is the water level from inundation scenarios.

The raster layer containing the PIAs was clipped with the coastline boundary, digitized from an orthophoto, using an Extract by Mask tool to delimit the inundation surface at the case study level. The resultant grid was then converted to a vector polygon which produces a flood boundary of current and future scenarios with a magnitude of h to facilitate the spatial overlay analysis for exposure assessment and damage estimation. These procedures were repeated for a series of sea-level rise scenarios.

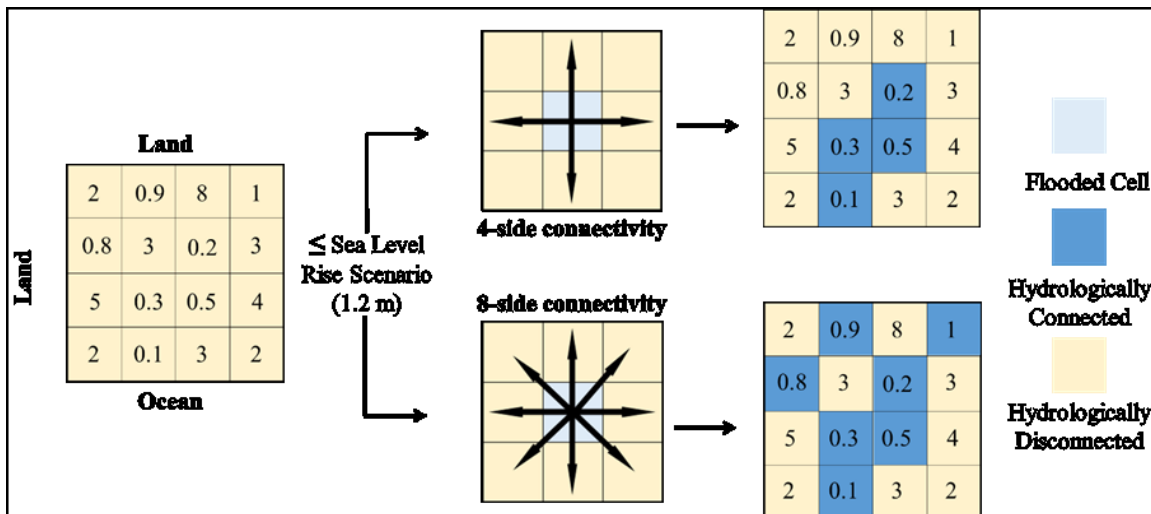


Figure 11: Hydrologic Connectivity using 4-side and 8-side rule (Poulter and Halpin, 2008)

4.7 Exposure analysis

The persistent trend and acceleration of rising sea levels have a profound interaction with extreme sea level events (Hunter, 2009; Oppenheimer et al., 2019) which as a result, augment the exposure of coastal zones to a more frequent and severe sea flooding. The United Nations Office for Disaster Risk Reduction defines exposure as “the situation of people, infrastructure, housing, production capacities and other tangible human assets located in hazard-prone areas” (UNISDR, 2016, p. 18). In accordance with the requirements predicated by the European Flood Directives, people, cultural heritage sites, economic activities and the environment are the essential elements to be considered in any flood risk analysis (Council of the European Communities, 2007) and exposure is one of the components in quantifying this risk. Exposure analysis describes the number and type of elements that may be adversely affected by a particular flood hazard scenario via operations within a geo-information system. In most cases, land use/cover data are generally utilized to characterize exposure in terms of affected sectors or economic activities while the official statistics of the population can be employed directly as exposure data (Merz et al., 2010; Tate et al., 2021). A leading measure to quantify exposure is expressed as the number of buildings, length of roads, types of assets, and the number of population affected in an area (Papilloud et al., 2020; UNISDR, 2016).

In the present study, the exposure of the elements displayed in Table 4 was assessed through a spatial query in a GIS environment by overlaying the predicted flood footprints of each scenario to different geospatial datasets such as population distribution, land use, buildings, public infrastructures, and cultural heritage sites. The spatial distribution of inundated areas generated from bathtub modelling

shows the propagation of hazards in the affected areas as a function of depth as well as the potential impact of varying sea levels on the built environment. This overlay operation defines the exposure of people, buildings, critical infrastructures and economic activities in the city of Piran to the identified coastal flood hazards which provides a valuable estimate of the physical impacts of rising sea levels. Typical built-up structures in the study area include residential buildings, town hall, business establishments (i.e. hotels, restaurants, café, and souvenir shops), museums, and cultural heritage buildings. Also, the total land area exposed to flood hazards was computed to investigate the spatial extent of land loss due to rising sea levels as well as the total number of affected population and buildings. The different types of elements at risk in Table 4 for exposure analysis were identified more specifically according to the setting of the study area but for this study, the assessment was limited to analyzing the exposure of the existing population, residential buildings, non-residential properties, public infrastructures, and cultural heritage.

Table 4: Identified elements at risk in Piran

Physical Elements	Public Infrastructures	Population	Economic Activities
- Land use	- Local roads	- Spatial distribution	- Revenue and income from different company size (micro, small, medium and big)
- Buildings: construction types, contents	- Water supply network - Sewage system - Underground electricity and telecommunication networks	of total population in 100 m grid	
- Monuments and cultural heritage (i.e. archaeological, memorial, sacred, profane building)			
- Vehicles			

4.8 Flood damage estimation

Quantitative estimation of flood damage is an important component of comprehensive flood risk analysis (Kang et al., 2005) which offers essential information for cost-benefit analysis of any proposed flood protection strategies, for disaster relief assistance, reconstruction and research priorities (Middelmann-Fernandes, 2010). Managing flood risk is vital from both a societal and economic perspective to avoid loss of life, ensure public safety and reduce economic losses. Data from exposure assessment can be combined with the information on the vulnerability of each element at risk and the hazard characteristics to obtain the potential cost of damage (De Moel et al., 2015). These damages are generally classified into direct and indirect losses which can be determined by identifying whether the objects have immediate physical contact with flood water or not. Subsequently, both types are further categorized into tangible and intangible consequences depending on whether or not they can be assessed in monetary terms (Messner et al., 2007). Thus, the components and methodology of flood damage appraisal differ from country to country and generally, the estimation can be accomplished in two ways, either thru post-flood survey or with the use of damage or loss functions. In practice, conducting a detailed survey in the aftermath of flood events to estimate the incurred losses is laborious, expensive, and time-consuming. The inherent variation in the results depends on the perceptions of individual respondents and survey personnel (Herath, 2003). As a result, the use of damage functions as a standard methodology has become a consensus in the scientific community to evaluate the economic damage caused by floods (Herath, 2003; Smith, 1994). This flood damage function is an umbrella term for functions expressing the degree of damage determined by inundation parameters considered in the analysis such as depth of flooding, velocity, duration, sediment loads, contamination of flood water, and

the availability of flood warning systems (Merz et al., 2010). As reported by Dutta et al. (2003), any of the mentioned parameters have a significant influence on the extent of the damage but in most cases, inundation depth is regarded as the determining variable to quantify the economic losses caused by floods (Burnham and Davis, 1997; Dutta et al., 2003; Merz et al., 2007; Smith, 1994) due to limited data on the joint effects of other influencing factors (Schröter et al., 2014). Besides, depth-damage curves are the most commonly used approach to assess flood losses in monetary terms by relating the flood depth to the degree of damages for a specific element at risk (Merz et al., 2007; Smith, 1994). Moreover, a wide variety of flood damage estimation models have already been developed and in use internationally for qualitative and quantitative assessments of losses inflicted by floods to different sectors under investigation. These damage models are developed using an empirical and/or synthetic approach depending on the availability of information (Merz et al., 2010). Some of the models that were successfully applied in flood damage assessments in different countries include The Multi-Coloured Manual in the UK, HAZUS-MH and HEC-FDA in the USA, FLEMO in Germany, DSM in the Netherlands, Anuflood in Australia and among others (See Section 2.4 for descriptions of these models and flood damage categories). Among them, a country-wide flood loss model called KRPAN (Vidmar et al., 2019) was successfully developed for the entire territory of Slovenia and applied in several detailed case studies.

4.8.1 KRPAN model

In this study, the KRPAN model (*Kumulativni Računi Poplavnih škod in ANalize / Cumulative Calculation of Flood Damage and Analyses*) developed by Vidmar et al. (2019) for the whole territory of Slovenia was used to estimate the flood damage caused by rising sea levels in Piran. The development of the KRPAN model was based on the upgraded methodology of the Institute for Water of the Republic of Slovenia (IZVRS, 2014 as cited in Vidmar et al., 2019, p. 2) for assessing the benefits of structural and non-structural flood reduction measures in Slovenia. As part of the improvements in the former methodology, the latest data on flood damage to cultural heritage, critical infrastructures, watercourses, and water structures after the 2012 flood event were taken into account. Whilst, the objective of the original and upgraded methodology remains the same, as a decision-support tool in evaluating the economic benefits of flood mitigation measures (Vidmar et al., 2019).

The application of KRPAN in calculating the expected annual flood damage for different sectors such as the environment, cultural heritage, and economic activities is intended for the entire territory of Slovenia. For each sector, the general expression in Eq. 6 is applied to calculate the expected damage (ED) in a given area during a certain flood event with a recurrence interval of 2-, 5-, 10-, 100-, 500- and 1000-year.

$$ED = M \times D \times E \times Vu \times Va \quad (6)$$

where M represents flood magnitude (depth and/or velocity), D is the dimension that refers to the number or size of objects at risk in a given area, E is the exposure of elements in the selected area for a given hazard, Vu is the vulnerability describing the damage of individual elements and Va is the economic value or cost (€) of every single element in the given area (Vidmar et al., 2019).

Within the KRPAN methodology, direct economic losses are either based on synthetically-derived depth-damage curves or empirical data depending on the availability of data for different sectors. As such, the direct tangible damages to residential buildings, business entities and building contents are estimated based on the depth-damage curves adapted from FEMA (2014). It also includes tangible losses to vehicles as well as the cost of cleaning the built-up areas and the exterior surfaces of nearby buildings. On the other hand, damages to cultural heritage, public infrastructures, and watercourses are appraised

based on the average of actual damages from past flood events archived in AJDA web application which is a Slovenian application for damage assessment on agricultural products and property operated by the Administration for Civil Protection and Disaster Relief (ACPDR). Also, using the damage database in AJDA, the loss of revenue and income from economic activities are calculated in four different company size classes: micro, small, medium-sized, and big companies (Vidmar et al., 2019).

Open-source GIS tools (e.g. SAGA, GDAL) were used as the base of the KRPAN model to operate by connecting the necessary input data and depth-damage functions. It is designed as a console application via a text-only computer interface (Figure 12) due to a large amount of data to be processed. Spatial data is based on the three basic vector building blocks of GIS databases - polygon, line, point. Polygon layers include building cadastre, land-use, water, land, and cultural heritage sites which are the basis for determining the damage to individual entities, expressed per surface unit. A spatial layer called KrpaP has been established for the entire country consisting of 1.3 million complex polygons while KrpaK was created separately to calculate the expected damage to cultural heritage. Whereas, public roads (state, local, forest), electricity network (underground part), water supply and sewerage network are expressed as line entities per unit length. A relational database KrpaL was created from these 110,095 line layers which is the basis for calculating the expected damage to line elements in the application. The point features (KrpaT) cover industrial buildings, passenger cars, and compensations for shelter needs while the availability of databases that relate to personal data (population records, personal cars) are subjected to legal provisions on personal data protection. However, the software still captures the number of people and cars as a generalization, computed from the total number of entities in each spatial district (Vidmar et al., 2019; Zabret et al., 2018). All these data were prepared and established in GIS tools to build appropriate relational databases of KRPAN operation.

Damage estimation within the KRPAN model can be executed in two ways: (1) when the depth of flooding is known from a specific event or scenario, the damage is estimated using stage-damage curves; and (2) when the depth of flooding is unknown, the model automatically use the average depth of floods in Slovenia (0.62 m) to compute the damage (Vidmar et al., 2019).

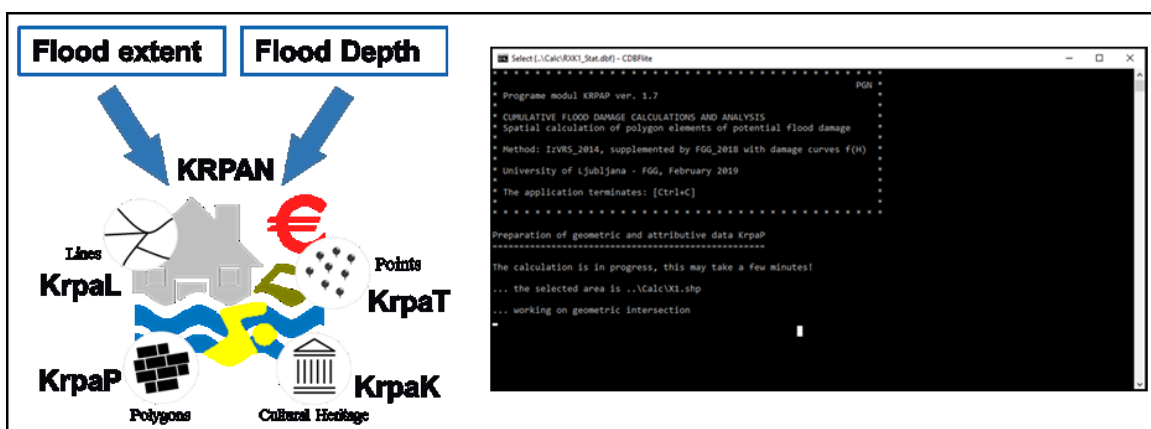


Figure 12: KRPAN model application

Therefore, this study mainly focused on the use of flood depth as the main determinant of direct economic damage, albeit it is acknowledged that other influencing factors and damage categories play an important role in evaluating flood impacts. However, the findings of several studies revealed that the depth of flooding has the largest influence on the flood damage among other inundation parameters (Büchele et al., 2006; Pistrika et al., 2014). The inundation depth grid datasets for each scenario were generated by subtracting the scenario water level from the elevation data using the raster calculator in ArcGIS. The combined information from the flood extent map and inundation depth distribution were used as inputs to the KRPAN application in calculating the total estimated annual flood damage in Piran

for 42 different scenarios. Thus, only tangible damages which can be assessed in monetary values and are within the flood zone were taken into account in the calculation, as well as, the indirect damages incurred by a certain flood scenario such as loss of revenues and cost of temporary housing for distressed inhabitants. The output reflects the estimated breakdown of damages for different sectors and a curve of the expected annual damage as a function of the recurrence interval. Additionally, the spatial distribution of expected flood damage over the area for different sea level rise scenarios can also be projected visually in the GIS environment.

The methods outlined in the KRPAN model employ a depth-damage function that only allows estimation of damages from freshwater flooding, but considering the location of Piran, it is mainly impacted by saltwater flooding. Considering the same flood water depth, the economic losses from sea water flooding are more extensive than freshwater, especially in structural components of a building and house installations due to its corrosive influence (Glas et al., 2017; Olesen et al., 2017; Prime et al., 2015). Consequently, this influence needs to be taken into account in damage assessment, however, there is a considerable paucity of information presently available on the differences of damages between a freshwater and saltwater inundation. Vanneuville et al. (2003 as cited in Glas et al., 2017, p. 1880) found out that the damage function for building contents from a short- and long-term duration flooding, which they respectively refer to as freshwater and saltwater is very similar while for building structures, the latter is higher by up to 12%. The catalog of residential depth-damage functions by USACE (Davis and Skaggs, 1992) also showed equal percent damages to contents value and a little variation to structure value which confirmed the findings of Vanneuville et al. (2003). In addition to this, USACE (2006) expressed this idea as “flooding is flooding” originating from the varying judgments of experts in the fields of construction, repair, and restoration, but some damages due to saltwater flooding are more pronounced in the longer term. Since the damages between the two types of flooding are not also clearly differentiated in the investigated area and KRPAN model, this study incorporates the influence of saltwater as unforeseen damage by defining a general percent of increase to the obtained calculations as given by Penning-Rowsell et al. (2005) who reported that the damage repair costs to building fabrics within a flood zone where the saltwater effect is expected should be increased by 10%. Consequently, in order to have a better understanding of the distribution of damages in Piran, the share of losses inflicted on residential buildings, public infrastructures, cultural heritage, business establishments and the costs of cleaning and temporary residence relative to the estimated damage of each flood scenario were presented separately. Results of the calculation for different scenarios are presented in the following chapter.

4.8.2 Damage-probability Curve

Expected annual damage (EAD) is a risk indicator (Romali and Yusop, 2020; Zhou et al., 2012) used to describe an estimate of the average flood damage that is expected to occur each year (Arnell, 1989; Messner et al., 2007; Olsen et al., 2015). It can be approximated by estimating the area under a flood damage (or loss) – probability curve (Arnell, 1989; Dawson et al., 2008; Messner et al., 2007; Ward et al., 2011) which relates the annual exceedance probability of a flood event with the corresponding cost of damage (Dawson et al., 2008; Romali and Yusop, 2020) as expressed in Eq. 7. In practice, there are several existing methods to calculate the EAD, such as numerical integration of Eq. 7, analytical solution, and simulated time series of costs (Olsen et al., 2015). However, an adequate number of flood events must be simulated and appraised to accurately depict the shape of the curve for a better approximation of associated risks (Foudi et al., 2015). Penning-Rowsell et al. (2005) recommended that damages from at least 5 return period flood events need to be evaluated while Messner et al. (2007) suggested at least 3 and preferably 6 events with different return periods should be used. Romali and Yusop (2020) used 10, 25, 50, 100, 200, and 1000-year return periods to develop

a damage-frequency curve for an urban area in Malaysia, while Foudi et al. (2015) appraised the damages of flood events in Zaragoza, Spain with a recurrence interval of 5, 10, 25, 50, 100 and 500-year. On the other hand, Ward et al. (2011) argue that there is no enough concrete scientific basis behind this guidance due to a lack of research in this direction.

$$EAD = \int_0^1 D(P)dP \quad (7)$$

where P is the exceedance probability of a certain flood event and D(P) refers to the direct – tangible damage caused by that flood event (Arnell, 1989; Foudi et al., 2015; Verkade and Werner, 2011).

Damage-probability curves and EAD define the complete distribution of flood risk which work as complementary tools for the design of flood mitigation measures (Foudi et al., 2015) and financial risk management of insurance companies (Aerts et al., 2013). EAD assists decision-makers in determining what measures need to be prioritized in terms of both location and sector by assessing the current risk level of floods and calculating the benefits, while the loss-probability curve provides important risk-related information as to whether the risk originates from periodic flooding with smaller economic losses or from exceptional floods with greater consequences (Aerts et al., 2013; Foudi et al., 2015). The risk profile plays a crucial role in the selection of return period for determining the optimal design of flood protection measures (Foudi et al., 2015; Ward et al., 2011) and for decision-making on flood risk management policy (Messner et al., 2007).

The estimated damage costs of different flood events with return periods of 2-, 5-, 10-, 100-, 500-, and 1000-year from KRPAN calculation were used to construct the localized damage-probability curves in Piran. Subsequently, the EAD of each SLR scenario was calculated by numerical integration of the loss-probability curve using the trapezoidal rule in Eq. 8 (Olsen et al., 2015).

$$EAD = \frac{1}{2} \sum_{i=1}^n \left(\frac{1}{T_i} - \frac{1}{T_{i+1}} \right) (D_i + D_{i+1}) \quad (8)$$

where T_i is the i^{th} return period (its inverse is the probability) of a certain flood event and D_i denotes the corresponding total damage from the return period T_i .

5 RESULTS AND DISCUSSION

This chapter deals with the presentation of results and discussion of relevant implications with reference to the main objective of the study which is to evaluate the costs of flood damage under a series of sea level rise scenarios. The chapter also explains the limitations and strengths of the methodology employed in the present study and their linkages to the existing literature to ascertain whether the result supports or contradicts the existing information. Thus, the results are elaborated according to the specific areas of interest defined in the methodological framework, namely extreme value analysis, coastal flood hazard analysis, exposure assessment and flood damage estimation.

5.1 Estimates of current and scenario-based extreme sea levels

The extreme sea levels in Piran for different return periods as presented in Table 5 were estimated based on parametric extreme value analysis using a block maxima approach. GEV and Gumbel distributions were fitted to the annual maximum series of historical sea levels from the Koper mareographic station with 60 years of data. It is evident that the GEV model gives considerably higher values of extreme sea level for return periods longer than approximately 100-year compared to the values provided by ARSO (Centa et al., 2014) and from Gumbel distribution. The discrepancy between the return values from GEV and Gumbel distributions generally constitutes a practical matter of eminent significance in planning for structural flood protection measures as they are often dependent on design return periods and limited to design performance. In this account, the performance of both models was evaluated using standard diagnostic graphical checks (Coles, 2001) and a criterion-based model selection procedure that includes employing AIC and BIC indices. These goodness-of-fit criteria are based on likelihood functions that allow the selection of best-fitted distribution when the model parameters are estimated via MLE. The positive shape parameter of the GEV model in Table 6 implies a Frechet distribution of annual peak values which is characterized by a heavy-tail distribution (Koutsoyiannis, 2007). The implication of using a heavy-tailed distribution is the large probability of predicting extremely large values for higher return periods (Koutsoyiannis, 2007; Papalexiou et al., 2013). Although, several authors agreed that Frechet distribution (or EV type II) performs better in analyzing and predicting hydrological extremes compared to Gumbel due to its ability to predict more frequent and severe events (Koutsoyiannis, 2007; Moccia et al. 2021; Papalexiou et al., 2013), some studies still argued that Gumbel distribution is often used to describe the annual maximum series data and appears to provide the best fit to a given sea level data (Paprotny, 2014; Ribeiro et al., 2014; Suursaar and Sooäär, 2007).

Moreover, the adequacy of both models is assessed by using various diagnostic plots (Coles, 2001) as illustrated in Figure 13 which provides a prerequisite visual test on the consistency of GEV and Gumbel distributions with the observed data. The probability plot compares the fitted value of the distribution functions against the empirical data while a quantile – quantile (QQ) plot relates the empirical quantiles from the sample to the modelled quantiles of each data point (Coles, 2001). It is noticeable from both plots that the locus of points of the GEV and Gumbel model converges with the 1:1 reference line indicating the validity of the fitted model to the annual sea level maxima. On the other hand, the obvious dissimilarity of the return level plots can be attributed to the effect of the estimated shape parameter from GEV which renders a concave plot (curve) with no finite bound as a consequence of a positive $\xi = 0.13$ (Coles, 2001) while Gumbel ($\xi = 0$) follows the linearity of the plot. The greatest difference between the two models is in terms of their confidence intervals which describes the range in which the true value of return level lies and defines the uncertainty present in the estimate (Benstock and Cegla, 2017). GEV has a broader range of 95% point-wise confidence intervals (gray dashed lines and refer to the values in Table 5) particularly for higher recurrence intervals which signal greater

uncertainty in model extrapolation. Also, Fredriksson et al. (2016) reported that when the confidence interval becomes wider for larger return periods, the applicability of the model is no longer suitable for practical purposes. This observation can be explained by the influence of the additional shape parameter which has an inherent uncertainty about its value (Coles, 2001) that contributes to the underlying error. Finally, the corresponding density estimates favor the Gumbel model as it fits the observed data reasonably well compared to GEV. The diagnostic plots reveal a good representation of the annual maximum sea level from the Koper tide gauge station but generally lend support to the Gumbel model.

Table 5: Extreme sea level for various return periods using GEV and Gumbel distribution models (with 95% confidence interval inside the brackets)

Return Period	Sea Level Elevations (cm)		
	GEV	Gumbel	ARSO (Centa et al., 2014)
2-year	326.91 (322 – 331)	328.00 (324 – 332)	-
5-year	342.98 (336 – 350)	343.07 (337 – 349)	-
10-year	355.03 (344 – 366)	353.05 (345 – 361)	355
100-year	401.51 (355 – 448)	384.29 (370 – 398)	388
500-year	442.90 (344 – 542)	405.73 (387 – 424)	408
1000-year	463.60 (333 – 594)	414.96 (394 – 435)	419

Table 6: Distribution parameters of the GEV and Gumbel ($\xi = 0$) model (with standard error estimates inside the brackets) using MLE technique

Parameter	GEV	Gumbel
Location, μ	322.21 (1.89)	323.13 (1.80)
Scale, σ	12.52 (1.48)	13.29 (1.39)
Shape, ξ	0.13 (0.12)	0

The goodness-of-fit test results in Table 7 reveal that Gumbel distribution has lower AIC and BIC values compared to GEV which confirms that it fitted the data very well. It is further verified by a smaller standard error of estimates for the location and scale parameters of Gumbel as shown in Table 6 which represents the estimated standard deviations of each parameter indicating lower prediction errors in contrast to GEV distribution. Consequently, all four diagnostic plots along with AIC and BIC values back up the use of fitted Gumbel model for further analysis as it gives more acceptable approximation of extreme sea levels with narrower range of confidence intervals.

Table 7: Model performance of GEV and Gumbel distribution using criterion-based goodness-of-fit test

Goodness-of-fit Criteria	GEV	Gumbel
AIC	508.02	507.36
BIC	514.30	511.55

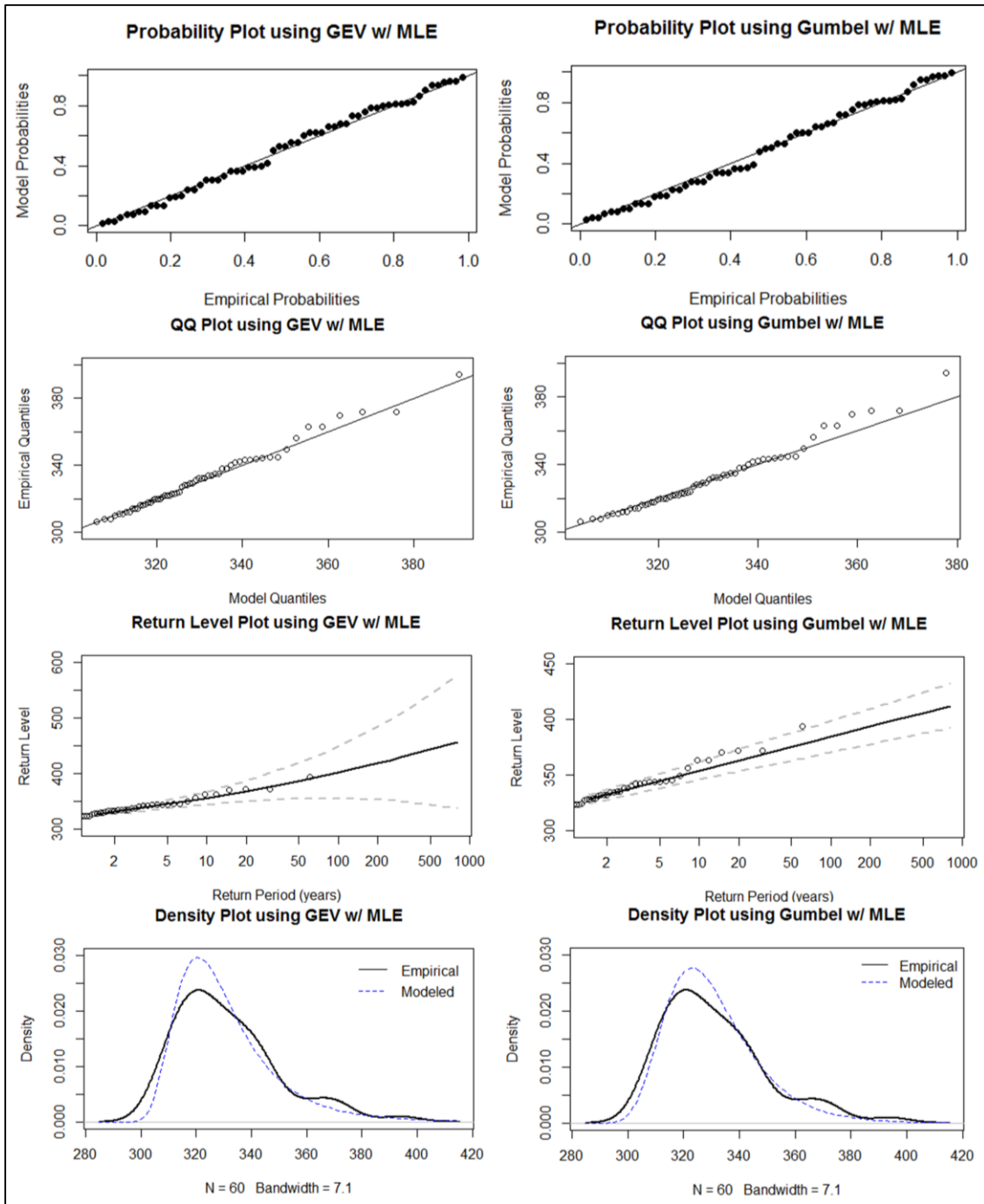


Figure 13: Diagnostic plots from fitting a GEV (left) and Gumbel (right) distribution to the annual maximum sea level dataset

5.1.1 Return period variation of extreme sea levels

The accelerating rate of sea level rise directly influences the frequency of extreme sea level events and the severity of its accompanying hazards. Once the Gumbel model is applied, the recurrence intervals of extreme sea levels were re-evaluated by considering the imminent impacts of sea level rise as a consequence of the warming global temperature. This analysis conveys information about how rising sea levels amplify the occurrence probability of rare events and change the relation of the critical threshold to the associated frequency of exceedances (Fang et al., 2021). Thus, the return period variation of extreme sea levels in Piran was estimated by superposing a series of SLR scenarios to

CEWLs. As clearly illustrated in Figure 14, the recurrence period of present extreme sea levels in Piran has declined considerably due to SLR and the downward trend is more evident under the worst-case SLR scenarios (0.84 m and 1.46 m) where the greenhouse gas emissions continue on a high trajectory of RCP 8.5 scenario. The frequency of high sea level events has already escalated significantly during the last few decades due to the 10 cm rise in the mean sea level of the Slovenian coast. The results of the evaluation in Table 8 demonstrate that an additional 10 cm increase would dramatically shift the highest recorded sea level of 394 cm in November 1969 with a return period of approximately 200 years into a 100-year event which indicates a higher probability of occurrence every year. Considering that the probable rise in sea level by 2100 is 30 cm (Ličer, 2019), the 1969 extreme event is shortened to about 25 years which is a four-fold increase in the exceedance probability and the 5-year event would become an annual occurrence at the end of 2100. Whereas, a 10-year return period event is predicted to occur more frequently under a sea level increment of 10 to 20 cm and is likely to become normal when the SLR hits 40 cm by 2100. Similarly, the 50- and 100-year recurrence intervals of CEWLs have also shortened remarkably, occurring once in every 2 – 25 years and 3 – 50 years, respectively when the SLR values are within the range of 10 to 50 cm. A significant change in larger return periods can be observed from the reduction of a 500-year to a return period of 13 – 235 years and a 1000-year to 25 – 458 years under the same series of SLR values. For low-probability high-impact scenarios, which represent the contributions of Antarctic ice-sheet melting on future SLR, the small probability events like 500- and 1000-year would drastically become an annual occurrence in Piran during a normal high tide cycle as shown in Table 8.

In general, the shortening of the extreme sea levels occurrence in Piran follows an approximate trend where every 10 cm increment in sea level is equivalent to a 50% reduction in the corresponding recurrence interval and consequently, increases the probability of occurrence by two. However, these estimates assume that the variation in extreme sea levels is a result of the direct increase of mean sea level without considering the changes in storm surge activity and other climatic conditions. Nonetheless, this is already a clear manifestation of how the future SLR modulates the extreme values of sea level which can lead to a large jump in the number of exceedances above the defined flood threshold and would markedly magnify the inundation risk in Piran.

Table 8: Average recurrence intervals of scenario extreme sea levels for different SLR projections

Return Period of CEWLs (years)	Return Period of SEWLs (years)						
	SLR1	SLR2	SLR3	SLR4	SLR5	SLR6	SLR7
2	<1	<1	<1	<1	<1	<1	<1
5	2.5	1.2	<1	<1	<1	<1	<1
10	5.2	2.5	1.2	<1	<1	<1	<1
20	10.3	5.0	2.4	1.2	<1	<1	<1
50	25.3	12.3	5.9	2.9	1.4	<1	<1
100	49.7	24.1	11.7	5.6	2.7	<1	<1
500	235.0	113.8	55.1	26.7	12.9	1.1	<1
1000	458.4	222.1	107.6	52.1	25.3	2.1	<1

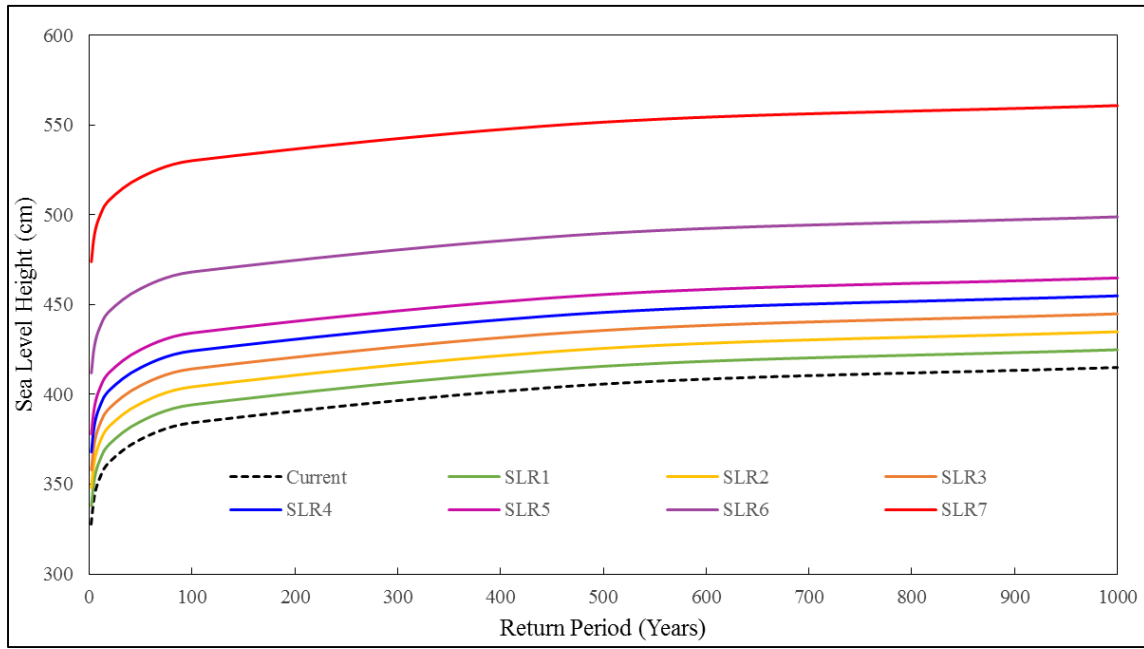


Figure 14: Changes in the return period of extreme sea levels in Piran under different sea level rise scenarios

5.2 Elevation-based inundation maps (PIAs)

The increasing risk of coastal communities to sea flooding urgently demands spatially-explicit estimates of areas vulnerable to the inexorable phenomenon of rising sea levels. In response, there is a need for local governments to develop a model-based map for areas threatened by coastal flooding and for adaptation guidance that integrates the potential effects of future sea level rise for local planning and decision-making. Mapping of the potential areas of coastal inundation in Piran for different scenarios was carried out via a GIS-based bathtub inundation model and high-resolution LiDAR DEM. The inundation modelling presented here imposes 7 sea level rise scenarios onto the Gumbel fitted extreme sea level values with a return period of 2-, 5-, 10-, 100-, 500-, and 1000-year. Figures 15 to 17 reflect the spatial extent of landward inundation in Piran for the baseline and future scenarios which were refined using the hydrologic connectivity criteria described above. While the severity of inland inundation was demonstrated by calculating its surface area as reflected in Figure 18.

The sea water primarily inundates the low-lying parts of the coastal land at a different pace depending on the return period of extremes and increments of sea level. The expanding trend of inundation would endanger the old town of Piran which is highly concentrated with economic activities, urban settlement, and cultural heritage sites (Vahter, 2006). Thus, the following inundation maps demonstrate that even for low recurrence period events, i.e. 2-year and 5-year, the promenade and Tartini Central Square are already susceptible to flooding as the latter was once part of the sea. Tartini square was originally a small inner harbor for fishing vessels until it was filled in 1894 and became ringed by historically significant buildings (Benčić, 2012), among them are the Town Hall, Venetian house, Tartini monuments, and the church of St. Peter. When the Adriatic Sea rises at least 10 cm above its present mean sea level, these scenarios dramatically expand the surface of inundation by 43% for a 2-year event and 36% for a 5-year event which further puts more important elements at risk. It is worth mentioning that even though these events including the 10-year return period are only associated with minor (less damaging) impacts, the shifts in their frequency into a normal occurrence due to sea level rise would cause huge inconveniences to the public by altering the daily economic activities in the city and compromising its present infrastructures. On one hand, Figures 16 and 17 depict that the present-day

low probability events eventually submerge the city's historic center but the further increase in the area of inundation slowly expands at a mean rate of 380 m^3 per 10 cm of SLR which could be attributed to the changes in the terrain of the area. Besides, the area at risk propagates most dynamically in 2-, 5-, and 10-year return periods with an average expansion rate of 850 m^3 per 10 cm of SLR as reflected in Figure 18. In the case of high-impact scenarios, the land area loss to flooding at 0.84 m of SLR will be 4.8 times greater than the present-day exposure of 2-year, 2.4 times of 10-year, 1.33 times of 500-year, and 1.27 times of 1000-year. These factors are magnified to 6, 2.8, 1.4, and 1.34 times, respectively for a 1.46 m of SLR which indicates that the extent of flooding does not significantly change at higher water levels. The significant slowdown in the extension variability of inundated areas for higher recurrence intervals and water levels can be attributed to the local characteristics of land topography in the area which varies from a flat coastal plain to a gently-sloping cliffs on its north side. The study of Paprotny and Terefenko (2017) observed a similar pattern at high water levels, starting at 1.5 to 5 m above MSL while Zhang et al. (2011) detected a slowdown in the pace of land inundation as the SLR reaches beyond 1.35 m. The minimal difference in the flood surface areas of 500- and 1000-year events for all SLR scenarios (Figure 18) confirms the role of topography in restricting the expansion of inundated areas during these flood events. Under these two extremely severe events, the predicted scope of flooding for a 10 to 50 cm ranges from 81,000 to 94,180 m^2 and 84,069 to 97,162 m^2 , respectively. According to these predictions, approximately 20% of the investigated land area would be inundated by 2100 given a 30 cm of SLR and heavy floods would occur during the normal tidal cycle.

The inundation analysis in the present study highlights the importance of mapping the spatial distribution of SLR-induced flooding which has a strong correlation with the terrain setting of the land and SLR scenarios. The acceleration of land inundation with respect to SLR is primarily governed by the flat and low-lying elevation of Piran and its proximity to the coastline. It is immediately evident that SLR intensifies the inundated areas and contributes to the growth rates of land exposure but its contribution is also dependent on the baseline sea level scenario. However, it is important to emphasize that the inundation effects in Piran obtained from a bathtub model do not account for dynamic factors such as erosion, wind forcing, wave action, groundwater level, vertical land movement, and future changes in storm surge activity. Several authors reported that the bathtub model overestimates the extent of inundation compared to a hydrodynamic approach (Gallien et al., 2011; Williams and Lück-Vogel, 2020; Li et al., 2009) but Cooper et al. (2013) and Anderson et al. (2019) argue that relying on the bathtub model will potentially underestimate the associated impacts of SLR-related hazards. The assessment of hydrologic connectivity constrains the spread of SLR and improves the performance of a bathtub model along with the fine-resolution of LiDAR DEM (Cooper et al., 2013) which yields a comparable result to the complex models (Breilh et al., 2013; Gesch, 2018). In the case of Piran, this specific criterion is not seen as a major problem especially in higher water levels because of its flat terrain and location with no existing large-scale flood protection structures. Still, due to the peninsular shape of Piran, the application of the bathtub model may generate an underestimation of flood extent because of its exposure to both southeasterly winds and standing waves along with cyclones and drop in air pressure could exacerbate the inundation field and boosts the depth of hazard. However, as mentioned by Ličer (2019), the tide is the chief indication of a flood warning on the Slovenian coast and SLR raises the height of the tidal system. The result confirms that SLR will trigger the Adriatic Sea to inundate the town of Piran during the normal high tide cycle even without any storm activity in the North Adriatic basin. Moreover, the most pronounced effect of SLR can be observed on the increasing depth of hazard which will then be reflected on the calculated flood damage. Overall, inundation maps facilitate the identification of areas at high risk of potential SLR alone which can be used as baseline information for impact assessment.

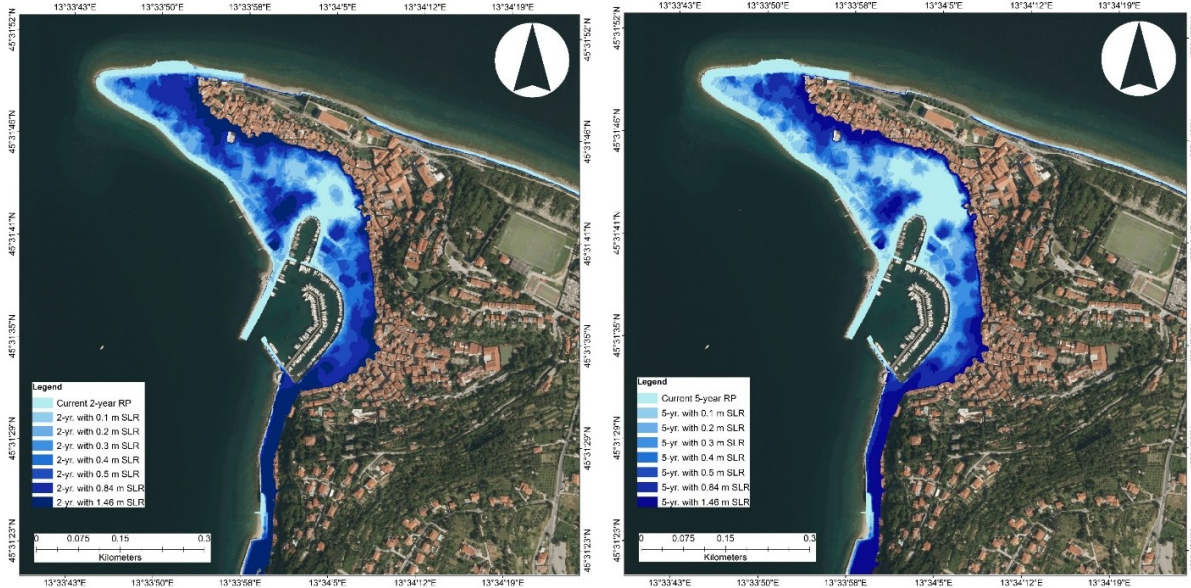


Figure 15: Inundation maps of Piran for 2-year (left) and 5-year (right) return period imposed with varying SLR values

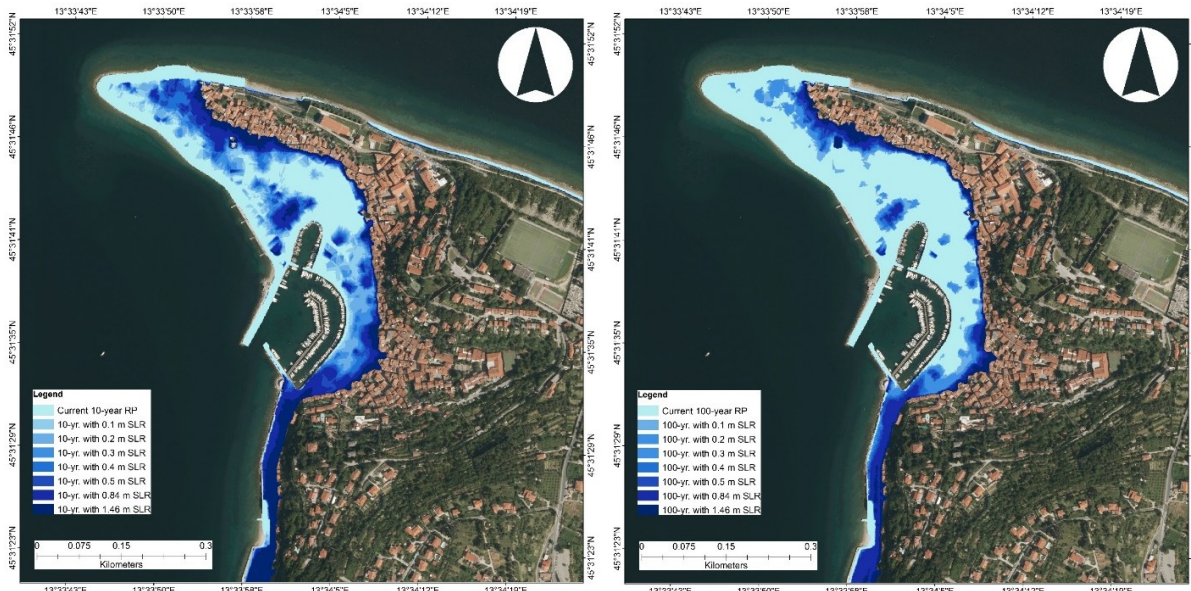


Figure 16: Inundation maps of Piran for 10-year (left) and 100-year (right) return period imposed with varying SLR values

5.3 Exposure analysis

The estimates of land inundation described above, provide the basis for estimating the exposure of population and physical elements to SLR-induced coastal flooding. Overlaying the simulated flood footprints of varying scenarios with the geospatial datasets has quantified the statistics of exposed residential buildings, non-residential properties, public infrastructures, cultural heritage, and populations located in a particular hazard scenario. The exposure of different sectoral elements in Piran depends on the spatial distribution of flood hazards which are predicted to escalate with the accelerating trend of sea level along the coast of Slovenia. The succeeding results indicate that the number of endangered populations and physical assets followed an escalating tendency, but the growth dynamic of the exposure at smaller recurrence intervals is higher compared to larger return period events particularly for a 10 to

50 cm of SLR. On one hand, when the SLR crosses this range, the number of exposed elements soars swiftly for high-impact scenarios which highlights the relative influence of long-term changes in SLR on the inundation and exposure of the city of Piran. Thus, the following exposure information for different elements is based on coastal flood events of different recurrence intervals and specified levels of SLR which could significantly help local governments in identifying which sectoral asset is mostly exposed to the hazard and in planning interventions on preparedness and response recovery.

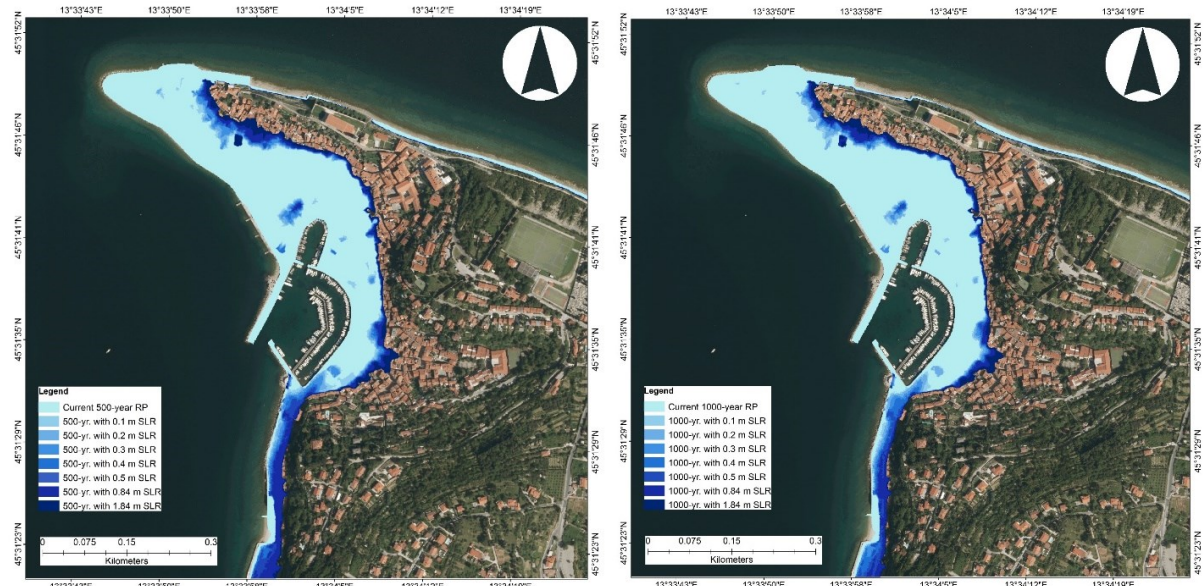


Figure 17: Inundation maps of Piran for 500-year (left) and 1000-year (right) return period imposed with varying SLR values

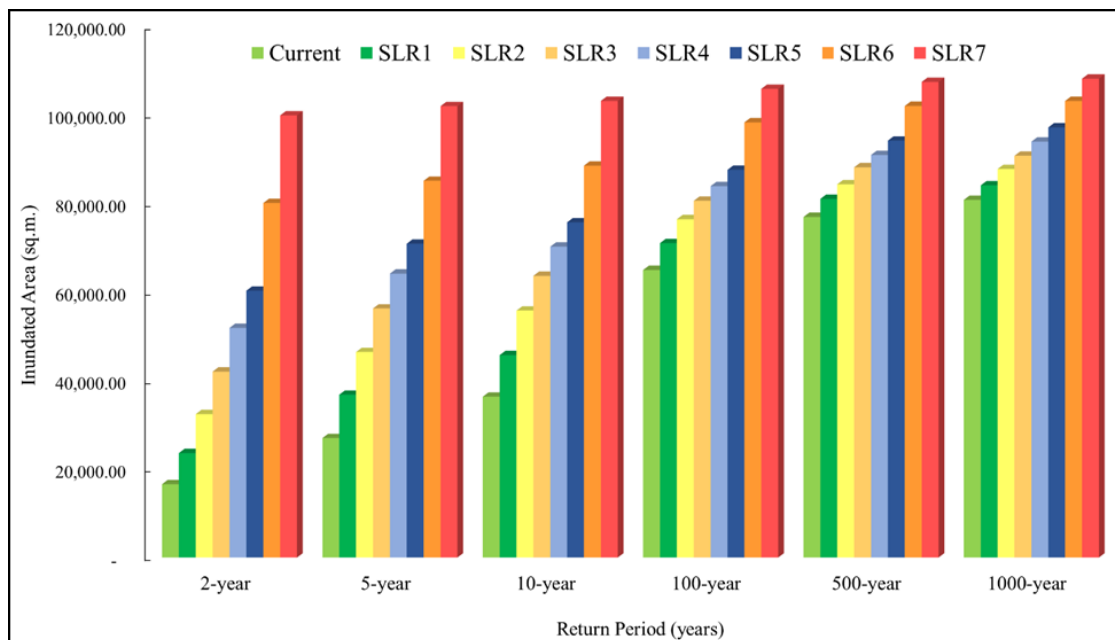


Figure 18: Inundated land area in Piran for a series of SLR scenarios

5.3.1 Population

As reported by the Slovenian Statistical Office, Piran is the most densely populated urban settlement in the country relative to its surface area (Razpotnik, 2020). Based on the 100-m population grid statistics, 3,568 inhabitants are residing within the study area and the proportion of urban dwellers is relatively higher in the low-lying city center of Piran. According to the chart presented in Figure 19, the result of exposure analysis reveals that the number of exposed populations increases proportionally with the accelerating rate of land inundation attributed to different SLR scenarios. Consequently, the current extreme sea level with a return period of 100-year is predicted to affect 939 people, accounting for 26% of the population in the study area while 1,472 people (41% of the population) are living within the 1000-year floodplain. Correspondingly, these populations will be dramatically exposed to a 12- and 108-year event in 2100 due to a 30 cm rise in sea level from its current 100- and 1000-year recurrence intervals, respectively. Additionally, a 10 cm rise in sea level will trigger the 100-, 500-, and 1000-year flood events to endanger 1,159, 1,478, and 1,620 residents, respectively. Meanwhile, 746 people are added to the affected population of the present 10-year flood and 528 people for a 100-year event when the sea level rises to 30 cm. Similarly, more than 50% of the inhabitants will be inundated more frequently by 500- and 1000-year events given a 30 to 50 cm of SLR. Once the sea level reaches 0.84 m, which corresponds to the RCP 8.5 scenario of the IPCC SROCC projection, 40 to 49% of the population will be exposed to a 2- to 10-year flood while 53 to 58% will be more prone to more extreme events. Similarly, the result of high-end SLR scenarios demonstrates that a 1.46 m of SLR is expected to impact 1,910 to 2,274 inhabitants every year, representing 54 to 64% of the total population under study.

In general, the analysis indicates that a significant number of Piran inhabitants live in the 100-year flood plain and more people are projected to be exposed to the varying magnitude of SLR, reinforcing the importance of implementing flood protection measures in the area.

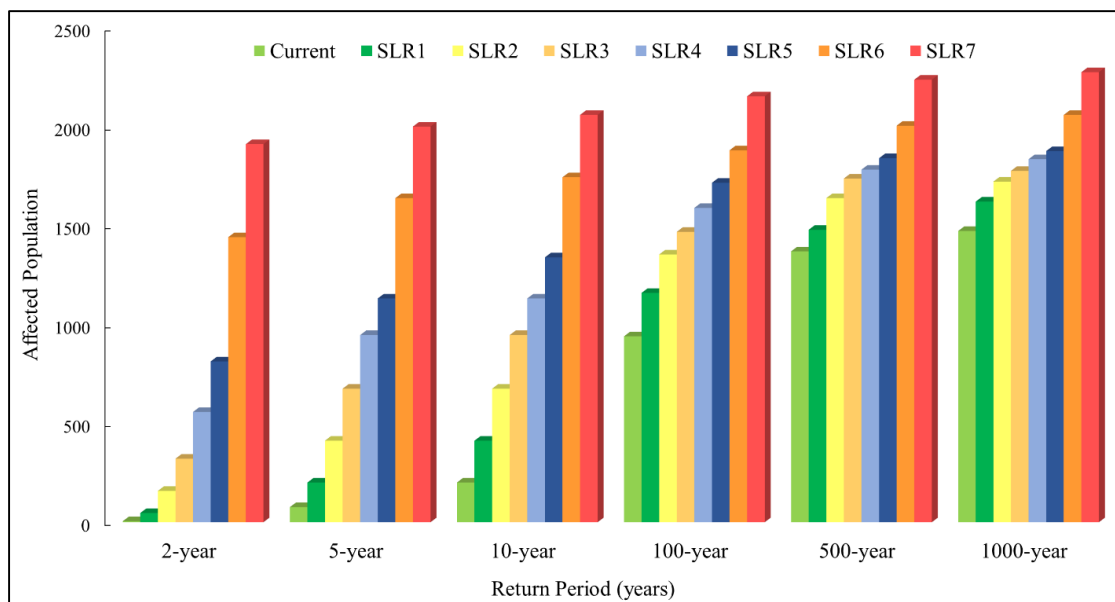


Figure 19: Number of endangered population in Piran for a series of SLR scenarios

5.3.2 Built-up structures

Built-up areas take the dominant portion of land-use in Piran accounting for 73.7% of the study domain which comprises predominantly of residential buildings. There are 1,231 buildings in the investigated area and 1,024 of them are used for dwelling purposes while the remaining 207 are classified as non-residential buildings. The Housing Act of Slovenia classifies residential buildings as single-family houses, villas, atrium houses, terraced houses, holiday houses, apartment blocks, student dormitories, workers' homes, and among others which are intended for dwelling. The act also specifies that if there are business premises within the building and more than 50% of the area is used as apartments, such building is classified as residential-commercial building (Legal Information System, 2003). Since Piran is a major tourist hotspot on the Slovenian coast, it can be expected that some parts of these dwelling spaces are used for tourist accommodation but in this study, it was not identified further which buildings are used for such purposes. Most of the buildings in Piran are located in the flood zones and residential properties are the worst affected sector in this respect as shown in Figure 20. When the sea level hits 1.41 m above MSL, which corresponds to the red warning level issued by ARSO, about 93 dwelling places and 21 non-residential buildings are expected to be flooded. The number of affected residential buildings abruptly grows to 286, 370, and 391 once the sea level crosses the red warning threshold and respectively follows the present-day 100-, 500-, and 1000-year extreme sea level heights. In the case of a 10 cm SLR, 71 to 75 more buildings are affected by 5- and 10-year floods, while on average 27 new buildings are added to the current exposure produced by less frequent events. For a 2-year scenario, 14% of the residential properties are projected to be inundated under a 30 cm SLR while 38 to 43% of them will be exposed to a more devastating sea level event by 2100. On the other hand, the share of non-residential buildings to the total exposure of built-up areas is fairly minimal as it only accounts for 17% of the total buildings inside the study domain. Despite its small proportion, it is important to note that the majority of the buildings located in the hazard zones include business establishments such as restaurants, café shops, and souvenir stores. Hence, the gradual increase in the statistics of endangered non-residential buildings (Figure 21) can be attributed to its dispersed location. Most of the affected business establishments are positioned in a strategic location that is appealing to the tourists, among them are restaurants at the seaside, museums near the Piran harbor, and souvenir shops adjacent to local roads, which makes them more vulnerable to any coastal hazards. Aside from these, a larger fraction of the local museums will be affected by the impact of coastal inundation which includes Sergej Mašera Maritime Museum, Museum of Underwater Activities, Piran Aquarium, and Magical World of Shells. In addition, the two worst-case projections of SLR for the 21st century are estimated to put more buildings at risk ranging from 443 to 625 which accounts for 36 to 51% of the total buildings under study. However, the actual number of business establishments may be greater than what is reported here because of the possibility that many independent businesses are operating under a single roof due to the monumental protection of Piran which prohibits any further developments inside the city. Also, most of these buildings regardless of their category are centuries-old and some of them have significant cultural value to the state that is under the protection of the Ministry of Culture.

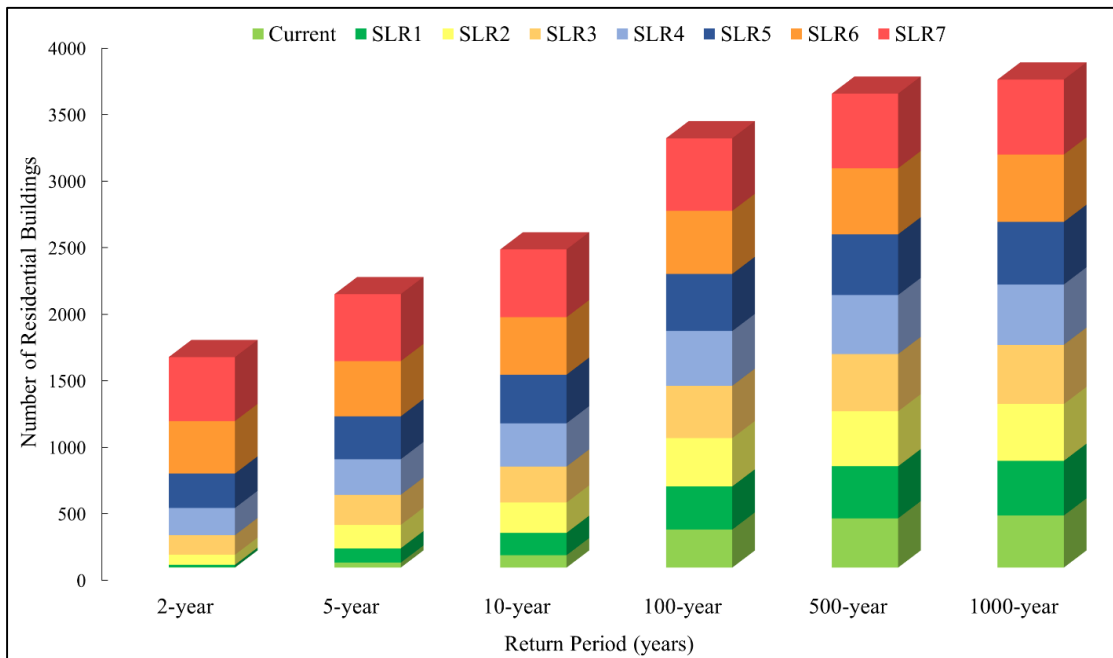


Figure 20: Number of exposed residential buildings in Piran for a series of SLR scenarios

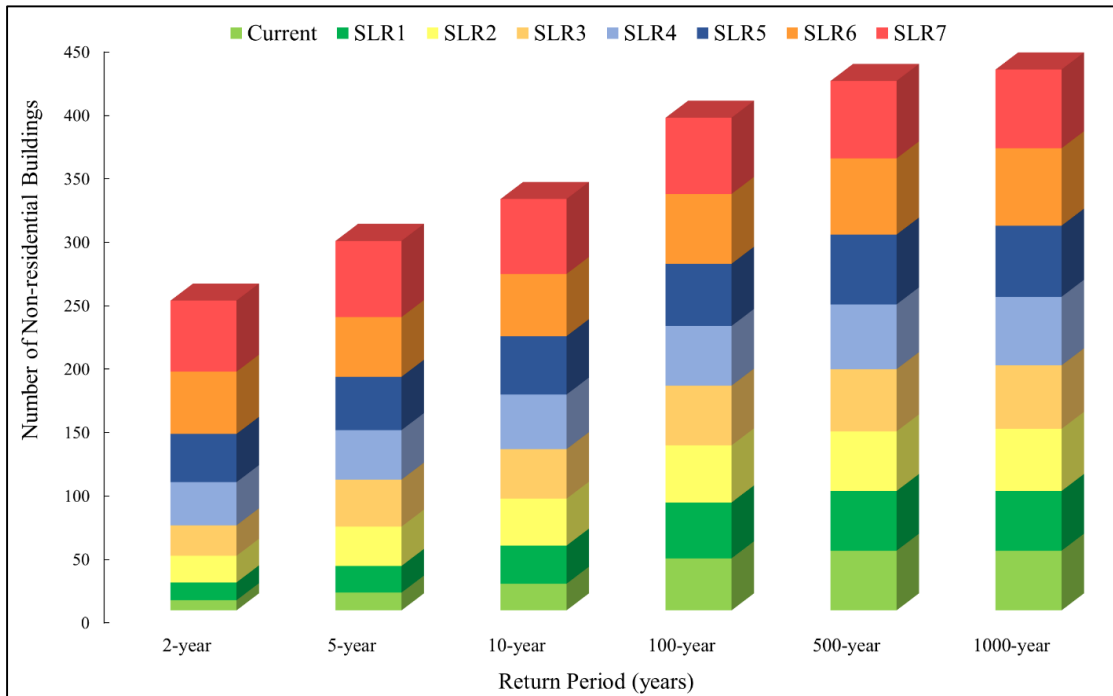


Figure 21: Number of exposed non-residential buildings in Piran for a series of SLR scenarios

5.3.3 Public infrastructures

The exposure of public infrastructures is expressed in linear meters by identifying the length of local roads, electric cables, water pipes, and sewer systems located in a particular hazard scenario. These linear infrastructure systems are also considered as critical infrastructures in this study because their failure would endanger public health, safety and economic activities, with repercussions on the entire area (Arrighi et al., 2021). The following chart in Figures 22 to 25 represents the result of exposure analysis to public infrastructures which are generally more exposed and sensitive to the varying extent of flooding than the buildings. Sewer systems are the most exposed infrastructures which is an indication

that sewage leaking and intrusion of seawater in the sewage system can be a major concern especially in the case of Piran where the design (pipe diameter) is incapacitated to carry both storm and wastewater. It is followed by water supply systems and local roads. Their individual exposure contributes to the overall impacts of sea flooding such as saltwater contamination, electric power outage, and traffic disruption. Local roads of approximately 860 m length are inundated at 1.19 m above MSL (2-year) which is almost equivalent to the yellow warning signal of ARSO while affecting 61 m of underground electric cables, 320 m of water pipes, and 1,260 m of sewers. These numbers increase dramatically with return periods and SLR scenarios. The 10 cm SLR will magnify the exposure of the following infrastructures to 3,575 m of local roads, 642 m of underground electric cable, 3,389 m of water pipes, and 6,439 m of sewers for a 100-year flood event. Underground lines for power supply, water utility, and sewage conduits are directly submerged to flood water once the sea level crosses the threshold point. More of these infrastructures are predicted to be underwater if the SLR follows the high-end scenario projections of IPCC SROCC and Kopp et al. (2017). Although below-ground infrastructure systems are designed to meet rigorous weather events and high below-ground water tables, the long-term effects of SLR-induced flooding may lead to deterioration of the system and its components, resulting in failure of its operation. The frequent exposure of buried utilities to seawater increases the rate of corrosion in water and sewer pipelines, causes separation of pipe joints, leaks, loss of bedding material, and reduction in the life span of the components which could all lead to serious consequences. The safety, health, and livelihoods of coastal communities greatly depend on the safe and continuous operation of these critical infrastructures before, during, and after a large-scale disaster (Chilsum and Matthews, 2012; Azevedo de Almeida and Mostafavi, 2016). With the aging of these infrastructures and threats of SLR, investigating their exposure is of critical importance in upgrading the design capacity of these utilities, particularly the sewer system and also, for planning adaptation pathways to ensure public safety without hampering the economic activities of the area.

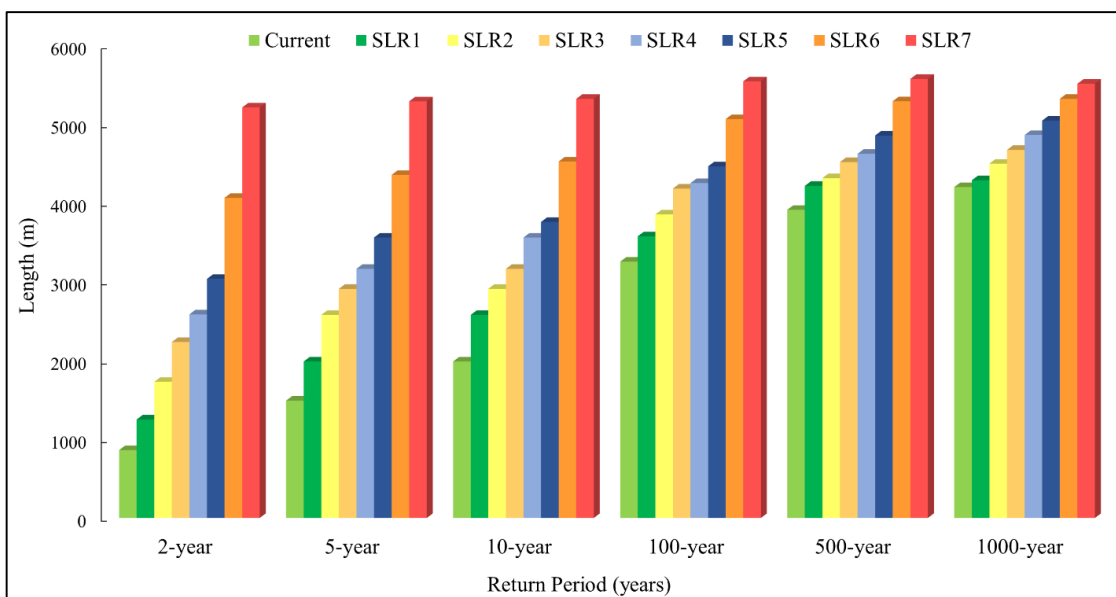


Figure 22: Estimated length of local roads exposed to a series of SLR scenarios

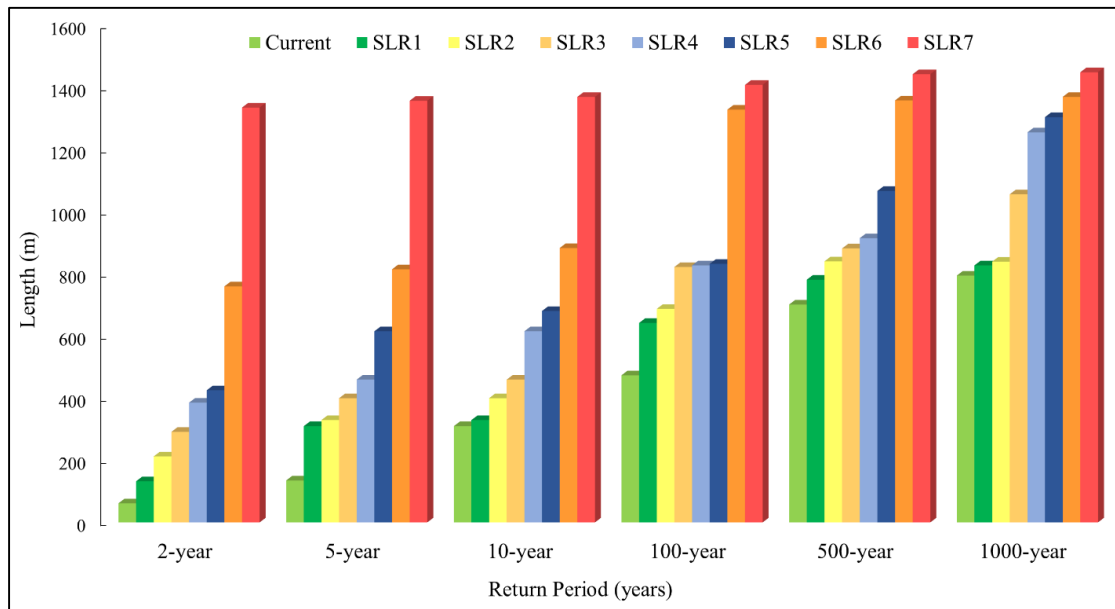


Figure 23: Estimated length of underground electric cables exposed to a series of SLR scenarios

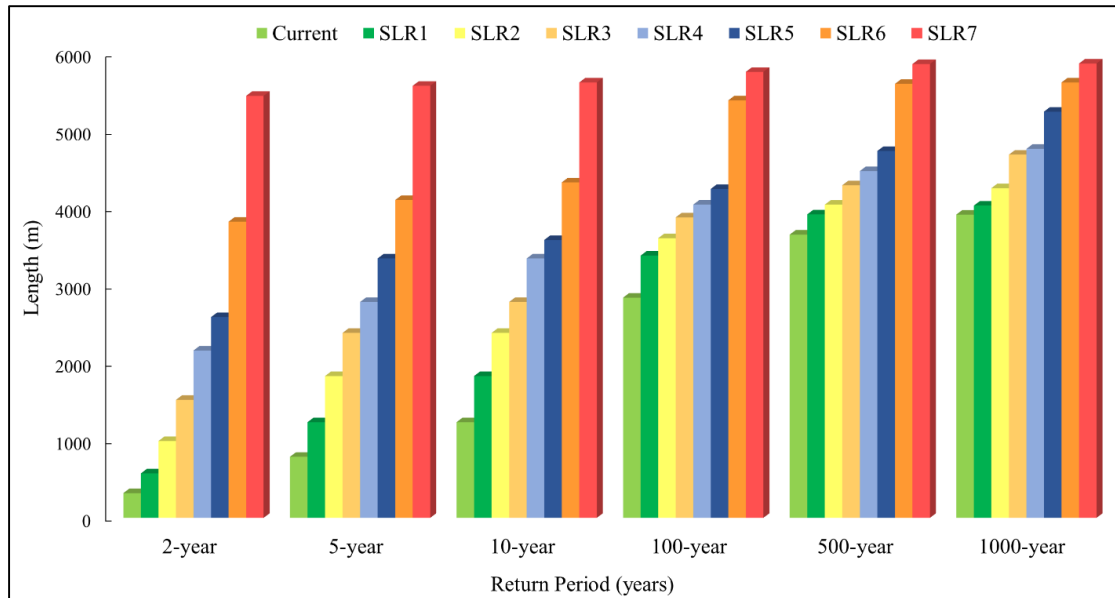


Figure 24: Estimated length of water supply networks exposed to a series of SLR scenarios

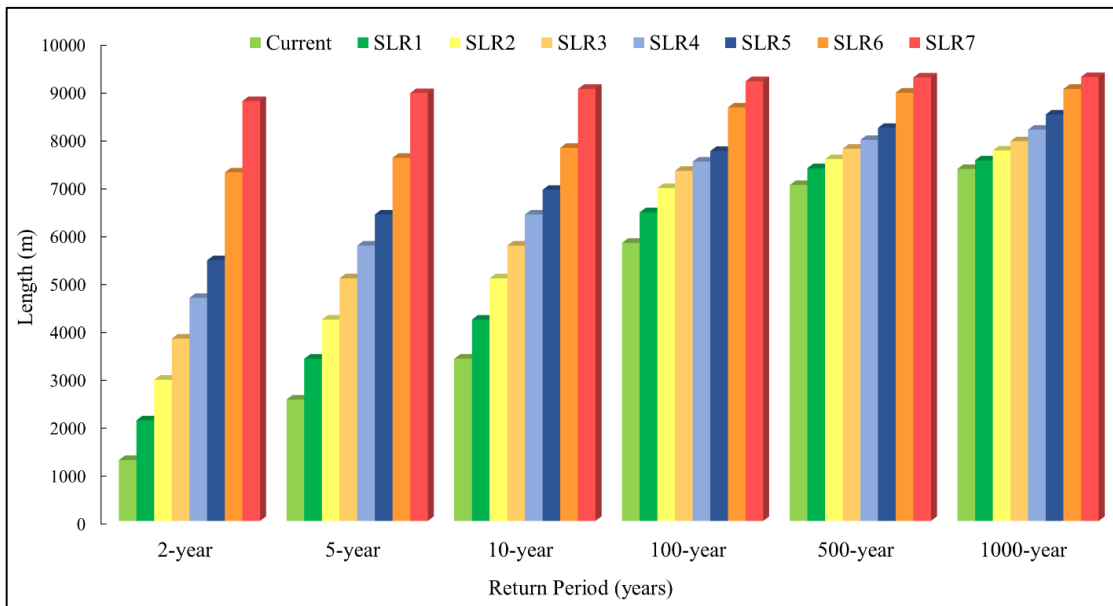


Figure 25: Estimated length of sewer systems exposed to a series of SLR scenarios

5.3.4 Cultural heritage

The integrity of cultural heritage in coastal regions is inarguably threatened by the accelerating pace of sea levels as a result of climate change which leads to degradation of the materials comprising the tangible cultural assets (Smith and ICLEI Canada, 2020; Sesana et al., 2018). The rich history and cultural heritage of Piran with many buildings and structures belonging to the category of protection and preservation are particularly at risk of rising sea levels and coastal flooding. Under every scenario, the identified 65 cultural heritage buildings and monuments in the historic center of Piran will be endangered by sea level rise and inundation. These sites include various key heritage tourism destinations in the area that attract visitors every year. Figures 26 and 27 exhibit the potential exposure of different tangible cultural heritage assets for 2-year and 1000-year return periods at varying SLR scenarios. In the lowest impact return level scenario, 17% of the currently known sites will be affected while 33 of them are expected to experience seawater inundation from a 1000-year flood. Among the most prone sites as shown in Figure 28 are Tartini square surrounded by Baroque houses, Venetian house, Tartini monument, Court Palace, Tartini's Birth house, Town hall, Piran lighthouse, Our Lady of Health Church, etc. The number of exposed cultural properties increases to 23 (35%) and 35 (54%), respectively given a 30 cm of SLR by 2100. The analysis further reveals that over 39 tangible cultural heritage assets will be exposed to sea flooding under the worst-case SLR scenarios. Overall, the medieval character and cultural features of Piran remain a vital part of the area's tourist industry today. Thus, the findings presented here highlight the need for safeguarding the cultural heritage sites of Piran against the devastating impact of future SLR to preserve its authentic image and well-developed cultural tourism.

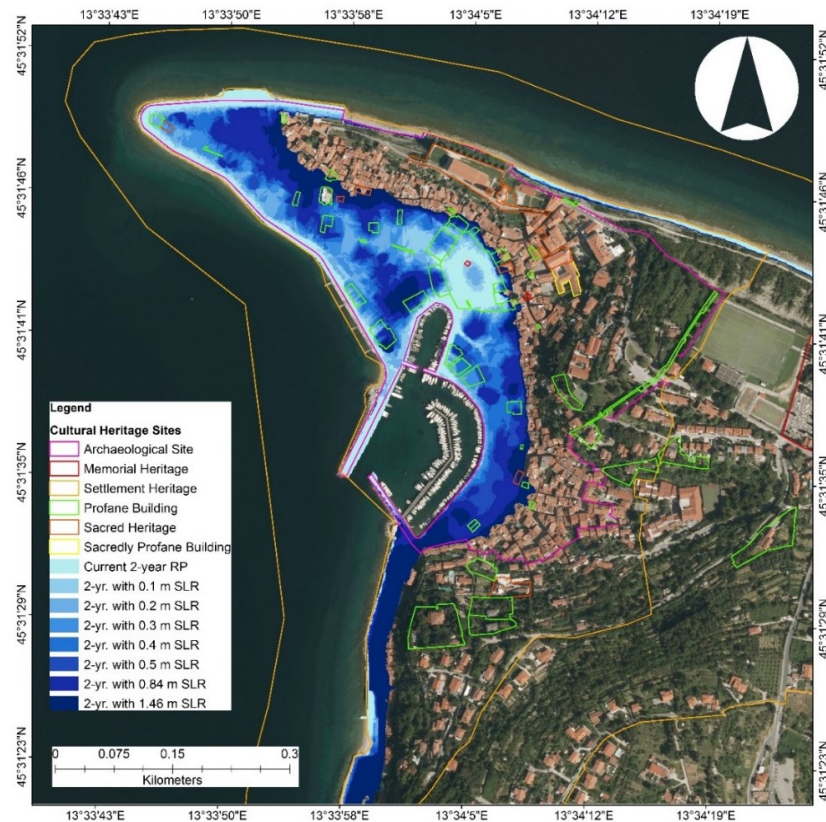


Figure 26: Endangered cultural heritage sites in Piran for 2-year return periods at different SLR scenarios

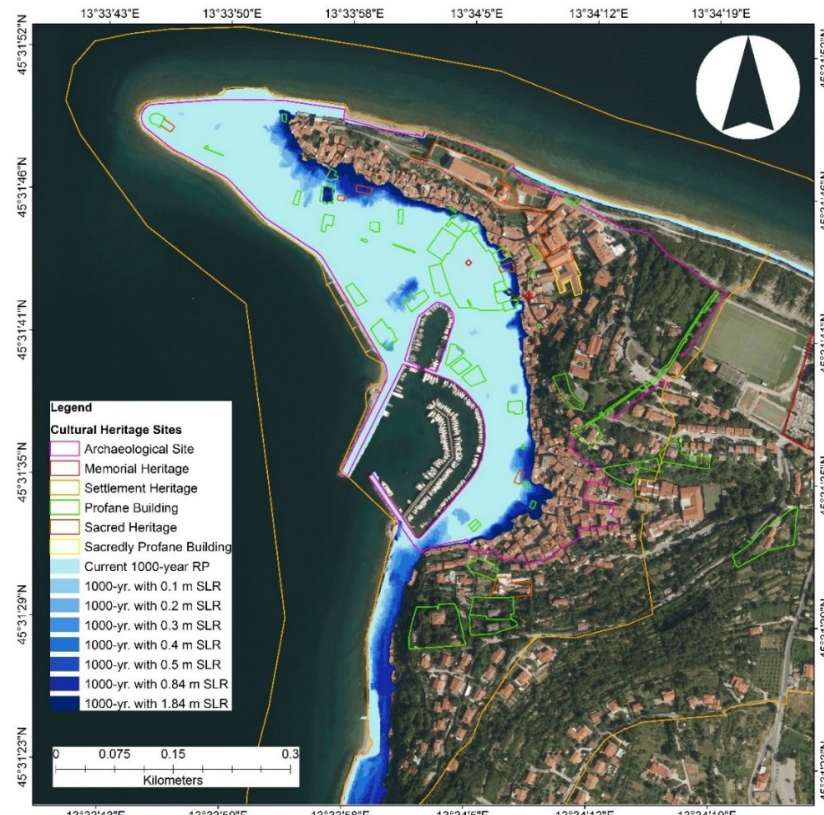


Figure 27: Endangered cultural heritage sites in Piran for 1000-year return periods at different SLR scenarios



Figure 28: Some of the most notable cultural heritage properties located in the low-lying center of Piran

5.4 Estimated costs of coastal flood damages

The estimation of flood damage for different sectors in Piran mainly focuses on the direct-tangible losses which are determined by the inundation depth as the governing parameter. The integrated information of flood extent map and water depth distribution from the bathtub model was utilized as the main inputs to the KRPAN model to calculate the cost of flood damage caused by various magnitude of extreme events and SLR. The result of the KRPAN calculation gives the estimated breakdown of damages inflicted by 6 hypothetical flood events to different sectoral entities present in the study area. It can be observed that the estimated flood damage, which ranges from 0.17 to 29 million euros (EUR), is mostly affected by the hazard components and SLR scenarios. In order to have an accurate picture of the damage situation in Piran, this study emphasized the share of calculated damages from residential buildings, business establishments, cultural heritage, public infrastructures, and the costs of cleaning, decontamination and temporary accommodation. The distribution of the evaluated damages in Figure 29 reveals that residential properties, which includes the costs of building structures and household contents, have the predominant share of flood damage estimated for a given flood return period which is congruent to the results of exposure assessment. The damage to residential properties for present-day low probability events (100-, 500-, and 1000-year) exceeds 4 million EUR with a maximum of nearly 8 million EUR in case of a 1000-year event which represents 66 to 71% of the total evaluated damage. Hence, the cost of every 10 cm rise in sea level to residential assets for these return period events is approximately 1.2 million EUR assuming no adaptation measures are undertaken. For high-occurrence events, the damage became significant with rising sea levels, the 10 cm will cause a 5-fold increase to the damage of a current 2-year event while the losses for a 5-year flood are 2.4 times higher than the baseline condition. In case the 2°C global temperature target is missed and greenhouse gas emissions continue to rise rapidly under the RCP 8.5 scenario, the costs of a 0.84 m and 1.46 m of SLR to residential properties are projected to reach approximately 9 and 15.7 million EUR, respectively. Given the shortening of the return periods of extreme sea level events, these costs of damages will be more likely in the future. For instance, a 10 cm rise in sea level will shift the occurrence of a 10-year flood

event, which is expected to cause a direct damage of 1.6 million EUR, to once in every 5 years with 20% annual exceedance probability or even a normal occurrence when the SLR hits 30 cm by 2100.

With major floods, residents may require temporary accommodation and local authorities are involved in the physical clean-up process and decontamination of inundated built-up structures. For a 100-year event, an inundated land area of 64,958 m² will cost about 41,500 EUR of cleaning and decontamination while the affected 939 inhabitants are estimated to require a temporary residence that will cost up to 0.62 million EUR. With a 10 cm of SLR, the cost of cleaning and temporary residence increases to over 1 million EUR, particularly for 500- and 1000-year floods. On average, the cumulative cost of these categories accounts for 9% of the total estimated damage for all flood scenarios. Due to the historic-cultural characteristics of Piran, the tangible losses to cultural heritage are relatively high, particularly for extreme events with recurrence levels of 100-, 500-, and 1000-year. The estimated damage for these events is between 0.35 and 0.46 million EUR which increases to a maximum of 0.65 million EUR with SLR. Interestingly, the average damage inflicted to business establishments, which also includes the damage to machinery, equipment, and supplies and the loss of revenue from micro and small companies, is only 2.4% of the expected direct losses while the proportion of public service infrastructures is quite high in lower return levels and decreases with escalating sea levels and return periods. However, it should be pointed out that the number of business enterprises in the area is relatively low compared to other activities (e.g. residential) and as previously mentioned, most of these businesses belong to the category of micro and small enterprises. Furthermore, the decreasing trend of percentage share for cultural heritage, critical infrastructures, and business properties could be explained by looking at the large increase in the accumulated damage of each scenario, which could be attributed to the contribution of residential buildings, while the increments of damage from these categories are relatively small. Other categories that follow as reflected in Figure 29 are damages to agricultural holdings and personal vehicles of which the latter has the largest fraction in this respect.

Further analysis shows that the projected SLR of 30 cm at the end of the 21st century will cause a damage of 1.3 – 11.2 million EUR to residential properties, 0.23 – 0.53 million EUR to cultural heritage, 0.14 – 0.31 million EUR to public infrastructures, 0.044 – 0.35 million EUR to business assets, and 0.24 – 1.2 million EUR of costs for cleaning and temporary accommodation. The two high-end SLR scenarios are predicted to incur a damage of 14.4 – 23.7 million EUR to residential properties, accounting for 71 – 83% of the aggregated direct losses of a specific flood return scenario. Aside from that, a current extreme water level of 1000-year, which is expected to cause 10.9 million EUR worth of damage, will become a common occurrence every year under a 1.46 m of SLR. Under these circumstances, 41% of the population, 36% of the total built-up structures, and most of the cultural heritage sites in Piran will be impacted by severe coastal flooding during normal high tide events with an assumption that the area remains unprotected.

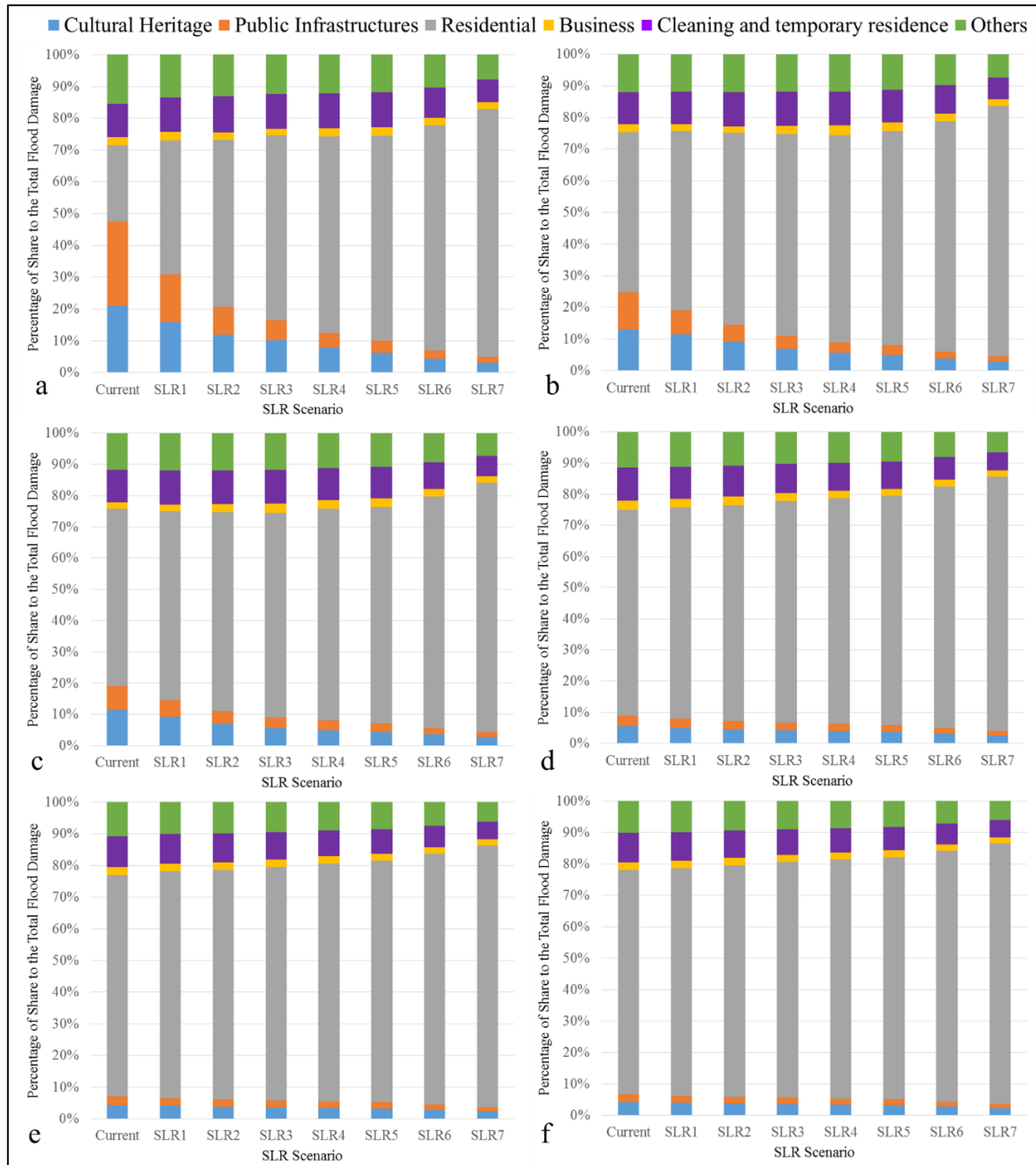


Figure 29: Shares of flood damages by sectors for (a) 2-year; (b) 5-year; (c) 10-year; (d) 100-year; (e) 500-year; and (f) 1000-year recurrence intervals at varying SLR scenarios

Based on the damage appraisals for different flood return period events, a damage-probability curve was constructed for each SLR scenario. The damage-probability curves in Figure 30 display the relationship of the potential flood losses in Piran with the exceedance probability of that damage. Apparently, the effect of SLR shifted the curve upward which indicates an increasing damage for the same probability of an event. The curves show an abrupt increase in the estimated direct damage for extreme sea level events with a probability of < 0.1 . This breaking point indicates that the damage-probability curves approximately follow a log-linear relationship of which high and low probability events follow different relations. The gentle slope of the log-linear trend for recurrence intervals smaller than 10-year denotes that the damages increase gradually with the intensity of sea level height while the steep slope of return periods higher than 10-year implies that the losses associated with these particular events escalate rapidly when sea levels are more extreme (Velasco et al., 2015). Studies of Olsen et al.

(2015) and Velasco et al. (2015) observed that a log-linear relationship exists in the flood damage curves and found a similar pattern in the shift of the curves at the 10-year return period. Thus, the propagation of the projected changes in the damage-probability curves due to SLR follows a similar trend with the return period variation of extreme sea levels as previously presented in Figure 14. These changes are markedly shown in the area beneath the curves which defines the total expected annual damage (EAD) of every SLR scenario. As being stressed above, EAD is of high interest in this study because it provides a detailed picture of the potential impacts of SLR on the cost of sea flooding in Piran. Total EAD is approximated using the trapezoidal rule (Olsen et al., 2015) to numerically integrate the 6 known combinations of the return frequency and damage estimates. EAD is often used to describe the flood risk of a given area and to estimate the benefits of implementing certain protection or adaptation measures (Aerts et al., 2013; Foudi et al., 2015; Olsen et al., 2015).

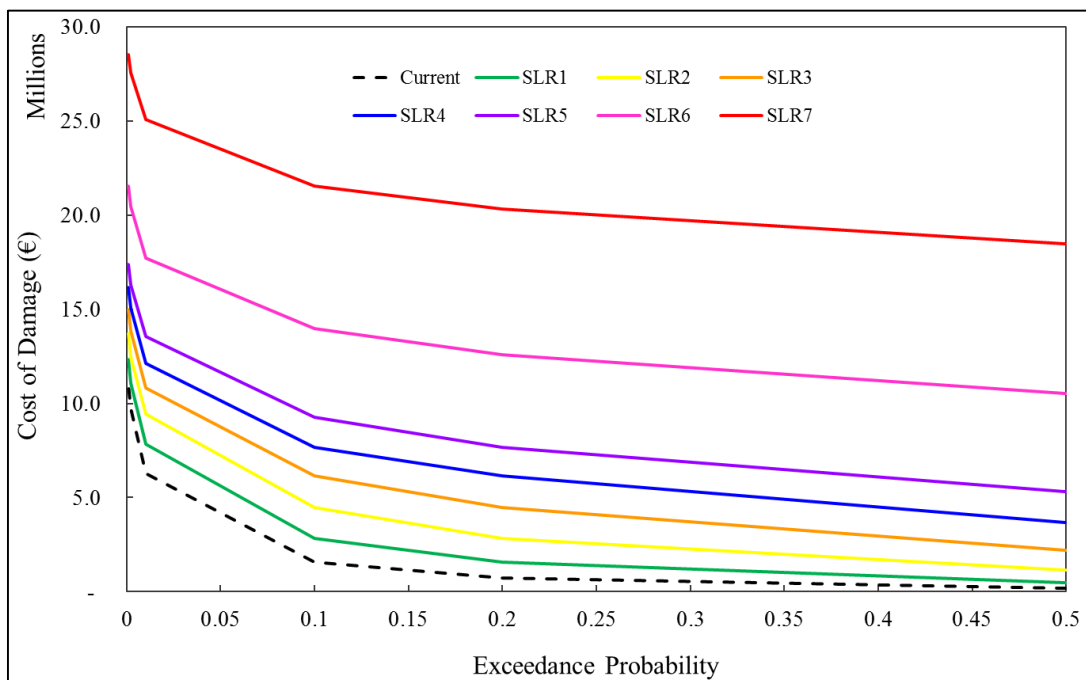


Figure 30: Damage-probability curves for Piran according to different SLR scenarios

It is immediately evident that SLR triggers an increase in the area under the damage-probability curve which corresponds to the escalation of EAD (Figure 31). The EADs from SLR-induced coastal flooding demonstrate a gradual increase between an SLR of 10 and 50 cm, but the further increments in EAD are relatively higher for the low-probability, high-impact SLR scenarios. The results of EAD calculations reveal that the aggregated cost of damage from flooding ranges from a minimum of 0.68 million EUR per annum (p.a.) for the baseline scenario to as much as 10.2 million EUR p.a. under a 1.46 m of SLR. The annual damage cost of flooding with a 10 cm SLR exceeds 1 million EUR which is 1.6 times higher than the current condition. Subsequently, the total EAD of flooding imposed with 20 cm of SLR is 2.5 times greater than the baseline value while for 30 cm, 40 cm, and 50 cm SLR, the EAD increases by a factor of 3.6, 4.7, and 5.8, respectively. However, the economic value of the damage for every 10 cm increment in sea level from 30 cm to 50 cm is nearly uniform and on average, it will cost about 0.76 million EUR p.a. Following the 30 cm SLR estimate of Ličer (2019), Piran is projected to experience a 2.4 million EUR worth of damage p.a. by 2100 from SLR-related coastal inundation. When the EAD of low-probability-high-impact SLR scenarios are considered, the losses are remarkably greater than the present-day value by a factor of about 9.4 and 15.1, respectively. Understanding the degree of risk associated with these SLR scenarios gives crucial information to city planners and

decision-makers regarding the possibility of the rapid melting of ice sheets of which its impacts should not be underestimated accordingly to planning and designing protection measures (Hinkel et al., 2015).

Additionally, analyzing the contributions of high and low-frequency events to the EAD of each SLR scenario reveals that the largest proportion of damage is attributed to more frequent events with a return period of less than 10-year. Even though extreme sea level events with a return period of more than 100-year are associated with widespread economic damage, their contributions to the EAD are reasonably low because of their small probability weights, P (see equation 7). The share of low probability events in the current scenario ranges from 12.4 – 23.1% which increases with SLR while high probability events only contribute less than 10% of the EAD. Under a 30 cm of SLR, 45.6% of the EAD is a result of a 2-year event while that of a 1000-year event is less than 1%. These results indicate that EAD is mainly governed by low consequence events due to its higher occurrence probability particularly in the case of Piran where a minor change in sea level equates to direct inundation of its low-lying zones. However, Merz et al. (2009) stressed out that extreme events with a low probability of occurrence and associated with higher damage are more significant in the societal view because such events have a devastating effect on the long-term development and economic activities of the affected area.

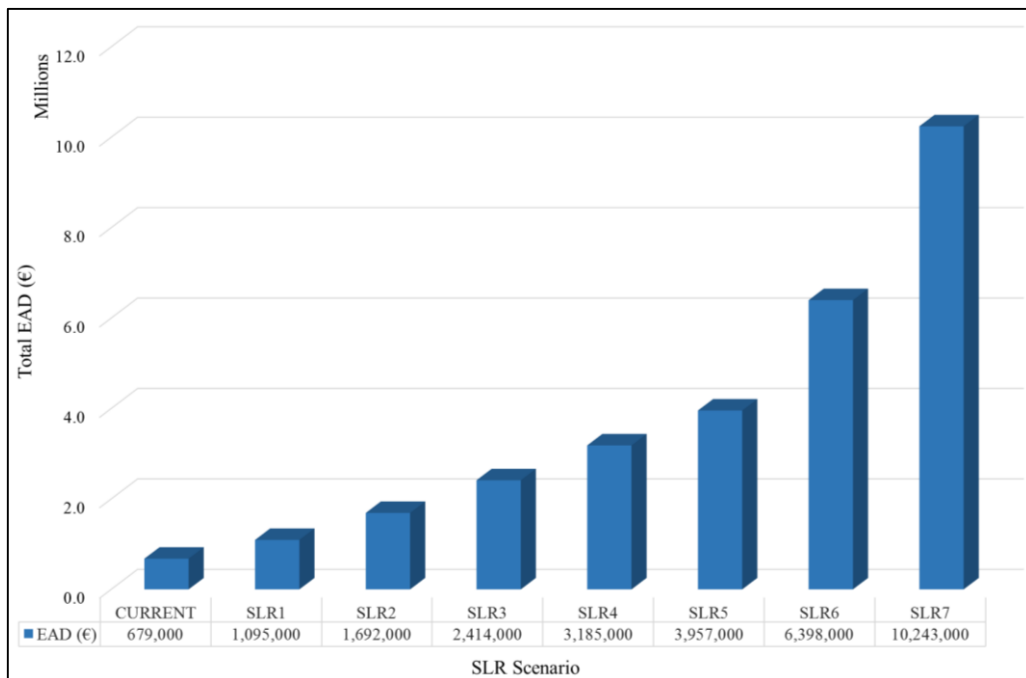


Figure 31: Total Expected Annual Flood Damage in Piran for different SLR scenarios

Figure 32 demonstrates that residential properties take the major fraction of the total EAD for all scenarios and even increases significantly with SLR, ranging from 59 – 79%. It is followed by the cumulative share of agriculture and personal vehicles which is represented as others in Figure 32. Since the area consists heavily of built-up structures and mostly are used for dwelling, the cost of cleaning after a flood event and temporary accommodation for affected residents will have a 7 – 10% share of the total EAD. On one hand, although the cultural heritage only accounts for 3 – 9% of the EAD, it is extremely important to the local identity of Piran and its preservation is of greatest concern to the state. Despite the touristic character of Piran, the business category has the lowest share in EAD even though most of the establishments are located in the most vulnerable parts of the old town. It is important to stress out that due to the monumental protection of Piran's old city center, only micro and small companies are present in the area and most of them are only operating during peak season. However, these values could be somewhat underestimated because indirect damages to businesses such as loss of

revenue are not represented entirely and satisfactorily relative to the area and the potential effect on the tourism sector is not taken into account in detail in the KRPAN model. Although the direct damage inflicted to public service infrastructures is only 2 – 7% of EAD, the indirect losses may constitute much larger share than what is simply reported here as e.g. malfunctioning of the public service infrastructure would affect many other cost categories. The shares of EAD by categories agree well with the damage estimates based on flood return period events (Figure 32) and reveal that the economic risk in Piran is borne mostly by the residential sector which also has substantial intangible values.

Overall, this study suggests that with the shortening of the recurrence intervals of extreme sea level events, the city of Piran will experience these costs of damage to properties, infrastructures, and cultural heritage more frequently in the future due to the inevitability of SLR which can lead to the paralysis of local economic activities (i.e. tourism), loss of cultural identity, and migration of residents to the hinterland.

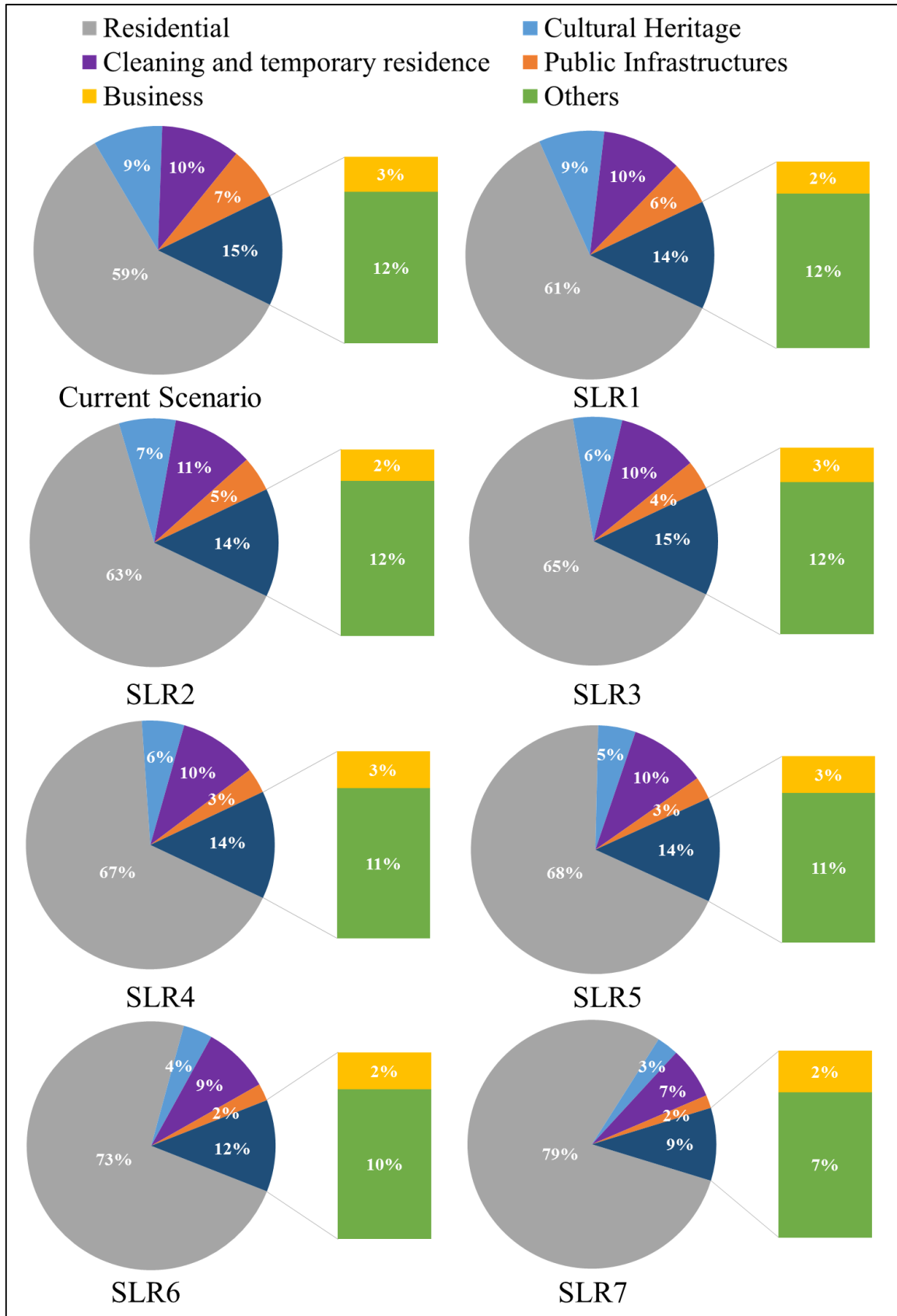


Figure 32: Shares of EAD in Piran by categories for different SLR scenarios

5.5 Response strategies and adaptation measures to reduce the impacts of SLR

In view of the significant losses inflicted to different exposed sectoral elements present in the city of Piran due to rising sea levels, there is a compelling need for a tailor-made response strategy and translating these adaptation plans into implementation. As mentioned by Nicholls (2011), the IPCC typology of planned adaptation strategies against SLR generally follows three approaches: retreat, accommodation, and protection. The retreat strategies mitigate the consequences of SLR by relocating and/or setting back existing assets out of the hazard zones or further from the coastline via land-use zoning, development controls, and other means. The accommodation strategies typically include employing methods that modify and regulate building development and increase awareness of the hazards (e.g. water proofing, elevating buildings on piles, retrofitting existing structures, improving flood warning systems). While, protection involves the use of hard (seawalls and dikes) and soft engineering measures (dunes and vegetation) in protecting the coastal plains from SLR-related hazards (Dronkers et al., 1990; Lee, 2014; Nicholls, 2011). Currently, the city of Piran is protected by submerged riprap breakwaters which are only intended to dissipate the energy of waves hitting the coast but do not provide protection against sea flooding. Moreover, local authorities are distributing flood protection sandbags and inflatable bags to the residents as part of the temporary preventive measures during flooding. It is also important to mention that the majority of the house and business owners in the city are manually installing flood barrier panels in front of their doors to prevent the sea water from entering the building and protect themselves and their assets against the direct impacts of flooding. Using the inundation maps and EAD from this study, the local governments can begin prioritizing site-specific flood protection measures in Piran that will reduce the overall severity of the impacts associated with SLR-induced flooding through cost-benefit analysis. Due to the local characteristics of Piran with high concentrations of population, economic activities, and cultural heritage in the urban core, the use of structural measures is inevitable as it offers the best option available for the adaptation of the city to rising sea levels and coastal flood hazards. This includes building a sea wall along the coastline of the city which is relatively accepted by the society as it provides a local defense for their home, infrastructures, assets, and especially for cultural heritage sites from coastal inundation. However, such measure is often limited to design performance, not well adaptable after implementation, and highly costly (i.e. construction and maintenance) with adverse environmental impacts. As part of the protection approach, installing a controlling flood barrier gate that will inflate during high tides or extreme sea level events to prevent ingress of water in the inner Mandrač of Piran delivers additional protection against direct inundation of the main Tartini Square and nearby buildings. Moreover, installing demountable or mobile temporary floodwalls is seen as an option to protect the city center from sea flooding but needs to be rigid to withstand strong winds and waves and requires efficient forecasting of sea level extremes and coordination among civil protection authorities. Any of these engineering structures could be implemented in parallel with several accommodation measures to reduce the risk of maladaptation. Under the umbrella of accommodation strategies, the local government of Piran could invest in improving the drainage facilities of the city while strengthening its flood warning system and preparedness plans. These measures do not, however, present a viable solution in protecting the vulnerable cultural heritage elements in the city Piran against the devastating effects of SLR. In this account, integrating protection and accommodation techniques may seem very costly and inconvenient to some, it provides better performance and cost-effective solutions in reducing the flood damage costs, protecting cultural heritage sites, and ensuring normal functioning of the city.

6 CONCLUSIONS AND RECOMMENDATIONS

A brief summary of the works that were carried out in this thesis was presented in this chapter together with the main findings of the study in fulfilment of the research objectives. The chapter also presents the limitations of the whole study and of the used approaches and methods. Furthermore, the applications of the outcomes and recommendations for the future development of this research are also presented below.

6.1 Summary

The accelerating rate of SLR is one of the most evident consequences of climate change which endangers the majority of the coastal areas in the world. The 10 cm rise in the sea level of the Slovenian coast in the last decades evokes widespread impacts over the historic core of the city of Piran as it experiences more frequent coastal flooding during normal high tide events. Accordingly, the sea level in the North Adriatic basin is projected to rise almost uniformly (Bonaduce et al., 2016; Ličer, 2019; Zanchettin et al., 2020) by 11.5 to 23.8 cm for the period of 2040 – 2050 (Galassi and Spada, 2014), 17 to 42 cm during 2070 – 2100 (Torresan et al., 2019), and 14 to 49 cm at the end of 21st century with the contribution of ice melt (Scarascia and Lionello, 2013). And as reported by Ličer (2019), the expected sea level rise along the coast of Slovenia is likely to be at least 30 cm by 2100. In this respect, Piran is at the greatest risk of the consequences of rising sea levels (Ministry of the Environment, Spatial Planning and Energy, 2002) as large part of the city is below 10 cm above MSL and highly concentrated with population, cultural and socio-economic values and tourism-related activities. However, there has been no study directed to analyzing the impacts of SLR on the existing coastal flood hazards and extreme sea level events in Piran which becomes the subject of the current research along with the estimation of the socio-economic costs associated with SLR.

The return periods of sea level extremes were calculated by fitting the GEV and Gumbel distributions to the block maxima of 60-year historical sea level data from the mareographic station in Koper. The performance of both distribution models was assessed using AIC and BIC goodness-of-fit criteria with visual inspections of various diagnostic plots. In this study, the impact of future SLR on the return periods of extreme sea level events was investigated by imposing seven SLR values on the CEWLs. Hence, the continuous increase in sea level will magnify both the frequency and severity of coastal flooding. Potentially inundated zones were generated using a bathtub model which integrates LiDAR-DEM and various water level scenarios in a GIS-raster environment. The inundation model that was employed here considers the hydrologic connectivity of flooded cells with each other and to the source of flooding via the eight-neighbor rule. Subsequently, each flood surface area (PIA) was overlaid to several geospatial datasets of built-up structures, 100-m population grid statistics, critical infrastructures, and cultural heritage sites to assess their exposure to a particular hazard scenario. The cost of flood damage for different scenarios was then estimated using the KRPAN model (Vidmar et al., 2019) which requires the spatial extension of flood hazard and distribution of water depth. The result of employing the KRPAN model was the breakdown of damages for each sectoral element and in this study, the losses to residential properties, cultural heritage, public infrastructures, business establishments, and the costs of cleaning and temporary accommodation were highlighted. The damage estimates based on six flood return period events (2-, 5-, 10-, 100-, 500-, and 1000-year) were used to construct the damage-probability curves of different SLR scenarios. Finally, the area under each curve was calculated using the trapezoidal rule in order to represent the expected annual flood damage of Piran for the different magnitudes of SLR.

6.2 Conclusions

The main objective of this study was to evaluate the impact of coastal flooding and the associated cost of flood damage caused by the varying magnitude of future sea level rise scenarios. Based on the results of the goodness-of-fit test, Gumbel distribution has a relatively lower Akaike Information Criterion value of 507.36 and Bayesian Information Criterion of 511.55 with a narrower range of confidence intervals compared to the GEV distribution. Lower AIC value provides a fitted likelihood function that minimizes the discrepancy measure between the observed and simulated data which indicates a good prediction performance of the approximating model (Dziak et al., 2012; Liao et al., 2009; Wong et al., 2020). Thus, the model with the smallest value of BIC implies a high posterior probability of a model being true (Dziak et al., 2012) while penalizing overparameterization more heavily than AIC (Liao et al., 2009; Wong et al., 2020). Hence, the lower values of AIC and BIC values together with visual analytics of various diagnostic plots confirmed that the current extreme sea levels (CEWLs) of Gumbel distribution was found to provide the best fit to the observed annual maximum sea level data. With rising sea levels, the recurrence intervals of these CEWLs have shortened considerably by about a factor of 2 for every 10 cm of sea level rise. Indeed, the occurrence probability of a 100-year return level declines remarkably to approximately 2% under a 10 cm of sea level rise and 8.5% for 30 cm, while a 1000-year is likely to occur once in every 458.4 and 107.6 years, respectively. The amplification of the frequency of extreme sea levels is most evident when the two high-end sea level rise scenarios trigger the 1000-year extreme sea level to be exceeded every normal high tide event (<1 return period). The shortening of recurrence intervals indicates a higher probability of flooding in the low-lying parts of the city for the next few decades.

Results from this study revealed that sea level rise magnifies the land inundation more rapidly at high probability events and earlier stages of sea level rise (10 to 30 cm). A 30 cm of sea level rise by 2100 would trigger the 2-, 5-, and 10-year events to inundate about 12% of the investigated land area annually which submerges the majority of the old town center of Piran. On average, this level of sea level rise is expected to impact 47% of the population, 38% of the total buildings of which 34% are residential buildings, 4,457 m of paved roads, 990 m of underground electric cables, 4,317 m of water distribution pipes, 7,660 m of sewers and most of the cultural heritage sites. As a result, the estimated damage of this sea level rise based on the return period events ranges from 10.8 to 15 million EUR, and approximately 73% of this damage is borne from residential buildings and household contents. A direct inundation of 22% of the study area for the same extreme events under a 0.84 m of sea level rise is predicted to endanger 40% of the residential buildings that would lead to the displacement of 76% of the residents and cause damage ranging between 17.7 and 21.5 million EUR. When the sea level rise hits 1.46 m, the entire low-lying areas of Piran would be submerged by the aforementioned extreme events affecting more than 50% of the total built-up structures and 62% of the population which leads to a mean damage of 27 million EUR. It is very clear from the result that with rising sea levels, it no longer takes a storm or gust of wind for the sea to flood the old town of Piran. While the risk of sea flooding in Piran continues to increase due to climate change-driven sea level rise, the associated economic losses are expected to escalate significantly along with the exposure of the population, properties, infrastructures, and assets. The constant exposure of critical components of lifeline infrastructure networks to frequent flooding will cause significant service disruptions in the area and even outside the flooded zone. The sewer system is among the most affected critical infrastructures in Piran which can lead to sewage leak that poses serious dangers to public health. Also, as the sea level rise drives coastal flooding to occur more frequently in higher magnitude, it is particularly pressing the cultural heritage value of Piran because majority of these historical and cultural sites are located within the inundation zone. It can also be inferred from the analysis of the results that residential properties are

principally the most at risk sector in Piran and the damage inflicted to the building structure and contents have a large contribution to the total damage.

The damage-probability curves of different sea level rise scenarios that were generated from the appraised damages of each return period event showed that the damage increases rapidly for events with an occurrence probability of less than 0.1 with over 1.2 million EUR for every 10 cm of sea level increments. Every increment in sea level has caused the curve to shift upward which signals escalating damage for the same probability of an event. The estimated economic value of a present-day 2-year event is about 0.17 million EUR which grows to 0.48 million EUR under a 10 cm of sea level rise and 2.22 million EUR for 30 cm by 2100. Whilst, a 10 cm of sea level rise is expected to cost an additional 1.4 million EUR for a 1000-year event from its baseline cost of 10.9 million EUR. This is further confirmed by the computed total EAD of each sea level rise value which increases from 0.68 million EUR per year for the current state to 1.1 million EUR per year for a sea level rise of 10 cm. Thus, assuming a 30 cm sea level rise in 2100, the annual cost of flood damage is projected to reach 2.4 million EUR which is 3.6 times higher than the present value. The EAD surges prominently under the two high-impact sea level rise scenarios when the expense of damage is estimated to be around 6.4 to 10.2 million EUR per year, which highlights the importance of considering the range of possibilities that frame the greatest risk and highest probable cost of implementing adaptation measures. The information from the damage-probability curves and EAD explains how rising sea levels lead to an unprecedented coastal flood risk level and a tremendous increase in flood damage.

Like any other studies directed to flood damage estimation, uncertainties of various kinds exist which stem from the uncertainty of underlying data and methodology limitations (Merz et al., 2004). First, the estimated return periods of extreme events do not consider the contribution and potential changes in the dynamics of storm surge activity and wave heights. The application of the static or bathtub approach in generating the extent and depth of inundation, which are key input parameters in the KRPAN model, neglects several coastal dynamic processes mentioned above. However, Breilh et al. (2013) reported that the bathtub model performs well in predicting inundation for areas with less than 3 km distance from the coastline and this is the case of Piran, practically the whole city center is less than a kilometer from the coast. Another concern is due to the unavailability of vertical land movement (e.g. due to earthquakes) and local sea level rise data, the present research only utilized the basin-wide sea level rise projections of the North Adriatic basin from previous studies with a large uncertainty range. However, this uncertainty in sea level rise projections was being handled by developing a series of sea level rise and inundation scenarios to create a considerably wide range of possible outcomes. In addition to this, the assumption of quantifying the effect of saltwater as an additional cause for unforeseen damage, accounting for 10% of the accumulated economic loss, faces uncertainty because of the long-term effects of saltwater on the structures of a building, household contents, equipment, and machinery which can be greater and more serious.

Nonetheless, the following results presented here are adequate to confirm that rising sea levels significantly contribute to the amplification of coastal flood hazards in Piran and the related damage while shortening the return periods of extreme sea level events. It highlights the need for flood protection measures and adaptation programs to deal with the increasing frequency of sea flooding. The use of high-resolution LiDAR DEM and GIS tools offers an efficient and less data-hungry approach to predicting the extent of inundation due to extreme sea level events and sea level rise. It provides an accessible communication tool for local authorities, coastal communities, state ministries and conservation managers in planning protective measures for cultural heritage elements and emergency action by identifying the hazard zones with special attention and utmost importance. The coupled information from damage-probability curves and EAD assists local governments and decision-makers in prioritizing flood protection measures that can effectively cope with the impacts of rising sea levels through cost-benefit analysis. But again, these results should be interpreted and utilized carefully with

the recognition of the study limitations and understanding the existing uncertainties is essential for detailed coastal risk management associated with the current trends of sea level rise.

6.3 Recommendations

In light of the discussion of results and aforementioned conclusions, the researcher recommends the following for further studies:

1. Inclusion of storm surges and wave setup in modelling the sea level extremes in the coast of Slovenia since the combined action of these drivers may increase the total sea level considerably which boosts the coastal flood hazard.
2. Evaluation of the performance of the bathtub inundation model in terms of flood extent by distributing random location points which will compare the observed and modeled flood surface areas through flood calibration/validation survey and fit measurement.
3. The contribution of local land subsidence in Piran, groundwater level, and storm drain backflow to SLR-induced flooding should be explored as these mechanisms are projected to exacerbate the impacts of SLR hazard.
4. In view of estimated flood damage, it is recommended to consider the direct and indirect losses to the tourism industry in Piran while differentiating the damage inflicted to tourist accommodation facilities from residential properties as the former may include considerable loss of revenues.

7 REFERENCES

- Aerts, J. C. J. H., Lin, N., Botzen, W., Emanuel, K., & de Moel, H. (2013). Low-Probability Flood Risk Modeling for New York City. *Risk Analysis*, 33(5), 772–788. Doi:10.1111/risa.12008
- Alahmadi, F., Rahman, N. A., & Abdulrazzak, M. (2014). Evaluation of the best fit distribution for partial duration series of daily rainfall in Madinah, western Saudi Arabia. *Proceedings of the International Association of Hydrological Sciences*, 364, 159–163. Doi:10.5194/piahs-364-159-2014
- Anderson, T. R., Fletcher, C. H., Barbee, M. M., Romine, B. M., Lemmo, S., & Delevaux, J. M. S. (2019). Publisher Correction: Modeling multiple sea level rise stresses reveals up to twice the land at risk compared to strictly passive flooding methods. *Scientific Reports*, 9(1). Doi:10.1038/s41598-019-45275-z
- Arnell, N. W. (1989). Expected Annual Damages and Uncertainties in Flood Frequency Estimation. *Journal of Water Resources Planning and Management*, 115(1), 94–107. Doi:10.1061/(asce)0733-9496(1989)115:1(94)
- Arrighi, C., Pagnolato, M., & Castelli, F. (2021). Indirect flood impacts and cascade risk across interdependent linear infrastructures. *Natural Hazards and Earth System Sciences*, 21(6), 1955–1969. Doi:10.5194/nhess-21-1955-2021
- Aucan, J. (2018) Effects of Climate Change on Sea Levels and Inundation Relevant to the Pacific Islands.
Pacific Marine Climate Change Report Card: Science Review 2018, pp 43-49.
<https://solomonislands-data.sprep.org/dataset/effects-climate-change-sea-levels-and-inundation/resource/c53c9689-1104-4c7d-84f8>
- Azevedo de Almeida, B., & Mostafavi, A. (2016). Resilience of Infrastructure Systems to Sea-Level Rise in Coastal Areas: Impacts, Adaptation Measures, and Implementation Challenges. *Sustainability*, 8(11), 1115. Doi:10.3390/su8111115
- Bali, T. G. (2003). The generalized extreme value distribution. *Economics Letters*, 79(3), 423–427. Doi:10.1016/s0165-1765(03)00035-1
- Ballu, V., Bouin, M.-N., Siméoni, P., Crawford, W. C., Calmant, S., Boré, J.-M., ... Pelletier, B. (2011). Comparing the role of absolute sea-level rise and vertical tectonic motions in coastal flooding, Torres Islands (Vanuatu). *Proceedings of the National Academy of Sciences*, 108(32), 13019–13022. Doi:10.1073/pnas.1102842108
- Bamber, J. L., Oppenheimer, M., Kopp, R. E., Aspinall, W. P., and Cooke, R. M. (2019). Ice sheet contributions to future sea-level rise from structured expert judgment. *Proceedings of the National Academy of Sciences*, 116(23), 11195–11200. Doi:10.1073/pnas.1817205116
- Bella, N., Dridi, H., & Kalla, M. (2020). Statistical modeling of annual maximum precipitation in Oued El Gourzi Watershed, Algeria. *Applied Water Science*, 10(4). Doi:10.1007/s13201-020-1175-6
- Benčič, N. (2012). Embrace Piran. Tourist Board Portorož. Piran, Slovenia (M. Perpar, Trans.).
<http://www.portoroz.si/si/files/default/PDF/Tiskovine/objemi-piran-zgibanka-eng.pdf>
- Benčič, N. (2018). Istria Slovenia: Koper, Izola, Piran, Portorož (V. Radulovič, Trans). Spirit Slovenia. Ljubljana, Slovenia. <https://www.slovenia.info/en/places-to-go/attractions/piran-and-salt-pans>
- Benstock, D., & Cegla, F. (2017). Extreme value analysis (EVA) of inspection data and its uncertainties. *NDT & E International*, 87, 68–77. Doi:10.1016/j.ndteint.2017.01.008
- Bezak, N., Brilly, M., & Šraj, M. (2014). Comparison between the peaks-over-threshold method and the annual maximum method for flood frequency analysis. *Hydrological Sciences Journal*, 59(5), 959–977. Doi:10.1080/02626667.2013.831174
- Blatnik, T. K. (2019 November 22). V obalnih mestih škoda zaradi poplav ob visoki plimi večmilijonska (In coastal cities, flood damage at high tide is in the millions). RTV Slo MMC.
<https://www.rtvslo.si/okolje/vreme/v-obalnih-mestih-skoda-zaradi-poplav-ob-visoki-plimi-vecmilijonska/505705>
- Bonaduce, A., Pinardi, N., Oddo, P., Spada, G., and Larnicol, G. (2016). Sea-level variability in the Mediterranean Sea from altimetry and tide gauges. *Climate Dynamics*, 47(9-10), 2851–2866. Doi:10.1007/s00382-016-3001-2

- Breilh, J. F., Chaumillon, E., Bertin, X., and Gravelle, M. (2013). Assessment of static flood modeling techniques: application to contrasting marshes flooded during Xynthia (western France). *Natural Hazards and Earth System Sciences*, 13(6), 1595–1612. Doi:10.5194/nhess-13-1595-2013
- Breili, K., Simpson, M. J. R., Klokkervold, E., and Roaldsdotter Ravndal, O. (2020). High-accuracy coastal flood mapping for Norway using lidar data, *Nat. Hazards Earth Syst. Sci.*, 20, 673–694. <https://Doi.org/10.5194/nhess-20-673-2020>
- Bureau of Transport and Regional Economics (BTR). (2002). Benefits of flood mitigation in Australia. Report 106. Canberra, Australia. https://www.bitre.gov.au/sites/default/files/report_106.pdf
- Büchele, B., Kreibich, H., Kron, A., Thielen, A., Ihringer, J., Oberle, P., ... Nestmann, F. (2006). Flood-risk mapping: contributions towards an enhanced assessment of extreme events and associated risks. *Natural Hazards and Earth System Sciences*, 6(4), 485–503. Doi:10.5194/nhess-6-485-2006.
- Burnham, M. W. and Davis, D. W. (1997). Risk-based analysis for flood damage reduction studies. *Proceedings on Hydrology and Hydraulics*. United States Army Corps of Engineers Hydrologic Engineering Center, California, USA. <https://www.hec.usace.army.mil/publications/SeminarProceedings/SP-28.pdf>
- Burton, T. I. (2016 June 9). Slovenia's Seaside Paradise: Piran. National Geographic. <https://www.nationalgeographic.com/travel/article/slovenia-secret-seaside-paradise-piran-adriatic-sea-balkan>
- Carillo, A., Sannino, G., Artale, V., Ruti, P. M., Calmanti, S., and Dell'Aquila, A. (2012). Steric sea level rise over the Mediterranean Sea: present climate and scenario simulations. *Climate Dynamics*, 39(9-10), 2167–2184. Doi:10.1007/s00382-012-1369-1
- Casas, A., Lane, S. N., Yu, D., and Benito, G. (2010). A method for parameterising roughness and topographic sub-grid scale effects in hydraulic modelling from LiDAR data. *Hydrology and Earth System Sciences*, 14(8), 1567–1579. Doi:10.5194/hess-14-1567-2010
- Central, M., Peček, M., Đurović, B., Gosar, L., Zupančič, G. (2014). Izdelava kart poplavne nevarnosti in kart razredov poplavne nevarnosti za dve območji pomembnega vpliva poplav v Republiki Sloveniji: Naloga I/2/1. Inštitut za vode Republike Slovenije. Slovenia, Ljubljana. http://www.statika.evode.gov.si/fileadmin/direktive/FD_P/2014/2014_I_2_01_P_01.pdf
- CEIWR-HEC. (2016 April). HEC-FDA Flood Damage Reduction Analysis: User's Manual Version 1.4.1. USACE, California. https://www.hec.usace.army.mil/software/hec-fda/documentation/CPD-72_V1.4.1.pdf
- Chang, B., Guan, J., and Aral, M. M. (2013). Modeling Spatial Variations of Sea Level Rise and Corresponding Inundation Impacts: A Case Study for Florida, USA. *Water Quality, Exposure and Health*, 6(1-2), 39–51. Doi:10.1007/s12403-013-0099-x
- Charras-Garrido, M. and Lezaud, P. (2013). Extreme Value Analysis: an Introduction. *Journal de la Societe Française de Statistique, Societe Française de Statistique et Societe Mathematique de France*, 154 (2), pp 66-97. <https://hal-enac.archives-ouvertes.fr/hal-00917995/document>
- Chisolm, E. I., & Matthews, J. C. (2012). Impact of Hurricanes and Flooding on Buried Infrastructure. *Leadership and Management in Engineering*, 12(3), 151–156. Doi:10.1061/(asce)lm.1943-5630.0000182
- Church, J.A., Clark, P.U., Cazenave, A., Gregory, J.M., Jevrejeva, S., Levermann, A., Merrifield, M.A., Milne, G.A., Nerem, R.S., Nunn, P.D., Payne, A.J., Pfeffer, W.T., Stammer, D., Unnikrishnan, A.S., 2013. Sea level change. In: Climate Change 2013: The Physical Science Basis. Contribution of Working Group I to the Fifth Assessment Report of the Intergovernmental Panel on Climate Change, T.F. Stocker, D. Qin, G.-K. Plattner, M. Tignor, S.K. Allen, J. Boschung, A. Nauels, Y. Xia, V. Bex and P.M. Midgley (Eds.). Cambridge University Press, Cambridge, UK and New York
- Coles, S. (2001). An Introduction to Statistical Modeling of Extreme Values. Springer Series in Statistics. Doi:10.1007/978-1-4471-3675-0
- Cooper, H., Fletcher, C., Chen, Q., and Barbee, M. (2013). Sea-level rise vulnerability mapping for adaptation decisions using LiDAR DEMs. *Progress in Physical Geography*. 10.1177/0309133313496835. https://www.researchgate.net/publication/258235472_Sea-level_rise_vulnerability_mapping_for_adaptation_decisions_using_LiDAR_DEMs

- Cooper, H. M., Chen, Q., Fletcher, C. H., and Barbee, M. M. (2012). Assessing vulnerability due to sea-level rise in Maui, Hawai'i using LiDAR remote sensing and GIS. *Climatic Change*, 116(3-4), 547–563. Doi:10.1007/s10584-012-0510-9
- Council of the European Communities. (2007). Directive 2007/60/EC of the European Parliament and of the Council of 23 October 2007 on the Assessment and Management of Flood Risks. Official Journal of European Union. <https://www.envir.ee/sites/default/files/flooddirective.pdf>
- Dasgupta, S., Laplante, B., Murray, S., and Wheeler, D. (2009). Climate Change and the Future Impacts of Storm-Surge Disasters in Developing Countries. *SSRN Electronic Journal*. Doi:10.2139/ssrn.1479650
- Davis S. A. and Skaggs, L. L. (1992). Catalog of Residential Depth-Damage Functions used by US Army Corps of Engineers in flood damage estimation: IWR Report 92-R-3. USACE Institute for Water Resources, Washington, DC. <https://usace.contentdm.oclc.org/digital/collection/p16021coll2/id/6789/>
- Dawson, R. J., Speight, L., Hall, J. W., Djordjevic, S., Savic, D., & Leandro, J. (2008). Attribution of flood risk in urban areas. *Journal of Hydroinformatics*, 10(4), 275–288. Doi:10.2166/hydro.2008.054
- DeConto, R. M., and Pollard, D. (2016). Contribution of Antarctica to past and future sea-level rise. *Nature*, 531(7596), 591–597. Doi:10.1038/nature17145
- De Moel, H., Jongman, B., Kreibich, H., Merz, B., Penning-Rowsell, E., & Ward, P. J. (2015). Flood risk assessments at different spatial scales. *Mitigation and Adaptation Strategies for Global Change*, 20(6), 865–890. Doi:10.1007/s11027-015-9654-z
- Deu, Ž. (2016). Dragocenosti starih mestnih jeder: monografija zgodovinskih mest Slovenije (J. Jarc, Trans.). Združenje zgodovinskih mest Slovenije. <https://issuu.com/simonpavlic/docs/dragocenosti-mestnih-jeder-issuu>
- Dronkers, J. Gilbert, J. T. E., Butler, L.W., Carey, J.J., Campbell, J., James , E., McKenzie, C., Misdorp, R., Quin, N., Ries, K.L., Schroder, P.C., Spradley, J.R., Titus, J.G., Vallianos, L. von Dadelszen, and J. (1990). Strategies for Adaption to Sea Level Rise. Report of the IPCC Coastal Zone Management Subgroup: Intergovernmental Panel on Climate Change. Geneva: Intergovernmental Panel on Climate Change. <http://papers.risingsea.net/IPCC-1990-Strategies-for-Adaption-to-Sea-Level-Rise.html>
- Doyle, T.W., Chivoiu, Bogdan, and Enwright, N.M. (2015). Sea-level rise modeling handbook—Resource guide for coastal land managers, engineers, and scientists: U.S. Geological Survey Professional Paper 1815, 76 p. <http://dx.doi.org/10.3133/pp1815>.
- Dutta, D., Herath, S., and Musiake, K. (2003). A mathematical model for flood loss estimation. *Journal of Hydrology*, 277(1-2), 24–49. Doi:10.1016/s0022-1694(03)00084-2
- Dziak, J. J., Coffman, D. L., Lanza, S. T., & Li, R. (12 June 2012). Sensitivity and specificity of information criteria. The Methodology Center, The Pennsylvania State University. <https://www.methodology.psu.edu/files/2019/03/12-119-2e90hc6.pdf>
- Elkabbany, M. F. (2019). Sea Level Rise Vulnerability Assessment for Abu Dhabi, United Arab Emirates (Publication No. 8998495) [Master's Thesis, Lund University]. LUP Student Papers, Lund University Libraries. <https://lup.lub.lu.se/student-papers/search/publication/8998495>
- Ernst, J., Dewals, B.J., Detrembleur, S., Archambeau, P., Erpicum, S., Pirotton, M., 2010. Micro-scale flood risk analysis based on detailed 2D hydraulic modelling and high resolution geographic data. *Natural Hazards*, 55(2), pp.181-209. Doi:10.1007/s11069-010-9520-y
- Erpicum, S., Dewals, B., Archambeau, P., Detrembleur, S., Pirotton, M., 2010. Detailed inundation modelling using high resolution DEMs. *Engineering Applications of Computational Fluid Mechanics*, 4(2), pp.196-208. Doi:10.1080/19942060.2010.11015310
- ESRI. (2020). Region Group—Help|ArcGIS for Desktop. <https://desktop.arcgis.com/en/arcmap/10.3/tools/spatial-analyst-toolbox/region-group.htm> (accessed on 27 May 2021)
- European Environment Agency (EEA). (2020 December 11). Global and European Sea Level Rise. European Union. <https://www.eea.europa.eu/data-and-maps/indicators/sea-level-rise-7/assessment>
- Fang, J., Wahl, T., Zhang, Q., Muis, S., Hu, P., Fang, J., ... Shi, P. (2021). Extreme sea levels along coastal China: uncertainties and implications. *Stochastic Environmental Research and Risk Assessment*, 35(2), 405–418. Doi:10.1007/s00477-020-01964-0

- FEMA. (2020). HAZUS-MH MR4 Flood Model Technical Manual, Federal Emergency Management Agency, Mitigation Division, Washington, DC. https://www.fema.gov/sites/default/files/2020-09/fema_hazus_flood-model_technical-manual_2.1.pdf
- Feng, A., Gao, J., Wu, S., Liu, L., Li, Y., & Yue, X. (2018). Assessing the inundation risk resulting from extreme water levels under sea-level rise: a case study of Rongcheng, China. *Geomatics, Natural Hazards and Risk*, 9(1), 456–470. Doi:10.1080/19475705.2018.1447026
- Fereshtehpour, M., & Karamouz, M. (2018). DEM Resolution Effects on Coastal Flood Vulnerability Assessment: Deterministic and Probabilistic Approach. *Water Resources Research*, 54(7), 4965–4982. Doi:10.1029/2017wr022318
- Foudi, S., Osés-Eraso, N., & Tamayo, I. (2015). Integrated spatial flood risk assessment: The case of Zaragoza. *Land Use Policy*, 42, 278–292. Doi:10.1016/j.landusepol.2014.08.002
- Fredriksson, C., Tajvidi, N., Hanson, H., & Larson, M. (2016). Statistical analysis of extreme sea water levels at the Falsterbo Peninsula, South Sweden. <https://www.semanticscholar.org/paper/STATISTICAL-ANALYSIS-OF-EXTREME-SEA-WATER-LEVELS-AT-Fredriksson-Tajvidi/45ebf40335850e63112dce70275f0d73ccb887cd>
- Fu, X., & Song, J. (2017). Assessing the Economic Costs of Sea Level Rise and Benefits of Coastal Protection: A Spatiotemporal Approach. *Sustainability*, 9(8), 1495. Doi:10.3390/su9081495
- Gabrovec, M. and Kladnik, D. (1997). Some new aspects of land use in Slovenia. *Geografski zbornik* 37:7–64. https://www.researchgate.net/publication/265063286_SOME_NEW_ASPECTS_OF_LAND_USE_IN_SLOVENIA_NEKAJ_NOVIH_VIDIKOV_RABE_TAL_V_SLOVENIJI_Some_New_Aspects_of_Land_Use_in_Slovenia
- Galassi, G., and Spada, G. (2014). Sea-level rise in the Mediterranean Sea by 2050: Roles of terrestrial ice melt, steric effects and glacial isostatic adjustment. *Global and Planetary Change*, 123, 55–66. Doi:10.1016/j.gloplacha.2014.10.007
- Galassi G, Spada G. (2015). Linear and non-linear sea-level variations in the Adriatic Sea from tide gauge records (1872–2012). *Ann Geophys* 57(6). Doi:10.4401/ag-6536
- Gallien, T. W., Schubert, J. E., and Sanders, B. F. (2011). Predicting tidal flooding of urbanized embayments: A modeling framework and data requirements. *Coastal Engineering*, 58(6), 567–577. Doi:10.1016/j.coastaleng.2011.01.011
- Gerl, T., Kreibich, H., Franco, G., Marechal, D., and Schröter, K. (2016). A Review of Flood Loss Models as Basis for Harmonization and Benchmarking. *PLOS ONE*, 11(7), e0159791. Doi:10.1371/journal.pone.0159791
- Gesch, D. B. (2009). Analysis of Lidar Elevation Data for Improved Identification and Delineation of Lands Vulnerable to Sea-Level Rise. *Journal of Coastal Research*, 10053, 49–58. Doi:10.2112/si53-006.1
- Gesch, D. B. (2018). Best Practices for Elevation-Based Assessments of Sea-Level Rise and Coastal Flooding Exposure. *Frontiers in Earth Science*, 6. Doi:10.3389/feart.2018.00230 <https://www.frontiersin.org/articles/10.3389/feart.2018.00230/full>
- Gilleland, E., & Katz, R. W. (2011). New Software to Analyze How Extremes Change Over Time. *Eos, Transactions American Geophysical Union*, 92(2), 13–14. Doi:10.1029/2011eo020001
- Gilleland, E. & Katz, R. W. (2016). extremes 2.0: An extreme value analysis package in r. *Journal of Statistical Software* 72, 1–39. <https://www.jstatsoft.org/article/view/v072i08>
- Gissing, A., & Blong, R. (2004). Accounting for variability in commercial flood damage estimation. *Australian Geographer*, 35(2), 209–222. Doi:10.1080/0004918042000249511
- Glas, H., Jonckheere, M., Mandal, A., James-Williamson, S., De Maeyer, P., & Deruyter, G. (2017). A GIS-based tool for flood damage assessment and delineation of a methodology for future risk assessment: case study for Annotto Bay, Jamaica. *Natural Hazards*, 88(3), 1867–1891. Doi:10.1007/s11069-017-2920-5
- Golian, S., Razmi, A., Mardani, H. A., & Zahmatkesh, Z. (2020). Nonstationary Bi-Variate Frequency Analysis of Extreme Sea Level and Rainfall Under Climate Change Impacts: South Carolina Coastal Area. Doi:10.5194/egusphere-egu2020-3098
- Golob, D. (2020 July 29). Slovenia – a maritime country. <https://slovenia.si/this-is-slovenia/slovenia-a-maritime-country/>

- Gorgoso-Varela, J. J., & Rojo-Alboreca, A. (2014). Use of Gumbel and Weibull functions to model extreme values of diameter distributions in forest stands. *Annals of Forest Science*, 71(7), 741–750. Doi:10.1007/s13595-014-0369-1
- Gracia, V., Sierra, J. P., Gómez, M., Pedrol, M., Sampé, S., García-León, M., and Gironella, X. (2019). Assessing the impact of sea level rise on port operability using LiDAR-derived digital elevation models. *Remote Sensing of Environment*, 232, 111318. Doi:10.1016/j.rse.2019.111318
- Griggs, G., Árvai, J., Cayan, D., DeConto, R., Fox, J., Fricker, H.A., Kopp, R.E., Tebaldi, C., Whiteman, E.A. (2017 April). Rising Seas in California: An Update on Sea-Level Rise Science. California Ocean Science Trust. California Ocean Protection Council Science Advisory Team Working Group. https://www.oceansciencetrust.org/wp-content/uploads/2017/04/OST-Sea-Level-Rising-Report-Final_Amended.pdf
- Griggs, G. (2017). 1. Human Settlement of the Coastal Zone. In *Coasts in Crisis* (pp. 1-20). Berkeley: University of California Press. <https://doi.org/10.1525/9780520966857-003>
- Habel, S., Fletcher, C. H., Anderson, T. R., & Thompson, P. R. (2020). Sea-Level Rise Induced Multi-Mechanism Flooding and Contribution to Urban Infrastructure Failure. *Scientific Reports*, 10(1). Doi:10.1038/s41598-020-60762-4
- Haigh, I. D., and Pattiaratchi, C. (2010). Estimating 21st century changes in extreme sea levels around Western Australia. *IOP Conference Series: Earth and Environmental Science*, 11, 012033. Doi:10.1088/1755-1315/11/1/012033
- Haigh, I., Nicholls, R., & Wells, N. (2011). Rising sea levels in the English Channel 1900 to 2100. *Proceedings of the Institution of Civil Engineers - Maritime Engineering*, 164(2), 81–92. Doi:10.1680/maen.2011.164.2.81
- Hawkes, P. J., Gonzalez-Marco, D., Sánchez-Arcilla, A., & Prinos, P. (2008). Best practice for the estimation of extremes: A review. *Journal of Hydraulic Research*, 46(sup2), 324–332. Doi:10.1080/00221686.2008.9521965
- Herath, S. (2003). Flood Damage Estimation of an Urban Catchment using Remote Sensing and GIS. Internation Training Program on Total Disaster Risk Management. United Nations University, Japan. <https://www.adrc.asia/publications/TDRM2003June/10.pdf>
- Hinkel, J., Lincke, D., Vafeidis, A. T., Perrette, M., Nicholls, R. J., Tol, R. S. J., ... Levermann, A. (2014). Coastal flood damage and adaptation costs under 21st century sea-level rise. *Proceedings of the National Academy of Sciences*, 111(9), 3292–3297. Doi:10.1073/pnas.1222469111
- Hinkel, J., Jaeger, C., Nicholls, R. J., Lowe, J., Renn, O., & Peijun, S. (2015). Sea-level rise scenarios and coastal risk management. *Nature Climate Change*, 5(3), 188–190. Doi:10.1038/nclimate2505
- Horton, B. P., Kopp, R. E., Garner, A. J., Hay, C. C., Khan, N. S., ... Shaw, T. A. (2018). Mapping Sea-Level Change in Time, Space, and Probability. Doi:10.1130/abs/2018am-318319
- Huang, W., Xu, S., & Nnaji, S. (2008). Evaluation of GEV model for frequency analysis of annual maximum water levels in the coast of United States. *Ocean Engineering*, 35(11-12), 1132–1147. Doi:10.1016/j.oceaneng.2008.04.010
- Huizinga, J., Moel, H. de, Szewczyk, W. (2017). Global flood depth-damage functions. Methodology and the database with guidelines. EUR 28552 EN. Doi: 10.2760/16510. <https://ec.europa.eu/jrc/en/publication/global-flood-depth-damage-functions-methodology-and-database-guidelines>
- Intergovernmental Panel on Climate Change (IPCC). (2013). Climate Change 2013: The Physical Science Basis - Contribution of Working Group I to the Fifth Assessment Report of the Intergovernmental Panel on Climate Change (Stocker, T.F., D. Qin, G.-K. Plattner, M. Tignor, S.K. Allen, J. Boschung, A. Nauels, Y. Xia, V. Bex and P.M. Midgley (eds.)). Cambridge University Press, Cambridge, United Kingdom and New York, New York, 1585 pp. <https://www.ipcc.ch/report/ar5/wg1/>
- IPCC. (2019). IPCC Special Report on the Ocean and Cryosphere in a Changing Climate [H.-O. Pörtner, D.C. Roberts, V. Masson-Delmotte, P. Zhai, M. Tignor, E. Poloczanska, K. Mintenbeck, A. Alegria, M. Nicolai, A. Okem, J. Petzold, B. Rama, N.M. Weyer (eds.)]. In press. <https://www.ipcc.ch/srocc/>
- Jacobs, J. M., Cattaneo, L. R., Sweet, W., and Mansfield, T. (2018). Recent and Future Outlooks for Nuisance Flooding Impacts on Roadways on the U.S. East Coast. *Transportation Research*

- Record: Journal of the Transportation Research Board, 2672(2), 1–10.
Doi:10.1177/0361198118756366
- Jevrejeva, S., Grinsted, A., and Moore, J. C. (2014). Upper limit for sea level projections by 2100. Environmental Research Letters, 9(10), 104008. Doi:10.1088/1748-9326/9/10/104008
- Jevrejeva, S., Jackson, L. P., Riva, R. E. M., Grinsted, A., & Moore, J. C. (2016). Coastal sea level rise with warming above 2 °C. Proceedings of the National Academy of Sciences, 113(47), 13342–13347. Doi:10.1073/pnas.1605312113
- Jevrejeva, S., Jackson, L. P., Grinsted, A., Lincke, D., & Marzeion, B. (2018). Flood damage costs under the sea level rise with warming of 1.5 °C and 2 °C. Environmental Research Letters, 13(7), 074014. Doi:10.1088/1748-9326/aacc76
- Jongman, B., Kreibich, H., Apel, H., Barredo, J. I., Bates, P. D., Feyen, L., ... Ward, P. J. (2012). Comparative flood damage model assessment: towards a European approach. Natural Hazards and Earth System Sciences, 12(12), 3733–3752. Doi:10.5194/nhess-12-3733-2012
- Jonsson, F., & Ryden, J. (2017). Statistical studies of the Beta Gumbel distribution: estimation of extreme levels of precipitation. Italian Journal of Applied Statistics, 29 (1). <https://www.saijas.org/ojs/journals/1/articles/28/submit/final/28-1-52-1-6-20200213.pdf>
- Kang, J.-L & Su, M.-D & Chang, L.-F. (2005). Loss functions and framework for regional flood damage estimation in residential area. Journal of Marine Science and Technology. 13. 193-199. <https://jmst.ntou.edu.tw/marine/13-3/193-199.pdf>
- Karamouz, M., Fereshtehpour, M., Ahmadvand, F., and Zahmatkesh, Z. (2016). Coastal Flood Damage Estimator: An Alternative to FEMA's HAZUS Platform. Journal of Irrigation and Drainage Engineering, 142(6), 04016016. Doi:10.1061/(asce)ir.1943-4774.0001017
- Katz, R. W., Parlange, M. B., & Naveau, P. (2002). Statistics of extremes in hydrology. Advances in Water Resources, 25(8-12), 1287–1304. Doi:10.1016/s0309-1708(02)00056-8
- Kirezci, E., Young, I. R., Ranasinghe, R., Muis, S., Nicholls, R. J., Lincke, D., & Hinkel, J. (2020). Projections of global-scale extreme sea levels and resulting episodic coastal flooding over the 21st Century. Scientific Reports, 10(1). Doi:10.1038/s41598-020-67736-6
- Kok, M., Huizinga, H. J., Vrouwenvelder, A. C. W. M., and Van den Braak, W. E. W. (2005). Standaardmethode 2005, Report PR999.10, HKV consultants and TNO Bouw, Lelystad.
- Kolega, Nataša. (2006). Slovenian coast sea floods risk. Acta Geographica Slovenica-geografski Zbornik - ACTA GEOGR SLOV. 46. 143-167. 10.3986/AGS46201. https://www.researchgate.net/publication/238454631_Slovenian_coast_sea_floods_risk.
- Kolega, N. (2015). Coastline changes on the Slovenian coast between 1954 and 2010. Acta Geographica Slovenica, 55(2). Doi:10.3986/ags.1887
- Kominz, M. A. (2013). Sea Level Variations over Geologic Time. Encyclopedia of Ocean Sciences, 575–582. Doi:10.1016/b978-0-12-409548-9.04349-9
- Kopp, R. E., DeConto, R. M., Bader, D. A., Hay, C. C., Horton, R. M., Kulp, S., ... Strauss, B. H. (2017). Evolving Understanding of Antarctic Ice-Sheet Physics and Ambiguity in Probabilistic Sea-Level Projections. Earth's Future, 5(12), 1217–1233. Doi:10.1002/2017ef000663
- Kopp, R. E., Horton, R. M., Little, C. M., Mitrovica, J. X., Oppenheimer, M., Rasmussen, D. J., and Tebaldi, C. (2014). Probabilistic 21st and 22nd century sea-level projections at a global network of tide-gauge sites. Earth's Future, 2(8), 383–406. Doi:10.1002/2014ef000239
- Koutsoyiannis, D. (2004). Statistics of extremes and estimation of extreme rainfall: I. Theoretical investigation / Statistiques de valeurs extrêmes et estimation de précipitations extrêmes: I. Recherche théorique. Hydrological Sciences Journal, 49(4). Doi:10.1623/hysj.49.4.575.54430
- Koutsoyiannis, D. (2007). A Critical Review of Probability of Extreme Rainfall. Advances in Urban Flood Management, 139–166. Doi:10.1201/9780203945988.ch7
- Kreibich, H., Seifert, I., Merz, B., & Thielen, A. H. (2010). Development of FLEMOcs – a new model for the estimation of flood losses in the commercial sector. Hydrological Sciences Journal, 55(8), 1302–1314. Doi:10.1080/02626667.2010.529815
- Kuleli, T., Şenkal, O. and Erdem, M. (2009). National Assessment of Sea Level Rise Using Topographic and Census Data for Turkish Coastal Zone. Environmental Monitoring and Assessment, 156, Article No. 425. <https://Doi.org/10.1007/s10661-008-0495-z>
- Kulp, S.A., Strauss, B.H. (2019). New elevation data triple estimates of global vulnerability to sea-level rise and coastal flooding. Nat Commun 10, 4844. <https://Doi.org/10.1038/s41467-019-12808-z>

- Kuza, I. and Merc, M. (2015 June 3). In STAGE every inhabitant of Slovenia play his or her part. Republic of Slovenia Statistical Office. <https://www.stat.si/StatWeb/en/News/Index/5238>
- Laio, F., Di Baldassarre, G., & Montanari, A. (2009). Model selection techniques for the frequency analysis of hydrological extremes. *Water Resources Research*, 45(7). Doi:10.1029/2007wr006666
- Le Bars, D., Drijfhout, S., and de Vries, H. (2017). A high-end sea level rise probabilistic projection including rapid Antarctic ice sheet mass loss. *Environmental Research Letters*, 12(4), 044013. Doi:10.1088/1748-9326/aa6512
- Lee, Y. (2014). Coastal Planning Strategies for Adaptation to Sea Level Rise: A Case Study of Mokpo, Korea. *Journal of Building Construction and Planning Research*, 02(01), 74–81. Doi:10.4236/jbcpr.2014.21007
- Legal Information System. (19 June 2003). Housing Act - SZ-1. Official Gazette of the Republic of Slovenia. <http://pisrs.si/Pis.web/pregledPredpisa?id=ZAKO2008#>
- Li, Xingong and Rowley, Rex and Kostelnick, John and Braaten, David and Meisel, Joshua and Hulbutta, Kalonie. (2009). GIS Analysis of Global Impacts from Sea Level Rise. *Photogrammetric Engineering and Remote Sensing*. 75. 807-818. 10.14358/PERS.75.7.807.
- Ličer, M. (2019). Podnebne spremembe in naraščanje gladine morja v Severnem Jadranu (Climate change and sea level rise in the North Adriatic). National Institute of Biology – Marine Biological Station Piran. <https://www.nib.si/mpb/sl/home/news/902-podnebne-spremembe-in-narascanje-gladine-morja-v-severnem-jadranu>
- Ličer, M., Fettich, A. and Jeromel, M. (2021 January). Prognozirano plimovanje morja (Tide tables 2021). Ministry of the Environment and Spatial Planning - Slovenian Environment Agency. Ljubljana, Slovenia. <http://www.arso.gov.si/vode/morje/>
- Ličer, M., Žagar, D., Jeromel, M., Jerma, J. (2009). Case Study: Application of an artificial neural network model for analysis of the extreme tide events in the Gulf of Trieste in the early December 2008. https://www.researchgate.net/publication/241506596_Case_Study_Application_of_an_artificial_neural_network_model_for_analysis_of_the_extreme_tide_events_in_the_Gulf_of_Trieste_in_the_early_December_2008
- Lichter, M., and Felsenstein, D. (2012). Assessing the costs of sea-level rise and extreme flooding at the local level: A GIS-based approach. *Ocean and Coastal Management*, 59, 47–62. Doi:10.1016/j.ocecoaman.2011.12.020
- Malik, A., Abdalla, R. (2016). Geospatial modeling of the impact of sea level rise on coastal communities: application of Richmond, British Columbia, Canada. *Model. Earth Syst. Environ.* 2, 146. <https://doi.org/10.1007/s40808-016-0199-2>
- Marcy, D., Brooks, W., Draganov, K., Hadley, B., Haynes, C., Herold, N., ... Waters, K. (2011). New Mapping Tool and Techniques for Visualizing Sea Level Rise and Coastal Flooding Impacts. *Solutions to Coastal Disasters* 2011. Doi:10.1061/41185(417)42
- Marcos, M., Chust, G., Jordà, G., and Caballero, A. (2012). Effect of sea level extremes on the western Basque coast during the 21st century. *Climate Research*, 51(3), 237–248. Doi:10.3354/cr01069
- Méndez, F. J., Menéndez, M., Luceño, A., & Losada, I. J. (2007). Analyzing Monthly Extreme Sea Levels with a Time-Dependent GEV Model. *Journal of Atmospheric and Oceanic Technology*, 24(5), 894–911. Doi:10.1175/jtech2009.1
- Mengel, M. et al. (2016). Future sea level rise constrained by observations and long-term commitment. *Proceedings of the National Academy of Sciences*, 113 (10), 2597-2602, Doi:10.1073/pnas.1500515113.
- Merz, B., Kreibich, H., Thielen, A., and Schmidtke, R. (2004). Estimation uncertainty of direct monetary flood damage to buildings. *Natural Hazards and Earth System Sciences*, 4(1), 153–163. Doi:10.5194/nhess-4-153-2004
- Merz, B., Thielen, A. H., & Gocht, M. (2007). Flood Risk Mapping At the Local Scale: Concepts and Challenges. *Advances in Natural and Technological Hazards Research*, 231–251. Doi:10.1007/978-1-4020-4200-3_13
- Merz, B., Elmer, F., & Thielen, A. H. (2009). Significance of "high probability/low damage" versus "low probability/high damage" flood events. *Natural Hazards and Earth System Sciences*, 9(3), 1033–1046. Doi: 10.5194/nhess-9-1033-2009.

- Merz, B., Kreibich, H., Schwarze, R., and Thielen, A. (2010). Review article "Assessment of economic flood damage". Nat. Hazards Earth Syst. Sci. 10, 1697–1724. <https://doi.org/10.5194/nhess-10-1697-2010>
- Messner, F., Penning-Rowsell, E., Green, C., Meyer, V., Tunstall, S. and Veen, A. (2007). Evaluating flood damage: guidance and recommendations on principles and methods. FLOOD Site Project Report. http://www.floodsite.net/html/partner_area/project_docs/T09_06_01_Flood_damage_guidelines_d9_1_v2_2_p44.pdf
- Mezek S., Bricelj M. (2002) A Review of Coastal Area Management in Slovenia. In: Sain B.C., Pavlin I., Belfiore S. (eds) Sustainable Coastal Management: A Transatlantic and Euro-Mediterranean Perspective. NATO Science Series (Series IV: Earth and Environmental Sciences), vol 12. Springer, Dordrecht. https://doi.org/10.1007/978-94-010-0487-9_12
- Middelmann-Fernandes, M. H. (2010). Flood damage estimation beyond stage-damage functions: an Australian example. Journal of Flood Risk Management, 3(1), 88–96. Doi:10.1111/j.1753-318x.2009.01058.x
- Millington, N., Das, S., Simonovic, S.P. (2011). The Comparison of GEV, Log-Pearson Type 3 and Gumbel Distributions in the Upper Thames River Watershed under Global Climate Models. Water Resources Research Report. Department of Civil and Environmental Engineering, The University of Western Ontario London, Ontario, Canada. <https://ir.lib.uwo.ca/wrrr/40/>
- Ministry of Agriculture, Forestry and Food (MAFF). (2019 August 22). Records of actual use by the farmer and forest land: Data on records of actual use for previous years (shape + metadata). <https://rkg.gov.si/vstop/>
- Ministry of Culture. (2018 September 24). Selection from the register of immovable cultural heritage. OPSI - Odprti podatki Slovenije. <https://podatki.gov.si/dataset/izbor-iz-registra-nepremicne-kulturne-dediscine>
- Ministry of the Environment, Spatial Planning and Energy. (2002). Slovenia's First National Communication under The UN Framework Convention on Climate Change. Ljubljana. https://www.gov.si/assets/ministrstva/MOP/Publikacije/podnebje_en.pdf
- Mlasko, J. (2011). Lasersko Skeniranje in Aerofotografiranje 2011 Blok B21: Tehnično Poročilo Izdelave. Agencija Republike Slovenije za okolje (ARSO). Ljubljana, Slovenia. http://gis.arso.gov.si/related/lidar_porocila/b_21_ijzelava_ijzelkov.pdf
- Moccia, B., Mineo, C., Ridolfi, E., Russo, F., & Napolitano, F. (2021). Probability distributions of daily rainfall extremes in Lazio and Sicily, Italy, and design rainfall inferences. Journal of Hydrology: Regional Studies, 33, 100771. Doi:10.1016/j.ejrh.2020.100771
- Moftakhar, H. R., AghaKouchak, A., Sanders, B. F., Allaire, M., and Matthew, R. A. (2018). What Is Nuisance Flooding? Defining and Monitoring an Emerging Challenge. Water Resources Research, 54(7), 4218–4227. Doi:10.1029/2018wr022828
- Moftakhar, H. R., AghaKouchak, A., Sanders, B. F., and Matthew, R. A. (2017). Cumulative hazard: The case of nuisance flooding. Earth's Future, 5(2), 214–223. Doi:10.1002/2016ef000494
- Moftakhar, H. R., AghaKouchak, A., Sanders, B. F., Feldman, D. L., Sweet, W., Matthew, R. A., and Luke, A. (2015). Increased nuisance flooding along the coasts of the United States due to sea level rise: Past and future. Geophysical Research Letters, 42(22), 9846–9852. Doi:10.1002/2015gl066072
- Mohammadi, S. A., Nazariha, M., & Mehrdadi, N. (2014). Flood Damage Estimate (Quantity), Using HEC-FDA Model. Case Study: The Neka River. Procedia Engineering, 70, 1173–1182. Doi:10.1016/j.proeng.2014.02.130
- Mudersbach, C., & Jensen, J. (2010). Nonstationary extreme value analysis of annual maximum water levels for designing coastal structures on the German North Sea coastline. Journal of Flood Risk Management, 3(1), 52–62. Doi:10.1111/j.1753-318x.2009.01054.x
- Muis, S., Verlaan, M., Winsemius, H. C., Aerts, J. C. J. H., & Ward, P. J. (2016). A global reanalysis of storm surges and extreme sea levels. Nature Communications, 7(1). Doi:10.1038/ncomms11969
- Mullin, C. and French, R. (4 February 2016). Mapping the damage from rising seas. GreenBiz. <https://www.greenbiz.com/article/mapping-damage-rising-seas>

- Murdukhayeva, A., August, P., Bradley, M., LaBash, C., and Shaw, N. (2013). Assessment of Inundation Risk from Sea Level Rise and Storm Surge in Northeastern Coastal National Parks. *Journal of Coastal Research*, 291, 1–16. Doi:10.2112/jcoastres-d-12-00196.1
- Nafari, R. H. (2018 January). Flood Damage Assessment in Urban Areas [Doctoral Dissertation, The University of Melbourne]. Minerva Access University Library. <https://minerva-access.unimelb.edu.au/handle/11343/212277>
- Neumann, J., Emanuel, K., Ravela, S., Ludwig, L., and Verly, C. (2015). Risks of Coastal Storm Surge and the Effect of Sea Level Rise in the Red River Delta, Vietnam. *Sustainability*, 7(6), 6553–6572. Doi:10.3390/su7066553
- New Zealand Institute of Economic Research. (2004). Economic impacts on New Zealand of climate change-related extreme events. Focus on freshwater floods. Report to the New Zealand Climate Change Office. Wellington, New Zealand: New Zealand Institute of Economic Research. <https://environment.govt.nz/assets/Publications/Files/economic-impacts-extreme-events-jul04.pdf>
- Nicholls, R.J. (2002). Rising sea levels: potential impacts and responses. In: Hester, R. and Harrison, R.M. (ed.) *Global Environmental Change. Issues in Environmental Science and Technology*, Number 17, Royal Society of Chemistry, Cambridge, pp. 83-107.
- Nicholls, Robert and Cazenave, Anny. (2010). Sea-Level Rise and Its Impact on Coastal Zones. *Science* (New York, N.Y.). 328. 1517-20. Doi: 10.1126/science.1185782. https://www.researchgate.net/publication/44683423_Sea-Level_Rise_and_Its_Impact_on_Coastal_Zones
- Nicholls, R., et al. (2008). Ranking Port Cities with High Exposure and Vulnerability to Climate Extremes: Exposure Estimates. *OECD Environment Working Papers*, No. 1, OECD Publishing, Paris, <https://Doi.org/10.1787/011766488208>
- Nicholls, R. (2011). Planning for the Impacts of Sea Level Rise. *Oceanography*, 24(2), 144–157. Doi:10.5670/oceanog.2011.34
- National Oceanic and Atmospheric Administration. (2000). Tidal datums and their applications. NOAA Special Publication NOS CO-OPS 1. https://tidesandcurrents.noaa.gov/publications/tidal_datums_and_their_applications.pdf
- NOAA National Centers for Environmental Information. (2018). State of the Climate: National Climate Report for May 2018, published online June 2018, retrieved on March 3, 2021 from <https://www.ncdc.noaa.gov/sotc/national/2018/05/supplemental/page-1>
- National Oceanic and Atmospheric Administration (NOAA). (2012). Mapping coastal inundation primer. United States of America. Retrieved from <https://coast.noaa.gov/data/digitalcoast/pdf/coastal-inundation-guidebook.pdf> on 05 March 2021
- National Oceanic and Atmospheric Administration (NOAA) Coastal Services Center. (2012). Lidar 101: An Introduction to LiDAR Technology, Data, and Applications. Revised. Charleston, SC: NOAA Coastal Services Center. <https://coast.noaa.gov/data/digitalcoast/pdf/lidar-101.pdf>
- Nicholls, R. J., Hanson, S. E., Lowe, J. A., Warrick, R. A., Lu, X., and Long, A. J. (2014). Sea-level scenarios for evaluating coastal impacts. *Wiley Interdisciplinary Reviews: Climate Change*, 5(1), 129–150. Doi:10.1002/wcc.253
- NOAA Office for Coastal Management. (2017). Digital Coast Sea Level Rise Viewer. United States of America. <https://coast.noaa.gov/data/digitalcoast/pdf/slris-faq.pdf>
- OECD (2019). Responding to Rising Seas: OECD Country Approaches to Tackling Coastal Risks. OECD Publishing, Paris, France. <https://Doi.org/10.1787/9789264312487-en>.
- Olesen, L., Löwe, R., and Arnbjerg-Nielsen, K. (2017). Flood damage assessment – Literature review and recommended procedure. Cooperative Research Centre for Water Sensitive Cities. <https://watersensitivocities.org.au/content/flood-damage-assessment-literature-review-recommended-procedure/>
- Olsen, A., Zhou, Q., Linde, J., & Arnbjerg-Nielsen, K. (2015). Comparing Methods of Calculating Expected Annual Damage in Urban Pluvial Flood Risk Assessments. *Water*, 7(12), 255–270. Doi:10.3390/w7010255
- Oppenheimer, M., B.C. Glavovic , J. Hinkel, R. van de Wal, A.K. Magnan, A. Abd-Elgawad, R. Cai, M. Cifuentes-Jara, R.M. DeConto, T. Ghosh, J. Hay, F. Isla, B. Marzeion, B. Meyssignac, and Z.

- Sebesvari, 2019: Sea Level Rise and Implications for Low-Lying Islands, Coasts and Communities. In: IPCC Special Report on the Ocean and Cryosphere in a Changing Climate [H.-O. Pörtner, D.C. Roberts, V. Masson-Delmotte, P. Zhai, M. Tignor, E. Poloczanska, K. Mintenbeck, A. Alegría, M. Nicolai, A. Okem, J. Petzold, B. Rama, N.M. Weyer (eds.)]. Cambridge University Press, Cambridge, UK and New York.
- Orovic, J. (2018 August 29). Adriatic Sea Warming – and Rising – At an Alarming rate. Total Croatia News. <https://www.total-croatia-news.com/news/30696-adriatic-sea-warming-and-rising-at-an-alarming-rate>
- Papalexiou, S. M., Koutsoyiannis, D., & Makropoulos, C. (2013). How extreme is extreme? An assessment of daily rainfall distribution tails. *Hydrology and Earth System Sciences*, 17(2), 851–862. Doi:10.5194/hess-17-851-2013
- Papilloud, T., Röthlisberger, V., Loreti, S., & Keiler, M. (2020). Flood exposure analysis of road infrastructure – Comparison of different methods at national level. *International Journal of Disaster Risk Reduction*, 101548. Doi:10.1016/j.ijdrr.2020.101548
- Paprotny, D., Terefenko, P. (2017). New estimates of potential impacts of sea level rise and coastal floods in Poland. *Nat Hazards* 85, 1249–1277. <https://doi.org/10.1007/s11069-016-2619-z>
- Paprotny, D. (2014). Trends in storm surge probability of occurrence along the Polish Baltic Sea coast. arXiv: 1410.2547. <https://arxiv.org/ftp/arxiv/papers/1410/1410.2547.pdf>
- Penning-Rowsell E., Johnson C., Tunstall S., Tapsell S., Morris J., Chatterton J. & Green C. (2005). The benefits of flood and coastal riskmanagement: a handbook of assessment techniques. Middlesex University Press, London. <https://citeserx.ist.psu.edu/viewdoc/download?Doi=10.1.1.958.5135&rep=rep1&type=pdf>
- Penning-Rowsell, E., Viavattene, C., Pardoe, J., Chatterton, J., Parker, D., and Morris, J. (2010). The Benefits of Flood and Coastal Risk Management: A Handbook of Assessment Techniques 2010. Flood Hazard Research Centre, Middlesex, London.
- Petek F. (2004). Land use in Slovenia, Slovenia: a geographical overview, ZRC SAZU, Ljubljana 105–108. http://zgs.zrc-sazu.si/Portals/8/Slo_Geo_Over/19.pdf
- Pistrika, A., Tsakiris, G., and Nalbantis, I. (2014). Flood Depth-Damage Functions for Built Environment. *Environmental Processes*, 1(4), 553–572. Doi:10.1007/s40710-014-0038-2
- Poulter, B., and Halpin, P. N. (2008). Raster modelling of coastal flooding from sea-level rise. *International Journal of Geographical Information Science*, 22(2), 167–182. Doi:10.1080/13658810701371858
- Prahl, B., Boettle, M., Costa, L. et al. (2018). Damage and protection cost curves for coastal floods within the 600 largest European cities. *Sci Data* 5, 180034. <https://doi.org/10.1038/sdata.2018.34>
- Prijatelj, M. (2019 February 28). In 2018 almost 15.7 million tourist overnight stays. Statistical Office of the Republic of Slovenia. Accessed on February 23, 2021 from <https://www.stat.si/StatWeb/en/news/Index/7978>
- Prime, T., Brown, J. M., Plater, A. J. (2015). Physical and Economic Impacts of Sea-Level Rise and Low Probability Flooding Events on Coastal Communities. *PLoS ONE* 10(2), e0117030. Doi:10.1371/journal.pone.0117030
- Pugh, D. T. (1987). Tides, Surges and Mean Sea-Level, 472 pp., John Wiley, Hoboken, N. J.
- Ramieri, Emiliano. (2000). An overview of the vulnerability of Venice to the impacts of climate change and sea level rise. Nota di Lavoro, No. 22. 2000, Fondazione Eni Enrico Mattei (FEEM), Milano, Italy. <https://www.econstor.eu/handle/10419/155076>
- Ray, R. D., and Foster, G. (2016). Future nuisance flooding at Boston caused by astronomical tides alone. *Earth's Future*, 4(12), 578–587. Doi:10.1002/2016ef000423
- Razpotnik, B. (2020 June 8). On 1 January 2020, 2,095,861 residents of Slovenia lived in 5,978 settlements; 57 settlements were unpopulated. Statistical Office of the Republic of Slovenia. <https://www.stat.si/StatWeb/en/News/Index/8857>
- Ribeiro, A., Barbosa, S. M., Scotto, M. G., & Donner, R. V. (2014). Changes in extreme sea-levels in the Baltic Sea. *Tellus A: Dynamic Meteorology and Oceanography*, 66(1), 20921. Doi:10.3402/tellusa.v66.20921
- Robič, M. and Vrhovec, T. (2002). Poplavljjanje Morske Obale. In B. Ušeničnik (Ed.), *Nesreče in varstvo pred njimi*. Ljubljana, Slovenia: Administration of the Republic of Slovenia for Civil Protection

- and Disaster Relief of the Ministry of Defense. http://www.sos112.si/slo/tdocs/nesrece_varstvo1.pdf
- Robič, M., and Strojan, I. (January 01, 2009). Izjemne višine morja leta 2008 (Extreme sea levels in 2008). Ujma, 27-36. Ljubljana, Slovenia: Administration of the Republic of Slovenia for Civil Protection and Disaster Relief of the Ministry of Defense. <http://www.sos112.si/slo/page.php?src=sv611.htm>
- Rocco, F.V. (2015). Sea level trends in the Mediterranean from tide gauges and satellite altimetry. Doctoral dissertation, Alma Mater Studiorum, University of Bologna, Italy. <https://core.ac.uk/download/pdf/31159452.pdf>
- Romali, N. S., & Yusop, Z. (2020). Flood damage and risk assessment for urban area in Malaysia. *Hydrology Research*, 52(1), 142–159. Doi:10.2166/nh.2020.121
- Rowley, R. J., Kostelnick, J. C., Braaten, D., Li, X., and Meisel, J. (2007). Risk of rising sea level to population and land area. *Eos, Transactions American Geophysical Union*, 88(9), 105–107. Doi:10.1029/2007eo090001
- R Core Team. (2020). R: A language and environment for statistical computing. R Foundation for Statistical Computing, Vienna, Austria. <https://www.r-project.org/>
- Sahin, O., & Mohamed, S. (2013). Coastal vulnerability to sea-level rise: a spatial-temporal assessment framework. *Natural Hazards*, 70(1), 395–414. Doi:10.1007/s11069-013-0818-4
- Scarascia, L., and Lionello, P. (2013). Global and regional factors contributing to the past and future sea level rise in the Northern Adriatic Sea. *Global and Planetary Change*, 106, 51–63. Doi:10.1016/j.gloplacha.2013.03.004
- Schmid, K., Hadley, B., and Waters, K. (2014). Mapping and Portraying Inundation Uncertainty of Bathtub-Type Models. *Journal of Coastal Research*, 295, 548–561. Doi:10.2112/jcoastres-d-13-00118.1
- Schröter, K., Kreibich, H., Vogel, K., Riggelsen, C., Scherbaum, F., & Merz, B. (2014). How useful are complex flood damage models? *Water Resources Research*, 50(4), 3378–3395. Doi:10.1002/2013wr014396
- Scialabba, Nadia (ed.). 1998. Integrated coastal area management and agriculture, forestry and fisheries. FAO Guidelines. Environment and Natural Resources Service, FAO, Rome. 256 p. <http://www.fao.org/3/W8440e/W8440e02.htm>
- Sesana, E., Gagnon, A., Bertolin, C., & Hughes, J. (2018). Adapting Cultural Heritage to Climate Change Risks: Perspectives of Cultural Heritage Experts in Europe. *Geosciences*, 8(8), 305. Doi:10.3390/geosciences8080305
- Siebentritt, M., 2016: Understanding sea-level rise and climate change, and associated impacts on the coastal zone. CoastAdapt Information Manual 2, National Climate Change Adaptation Research Facility, Gold Coast. https://coastadapt.com.au/sites/default/files/information-manual/IM02_Understanding_sea_level_rise.pdf
- Siegel, A. F. (2016). Correlation and Regression. *Practical Business Statistics*, 299–354. Doi:10.1016/b978-0-12-804250-2.00011-0
- Sindhu, B., & Unnikrishnan, A. S. (2011). Return period estimates of extreme sea level along the east coast of India from numerical simulations. *Natural Hazards*, 61(3), 1007–1028. Doi:10.1007/s11069-011-9948-8
- Slovenia in the laser scanning data. (5 November 2015). GEAVIS. <https://www.geavis.si/en/2015/11/slovenia-in-the-laser-scanning-data/> Accessed on 10 March 2021
- Slovenska tiskovna agencija (STA). (2019, November 13). Piran, Izola and Koper Flooded Due to Rain, Full Moon. Total Slovenia News. <https://www.total-slovenia-news.com/lifestyle/4964-piran-izola-koper-flooded-due-to-rain-full-moon-video>
- Slovenska tiskovna agencija (STA). (2020, December 9). Floods Hit Coast, Cause Power Cuts, Traffic Delays. Total Slovenia News. <https://www.total-slovenia-news.com/lifestyle/7458-floods-hit-coast-cause-traffic-delays-video>
- Smith, D. (1994). Flood damage estimation - A review of urban stage-damage curves and loss functions. *Water SA*, 20, 231-238. https://journals.co.za/Doi/10.10520/AJA03784738_1124
- Smith, N.F. and ICLEI Canada. (2020). Considering Sea Level Rise and Cultural Heritage: A Resource for Municipalities. An Initiative from the Together for Climate Project. ICLEI Canada, Toronto.

- https://icleicanada.org/wp-content/uploads/2020/10/Considering-Sea-Level-Rise-and-Cultural-Heritage_FINAL.pdf
- Stammer, D., Wal, R. S. W., Nicholls, R. J., Church, J. A., Le Cozannet, G., Lowe, J. A., ... Hinkel, J. (2019). Framework for High-End Estimates of Sea Level Rise for Stakeholder Applications. *Earth's Future*, 7(8), 923–938. Doi:10.1029/2019ef001163
- Stanchev, H., Palazov, A., and Stancheva, M. (2009). 3D GIS Model for Flood Risk Assessment of Varna Bay Due to Extreme Sea Level Rise. *Journal of Coastal Research*, 1597-1601. Retrieved February 25, 2021, from <http://www.jstor.org/stable/25738059>
- Statistical Office of the Republic of Slovenia (SURS). (2020 January 1). Settlement of Piran. <https://www.stat.si/KrajevnaImena/en/Settlements/Details/3227>
- Stephens, S. (2009). Toolbox 2.2.1 – Guidance on assessing sea-level rise in New Zealand. Impacts of Climate Change on Urban Infrastructure & the Built Environment. National Institute of Water and Atmospheric Research (NIWA). New Zealand. Retrieved from <https://niwa.co.nz/climate/urban-impacts-toolbox/toolbox-trays/second-tray-assess-the-likely-hazard/sea-level-rise-and-storm-surge>
- Strojan, I. and Robič, M. (15 September 2016). Sea level. Slovenian Environment Agency. <http://kazalci.arso.gov.si/en/content/sea-level-4>
- Surveying and Mapping Authority of the Republic of Slovenia (GURS). (2017). Real Estate Register. <https://www.e-prostor.gov.si/>
- Suursaar, Ü., & Sooäär, J. (2007). Decadal variations in mean and extreme sea level values along the Estonian coast of the Baltic Sea. *Tellus A: Dynamic Meteorology and Oceanography*, 59(2), 249–260. Doi:10.1111/j.1600-0870.2006.00220.x
- Sweet, W., Park, J., Marra, J., Zervas, C., and Gill, S. (2014). Sea level rise and nuisance flood frequency changes around the United States (NOAA Technical Report No. NOS CO-OPS 073) (p. 66). National Oceanic and Atmospheric Association. Retrieved from https://tidesandcurrents.noaa.gov/publications/NOAA_Technical_Report_NOS_COOPS_073.pdf
- Sweet, William and Zervas, Chris and Gill, Stephen and Park, Joseph. (2013). Hurricane Sandy Innundation Probabilities Today and Tomorrow. *Bulletin of the American Meteorological Society*. 94. S17-S20. https://www.researchgate.net/publication/262186934_Hurricane_Sandy_Innundation_Probabilities_Today_and_Tomorrow
- Tahvildari, N., and Castrucci, L. (2021). Relative Sea Level Rise Impacts on Storm Surge Flooding of Transportation Infrastructure. *Natural Hazards Review*, 22(1), 04020045. Doi:10.1061/(asce)nh.1527-6996.0000412
- Tate, E., Rahman, M. A., Emrich, C. T., & Sampson, C. C. (2021). Flood exposure and social vulnerability in the United States. *Natural Hazards*, 106(1), 435–457. Doi:10.1007/s11069-020-04470-2
- Thieken, A. H., Olschewski, A., Kreibich, H., Kobsch, S., & Merz, B. (2008). Development and evaluation of FLEMOps – a new Flood Loss Estimation MOdel for the private sector. *Flood Recovery, Innovation and Response I*. Doi:10.2495/friar080301
- Torresan, S., Gallina, V., Gualdi, S., Bellafiore, D., Umgiesser, G., Carniel, S., ... Critto, A. (2019). Assessment of Climate Change Impacts in the North Adriatic Coastal Area. Part I: A Multi-Model Chain for the Definition of Climate Change Hazard Scenarios. *Water*, 11(6), 1157. Doi:10.3390/w11061157
- Triglav-Čekada, M., Bric, V., Primož, K., Mongus, D., Lukac, N. and Zalik, B. (2015). Nationwide aerial laser scanning for 3D-acquisition of water surfaces in Slovenia. *CapturingReality*, 23-25 November 2015, Salzburg, Austria. https://www.researchgate.net/publication/291312265_Nationwide_aerial_laser_scanning_for_3D-acquisition_of_water_surfaces_in_Slovenia
- Tsimplis, M.N., Spencer, N.E., 1997. Collection and analysis of monthly mean sea level data in the Mediterranean and the Black Sea. *J. Coast. Res.* 13 (2), 534–544. https://www.jstor.org/stable/4298645?seq=1#metadata_info_tab_contents

- Tsimplis, M. N., Marcos, M., and Somot, S. (2008). 21st century Mediterranean sea level rise: Steric and atmospheric pressure contributions from a regional model. *Global and Planetary Change*, 63(2-3), 105–111. Doi:10.1016/j.gloplacha.2007.09.006
- Tsimplis, M. N., Raicich, F., Fenoglio-Marc, L., Shaw, A. G. P., Marcos, M., Somot, S., and Bergamasco, A. (2012). Recent developments in understanding sea level rise at the Adriatic coasts. *Physics and Chemistry of the Earth, Parts A/B/C*, 40-41, 59–71. Doi:10.1016/j.pce.2009.11.007
- Tyralis, H., Papacharalampous, G., & Tantanee, S. (2019). How to explain and predict the shape parameter of the generalized extreme value distribution of streamflow extremes using a big dataset. *Journal of Hydrology*. Doi:10.1016/j.jhydrol.2019.04.070
- UNEP/MAP-PAP/RAC. (2018). MAP Coastal Area Management Programme (CAMP) Slovenia: Final Integrated Report. MAP Technical Series No. 171. UNEP/MAP: Athens. <https://digitallibrary.un.org/record/648053?ln=en>
- UNISDR. (2016). Report of the Open-Ended Intergovernmental Expert Working Group on Indicators and Terminology Relating to Disaster Risk Reduction. United Nations, New York, USA. <https://digitallibrary.un.org/record/852089?ln=en>
- U.S. Army Corps of Engineers (USACE). (2013). Flood Risk Management National Economic Development Manual: IWR Report 2013-R-05. Institute for Water Resources. United States. <https://www.iwr.usace.army.mil/Portals/70/docs/iwrreports/2013-R-05.pdf>
- USACE. (2006). Depth-Damage Relationships for Structures, Contents, and Vehicles and Content-To-Structure Value Ratios (CSVR) in Support of the Donaldsonville to the Gulf, Louisiana, Feasibility Study. U.S. Army Corps of Engineers New Orleans District, Louisiana. <https://www.mvn.usace.army.mil/Portals/56/docs/PD/Donaldsv-Gulf.pdf>
- Vahter M. (2006). Institute for Integral Development and Environment. Euroision case study on the Slovenian coast, Euroision project. http://copranet.projects.euccd.de/files/000152_EUROSION_Slovenian_coast.pdf
- Van de Sande, B., Lansen, J., & Hoyng, C. (2012). Sensitivity of Coastal Flood Risk Assessments to Digital Elevation Models. *Water*, 4(3), 568–579. Doi:10.3390/w4030568
- Velasco, M., Cabello, À., & Russo, B. (2015). Flood damage assessment in urban areas. Application to the Raval district of Barcelona using synthetic depth damage curves. *Urban Water Journal*, 13(4), 426–440. Doi:10.1080/1573062x.2014.994005
- Verkade, J. S., & Werner, M. G. F. (2011). Estimating the benefits of single value and probability forecasting for flood warning. *Hydrology and Earth System Sciences*, 15(12), 3751–3765. Doi:10.5194/hess-15-3751-2011
- Vidmar, A., Zabret, K., Lebar, K., Pergar, P., and Kryžanowski, A. (2019). Development of an application for estimating the benefits of constructional and non-constructional measures for flood risk reduction. Conference: 7. Hrvatska konferencija o vodama - Hrvatske vode u zaštiti okoliša i prirode, Opatija, Croatia. https://www.researchgate.net/publication/333631413_Development_of_an_application_for_estimating_the_benefits_of_constructional_and_non-constructional_measures_for_flood_risk_reduction
- Vousdoukas, M.I., Mentaschi, L., Hinkel, J. et al. (2020). Economic motivation for raising coastal flood defenses in Europe. *Nat Commun* 11, 2119. <https://Doi.org/10.1038/s41467-020-15665-3>
- Vrščaj, B. (2011 December 28). Land Use Change and Agriculture. Slovenian Environment Agency. <http://kazalci.ars.si/en/teme/agriculture>
- Ward, P. J., de Moel, H., & Aerts, J. C. J. H. (2011). How are flood risk estimates affected by the choice of return-periods?. *Natural Hazards and Earth System Sciences*, 11(12), 3181–3195. Doi:10.5194/nhess-11-3181-2011
- Weber I. (2007) Heritage Narratives on the Slovenian Coast: The Lion and the Attic. In: Kockel U., Craith M.N. (eds) Cultural Heritages as Reflexive Traditions. Palgrave Macmillan, London. https://Doi.org/10.1057/9780230285941_10
- Webster, Tim and Forbes, Donald and MacKinnon, Edward and Roberts, Daniel. (2006). Flood-risk mapping for storm-surge events and sea-level rise using lidar for southeast New Brunswick. *Canadian Journal of Remote Sensing*. 32. 194-211. 10.5589/m06-016.

- Williams, L. L., and Lück-Vogel, M. (2020). Comparative assessment of the GIS based bathtub model and an enhanced bathtub model for coastal inundation. *Journal of Coastal Conservation*, 24(2). Doi:10.1007/s11852-020-00735-x
- Wong, T. E., A. M. Bakker and K. Keller. (2017). Impacts of Antarctic fast dynamics on sea-level projections and coastal flood defense. *Climatic Change*, 144 (2), 347-364. <https://Doi.org/10.1007/s10584-017-2039-4>
- Wong, T.E., Torline, T., & Zhang, M. (2020). Evidence for increasing frequency of extreme coastal sea levels. arXiv: Data Analysis, Statistics and Probability. <https://arxiv.org/abs/2006.06804>
- World Meteorological Organization (WMO). 2019. The Global Climate in 2015 – 2019. Geneva, Switzerland. https://library.wmo.int/doc_num.php?explnum_id=9936
- Wu, S., Feng, A., Gao, J., Chen, M., Li, Y., and Wang, L. (2016). Shortening the recurrence periods of extreme water levels under future sea-level rise. *Stochastic Environmental Research and Risk Assessment*, 31(10), 2573–2584. Doi:10.1007/s00477-016-1327-2
- Yunus, Ali P. and Avtar, Ram and Kraines, Steven and Yamamuro, Masumi and Lindberg, Fredrik and Grimmond, Christine. (2016). Uncertainties in Tidally Adjusted Estimates of Sea Level Rise Flooding (Bathtub Model) for the Greater London. *Remote Sensing*. 8. 366. 10.3390/rs8050366.
- Zabret, K., Vidmar, A., Sapač, K., Pergar, P., Klemen, K., Ivanuša, B., Kešeljević, A., Spruk, R., Kryžanowski, A. 2018. Razvoj enotne metode za oceno koristi gradbenih in negradbenih ukrepov za zmanjšanje poplavne ogroženosti. 29. Mišičev vodarski dan 2018. Vodnogospodarski biro Maribor, Maribor, 272-279. <http://www.mvd20.com/LETO2018/R34.pdf>
- Zanchettin, D., Bruni, S., Raicich, F., Lionello, P., Adloff, F., Androssov, A., ... Zerbini, S. (2020). Review article: Sea-level rise in Venice: historic and future trends. Doi:10.5194/nhess-2020-351
- Zhang, K. (2011). Analysis of non-linear inundation from sea-level rise using LIDAR data: a case study for South Florida. *Climatic Change*, 106(4), 537–565. Doi:10.1007/s10584-010-9987-2
- Zhang, K., Dittmar, J., Ross, M., & Bergh, C. (2011). Assessment of sea level rise impacts on human population and real property in the Florida Keys. *Climatic Change*, 107(1-2), 129–146. Doi:10.1007/s10584-011-0080-2
- Zhou, Q., Mikkelsen, P. S., Halsnæs, K., & Arnbjerg-Nielsen, K. (2012). Framework for economic pluvial flood risk assessment considering climate change effects and adaptation benefits. *Journal of Hydrology*, 414-415, 539–549. Doi:10.1016/j.jhydrol.2011.11.031